CHAPTER

4

LINEAR WIRE ANTENNAS

4.1 INTRODUCTION

Wire antennas, linear or curved, are some of the oldest, simplest, cheapest, and in many cases the most versatile for many applications. It should not then come as a surprise to the reader that we begin our analysis of antennas by considering some of the oldest, simplest, and most basic configurations. Initially we will try to minimize the complexity of the antenna structure and geometry to keep the mathematical details to a minimum.

4.2 INFINITESIMAL DIPOLE

An infinitesimal linear wire ($l \ll \lambda$) is positioned symmetrically at the origin of the coordinate system and oriented along the z axis, as shown in Figure 4.1(a). Although infinitesimal dipoles are not very practical, they are used to represent capacitor-plate (also referred to as *top-hat-loaded*) antennas. In addition, they are utilized as building blocks of more complex geometries. The wire, in addition to being very small ($l \ll \lambda$), is very thin ($a \ll \lambda$). The current is assumed to be constant and given by

$$\mathbf{I}(z') = \hat{\mathbf{a}}_z I_0 \tag{4-1}$$

where I_0 = constant.

4.2.1 Radiated Fields

To find the fields radiated by the current element, the two-step procedure of Figure 3.1 is used. It will be required to determine first **A** and **F** and then find the **E** and **H**. The functional relation between **A** and the source **J** is given by (3-49), (3-51), or (3-53). Similar relations are available for **F** and **M**, as given by (3-50), (3-52), and (3-54).

Since the source only carries an electric current $\mathbf{I}_e$, $\mathbf{I}_m$ and the potential function **F** are zero. To find **A** we write

$$\mathbf{A}(x, y, z) = \frac{\mu}{4\pi} \int_C \mathbf{I}_e(x', y', z') \frac{e^{-jkR}}{R} dl' \tag{4-2}$$

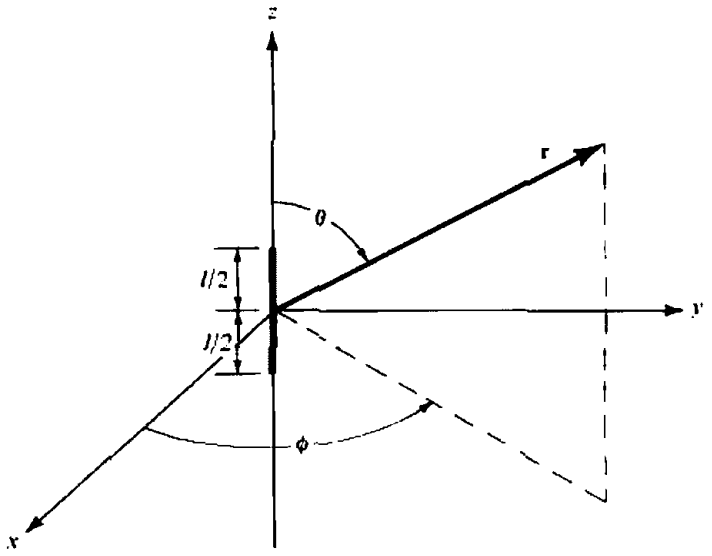

(a) Infinitesimal dipole

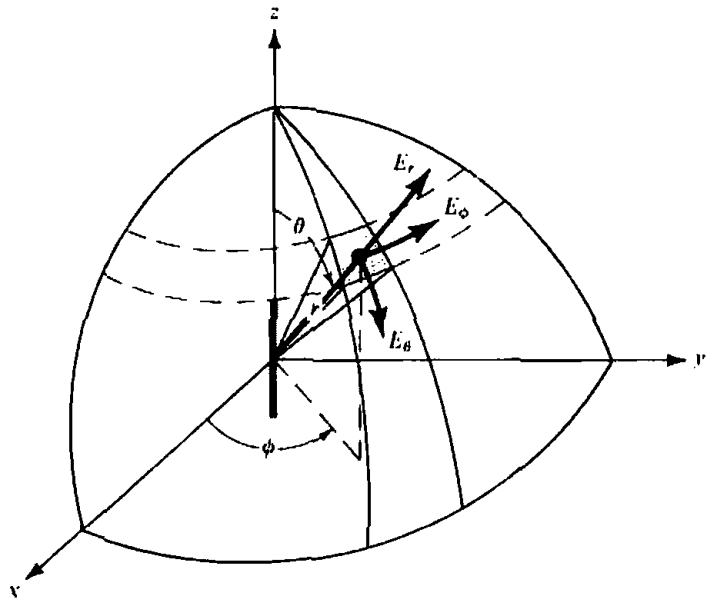

(b) Electric field orientation

Figure 4.1 Geometrical arrangement of an infinitesimal dipole and its associated electric field components on a spherical surface.

where (x, y, z) represent the observation point coordinates, (x', y', z') represent the coordinates of the source, R is the distance from any point on the source to the observation point, and path C is along the length of the source. For the problem of Figure 4.1

$$\mathbf{I}_e(x', y', z') = \hat{\mathbf{a}}_z I_0 \tag{4-3a}$$

$$x' = y' = z' = 0 \quad \text{(infinitesimal dipole)} \tag{4-3b}$$

$$R = \sqrt{(x - x')^2 + (y - y')^2 + (z - z')^2} = \sqrt{x^2 + y^2 + z^2}$$
$$= r = \text{constant} \tag{4-3c}$$

$$dl' = dz' \tag{4-3d}$$

so we can write (4-2) as

$$\boxed{\mathbf{A}(x, y, z) = \hat{\mathbf{a}}_z \frac{\mu I_0}{4\pi r} e^{-jkr} \int_{-l/2}^{+l/2} dz' = \hat{\mathbf{a}}_z \frac{\mu I_0 l}{4\pi r} e^{-jkr}} \tag{4-4}$$

The next step of the procedure is to find $\mathbf{H}_A$ using (3-2a) and then $\mathbf{E}_A$ using (3-15) or (3-10) with $\mathbf{J} = 0$. To do this, it is often much simpler to transform (4-4) from rectangular to spherical components and then use (3-2a) and (3-15) or (3-10) in spherical coordinates to find $\mathbf{H}$ and $\mathbf{E}$.

The transformation between rectangular and spherical components is given, in matrix form, by (see Appendix VII)

$$\begin{bmatrix} A_r \\ A_\theta \\ A_\phi \end{bmatrix} = \begin{bmatrix} \sin\theta\cos\phi & \sin\theta\sin\phi & \cos\theta \\ \cos\theta\cos\phi & \cos\theta\sin\phi & -\sin\theta \\ -\sin\phi & \cos\phi & 0 \end{bmatrix} \begin{bmatrix} A_x \\ A_y \\ A_z \end{bmatrix} \tag{4-5}$$

For this problem, $A_x = A_y = 0$, so (4-5) using (4-4) reduces to

$$A_r = A_z \cos\theta = \frac{\mu I_0 l e^{-jkr}}{4\pi r} \cos\theta \tag{4-6a}$$

$$A_\theta = -A_z \sin\theta = -\frac{\mu I_0 l e^{-jkr}}{4\pi r} \sin\theta \tag{4-6b}$$

$$A_\phi = 0 \tag{4-6c}$$

Using the symmetry of the problem (no variations in ϕ), (3-2a) can be expanded in spherical coordinates and written in simplified form as

$$\mathbf{H} = \hat{\mathbf{a}}_\phi \frac{1}{\mu r} \left[\frac{\partial}{\partial r}(rA_\theta) - \frac{\partial A_r}{\partial \theta} \right] \tag{4-7}$$

Substituting (4-6a)–(4-6c) into (4-7) reduces it to

$$\boxed{\begin{aligned} H_r &= H_\theta = 0 \qquad (4\text{-}8a) \\ H_\phi &= j \frac{kI_0 l \sin\theta}{4\pi r} \left[1 + \frac{1}{jkr} \right] e^{-jkr} \qquad (4\text{-}8b) \end{aligned}}$$

The electric field $\mathbf{E}$ can now be found using (3-15) or (3-10) with $\mathbf{J} = 0$. That is,

$$\mathbf{E} = \mathbf{E}_A = -j\omega\mathbf{A} - j\frac{1}{\omega\mu\epsilon} \nabla(\nabla \cdot \mathbf{A}) = \frac{1}{j\omega\epsilon} \nabla \times \mathbf{H} \tag{4-9}$$

Substituting (4-6a)–(4-6c) or (4-8a)–(4-8b) into (4-9) reduces it to

$$\boxed{\begin{aligned} E_r &= \eta \frac{I_0 l \cos\theta}{2\pi r^2} \left[1 + \frac{1}{jkr} \right] e^{-jkr} \qquad (4\text{-}10a) \\ E_\theta &= j\eta \frac{kI_0 l \sin\theta}{4\pi r} \left[1 + \frac{1}{jkr} - \frac{1}{(kr)^2} \right] e^{-jkr} \qquad (4\text{-}10b) \\ E_\phi &= 0 \qquad (4\text{-}10c) \end{aligned}}$$

The **E**- and **H**-field components are valid everywhere, except on the source itself, and they are sketched in Figure 4.1(b) on the surface of a sphere of radius r. It is a straightforward exercise to verify Equations (4-10a)–(4-10c), and this is left as an exercise to the reader (Prob. 4.9).

4.2.2 Power Density and Radiation Resistance

The input impedance of an antenna, which consists of real and imaginary parts, was discussed in Section 2.13. For a lossless antenna, the real part of the input impedance was designated as radiation resistance. It is through the mechanism of the radiation resistance that power is transferred from the guided wave to the free-space wave. To find the input resistance for a lossless antenna, the Poynting vector is formed in terms of the **E**- and **H**-fields radiated by the antenna. By integrating the Poynting vector over a closed surface (usually a sphere of constant radius), the total power radiated by the source is found. The real part of it is related to the input resistance.

For the infinitesimal dipole, the complex Poynting vector can be written using (4-8a)–(4-8b) and (4-10a)–(4-10c) as

$$\begin{aligned}\mathbf{W} &= \tfrac{1}{2}(\mathbf{E} \times \mathbf{H}^*) = \tfrac{1}{2}(\hat{\mathbf{a}}_r E_r + \hat{\mathbf{a}}_\theta E_\theta) \times (\hat{\mathbf{a}}_\phi H_\phi^*) \\ &= \tfrac{1}{2}(\hat{\mathbf{a}}_r E_\theta H_\phi^* - \hat{\mathbf{a}}_\theta E_r H_\phi^*)\end{aligned} \tag{4-11}$$

whose radial W_r and transverse W_θ components are given, respectively, by

$$W_r = \frac{\eta}{8}\left|\frac{I_0 l}{\lambda}\right|^2 \frac{\sin^2\theta}{r^2}\left[1 - j\frac{1}{(kr)^3}\right] \tag{4-12a}$$

$$W_\theta = j\eta\frac{k|I_0 l|^2 \cos\theta \sin\theta}{16\pi^2 r^3}\left[1 + \frac{1}{(kr)^2}\right] \tag{4-12b}$$

The complex power moving in the radial direction is obtained by integrating (4-11)–(4-12b) over a closed sphere of radius r. Thus it can be written as

$$P = \oiint_S \mathbf{W} \cdot d\mathbf{s} = \int_0^{2\pi}\int_0^{\pi} (\hat{\mathbf{a}}_r W_r + \hat{\mathbf{a}}_\theta W_\theta) \cdot \hat{\mathbf{a}}_r r^2 \sin\theta \, d\theta \, d\phi \tag{4-13}$$

which reduces to

$$P = \int_0^{2\pi}\int_0^{\pi} W_r r^2 \sin\theta \, d\theta \, d\phi = \eta\frac{\pi}{3}\left|\frac{I_0 l}{\lambda}\right|^2\left[1 - j\frac{1}{(kr)^3}\right] \tag{4-14}$$

The transverse component W_θ of the power density does not contribute to the integral. Thus (4-14) does not represent the total complex power radiated by the antenna. Since W_θ, as given by (4-12b), is purely imaginary, it will not contribute to any real radiated power. However, it does contribute to the imaginary (reactive) power which along with the second term of (4-14) can be used to determine the total reactive power of the antenna. The reactive power density, which is most dominant for small values of kr, has both radial and transverse components. It merely changes between outward and inward directions to form a standing wave at a rate of twice per cycle. It also moves in the transverse direction as suggested by (4-12b).

Equation (4-13), which gives the real and imaginary power that is moving outwardly, can also be written as [4]

$$P = \frac{1}{2}\iint_S \mathbf{E} \times \mathbf{H}^* \cdot d\mathbf{s} = \eta\left(\frac{\pi}{3}\right)\left|\frac{I_0 l}{\lambda}\right|^2\left[1 - j\frac{1}{(kr)^3}\right]$$

$$= P_{\text{rad}} + j2\omega(\tilde{W}_m - \tilde{W}_e) \tag{4-15}$$

where

P = power (in radial direction)
P_{rad} = time-average power radiated
$\tilde{W}_m$ = time-average magnetic energy density (in radial direction)
$\tilde{W}_e$ = time-average electric energy density (in radial direction)
$2\omega(\tilde{W}_m - \tilde{W}_e)$ = time-average imaginary (reactive) power (in radial direction)

From (4-14)

$$P_{\text{rad}} = \eta\left(\frac{\pi}{3}\right)\left|\frac{I_0 l}{\lambda}\right|^2 \tag{4-16}$$

and

$$2\omega(\tilde{W}_m - \tilde{W}_e) = -\eta\left(\frac{\pi}{3}\right)\left|\frac{I_0 l}{\lambda}\right|^2 \frac{1}{(kr)^3} \tag{4-17}$$

It is clear from (4-17) that the radial electric energy must be larger than the radial magnetic energy. For large values of kr ($kr \gg 1$ or $r \gg \lambda$), the reactive power diminishes and vanishes when $kr = \infty$.

Since the antenna radiates its real power through the radiation resistance, for the infinitesimal dipole it is found by equating (4-16) to

$$\boxed{P_{\text{rad}} = \eta\left(\frac{\pi}{3}\right)\left|\frac{I_0 l}{\lambda}\right|^2 = \frac{1}{2}|I_0|^2 R_r} \tag{4-18}$$

where R_r is the radiation resistance. Equation (4-18) reduces to

$$\boxed{R_r = \eta\left(\frac{2\pi}{3}\right)\left(\frac{l}{\lambda}\right)^2 = 80\pi^2\left(\frac{l}{\lambda}\right)^2} \tag{4-19}$$

for a free-space medium ($\eta \simeq 120\pi$). It should be pointed out that the radiation resistance of (4-19) represents the total radiation resistance since (4-12b) does not contribute to it.

For a wire antenna to be classified as an infinitesimal dipole, its overall length must be very small (usually $l \leq \lambda/50$).

Example 4.1

Find the radiation resistance of an infinitesimal dipole whose overall length is $l = \lambda/50$.

SOLUTION

Using (4-19)

$$R_r = 80\pi^2\left(\frac{l}{\lambda}\right)^2 = 80\pi^2\left(\frac{1}{50}\right)^2 = 0.316 \text{ ohms}$$

Since the radiation resistance of an infinitesimal dipole is about 0.3 ohms, it will present a very large mismatch when connected to practical transmission lines, many of which have characteristic impedances of 50 or 75 ohms. The reflection efficiency (e_r) and hence the overall efficiency (e_t) will be very small.

The reactance of an infinitesimal dipole is capacitive. This can be illustrated by considering the dipole as a flared open-circuited transmission line, as discussed in Section 1.4. Since the input impedance of an open-circuited transmission line a distance $l/2$ from its open end is given by $Z_{in} = -jZ_c \cot(\beta l/2)$, where Z_c is its characteristic impedance, it will always be negative (capacitive) for $l \ll \lambda$.

4.2.3 Radian Distance and Radian Sphere

The **E**- and **H**-fields for the infinitesimal dipole, as represented by (4-8a)–(4-8b) and (4-10a)–(4-10c), are valid everywhere (except on the source itself). An inspection of these equations reveals the following:

(a) At a distance $r = \lambda/2\pi$ (or $kr = 1$), which is referred to as the *radian distance*, the magnitude of the first and second terms within the brackets of (4-8b) and (4-10a) is the same. Also at the radian distance the magnitude of all three terms within the brackets of (4-10b) is identical; the only term that contributes to the total field is the second, because the first and third terms cancel each other. This is illustrated in Figure 4.2.

(b) At distances less than the radian distance $r < \lambda/2\pi$ ($kr < 1$), the magnitude of the second term within the brackets of (4-8b) and (4-10a) is greater than the first term and begins to dominate as $r \ll \lambda/2\pi$. For (4-10b) and $r < \lambda/2\pi$, the magnitude of the third term within the brackets is greater than the magnitude of the first and second terms while the magnitude of the second term is greater than that of the first one; each of these terms begins to dominate as $r \ll \lambda/2\pi$. This is illustrated in Figure 4.2. The region $r < \lambda/2\pi$ ($kr < 1$) is referred to as the *near-field* region.

(c) At distances greater than the radian distance $r > \lambda/2\pi$ ($kr > 1$), the first term within the brackets of (4-8b) and (4-10a) is greater than the magnitude of the second term and begins to dominate as $r \gg \lambda/2\pi (kr \gg 1)$. For (4-10b) and $r > \lambda/2\pi$, the first term within the brackets is greater than the magnitude of the second and third terms while the magnitude of the second term is greater than that of the third; each of these terms begins to dominate as $r \gg \lambda/2\pi$. This is illustrated in Figure 4.2. The region $r > \lambda/2\pi$ ($kr > 1$) is referred to as the *intermediate-field* region while that for $r \gg \lambda/2\pi$ ($kr \gg 1$) is referred to as the *far-field* region.

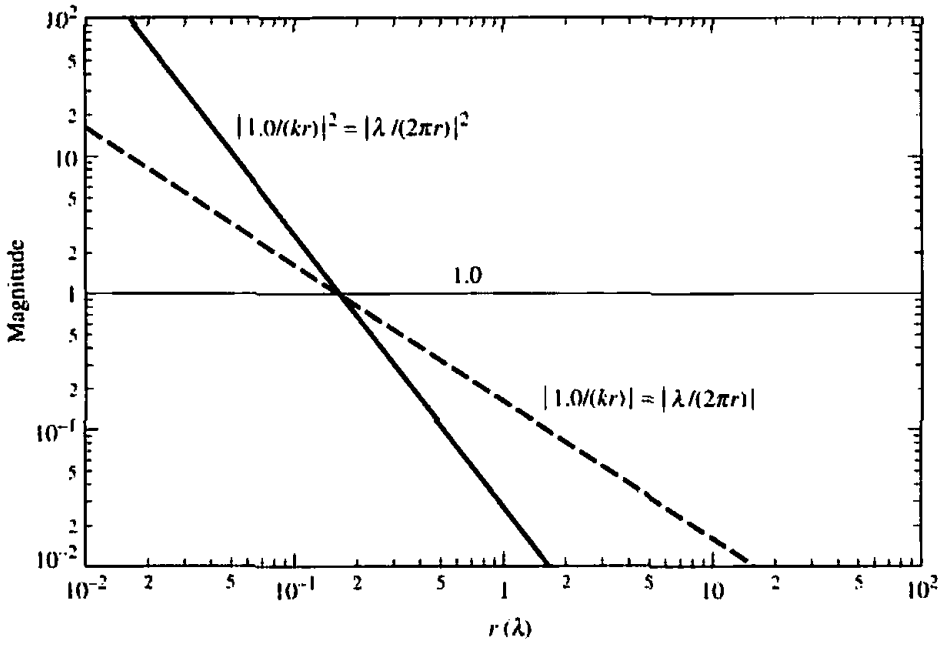

Figure 4.2 Magnitude variation, as a function of the radial distance, of the field terms radiated by an infinitesimal dipole.

(d) The sphere with radius equal to the radian distance ($r = \lambda/2\pi$) is referred as the *radian sphere*, and it defines the region within which the reactive power density is greater than the radiated power density [1]–[3]. For an antenna, the radian sphere represents the volume occupied mainly by the stored energy of the antenna's electric and magnetic fields. Outside the radian sphere the radiated power density is greater than the reactive power density and begins to dominate as $r \gg \lambda/2\pi$. Therefore the radian sphere can be used as a reference, and it defines the transition between stored energy pulsating primarily in the θ direction [represented by (4-12b)] and energy radiating in the radial (r) direction [represented by the first term of (4-12a); the second term represents stored energy pulsating in the radial (r) direction].

4.2.4 Near-Field ($kr \ll 1$) Region

An inspection of (4-8a)–(4-8b) and (4-10a)–(4-10c) reveals that for $kr \ll \lambda$ or $r \ll \lambda/2\pi$ they can be reduced in much simpler form and can be approximated by

$$\left.\begin{aligned} E_r &\simeq -j\eta \frac{I_0 l e^{-jkr}}{2\pi k r^3}\cos\theta && \text{(4-20a)}\\ E_\theta &\simeq -j\eta \frac{I_0 l e^{-jkr}}{4\pi k r^3}\sin\theta && \text{(4-20b)}\\ E_\phi &= H_r = H_\theta = 0 && \text{(4-20c)}\\ H_\phi &\simeq \frac{I_0 l e^{-jkr}}{4\pi r^2}\sin\theta && \text{(4-20d)} \end{aligned}\right\} \quad kr \ll 1$$

The E-field components, E_r and E_θ, are in time-phase but they are in time phase quadrature with the H-field component H_ϕ; therefore there is no time-average power

flow associated with them. This is demonstrated by forming the time-average power density as

$$\mathbf{W}_{av} = \tfrac{1}{2}\mathrm{Re}[\mathbf{E} \times \mathbf{H}^*] = \tfrac{1}{2}\mathrm{Re}[\hat{\mathbf{a}}_r E_\theta H^*_\phi - \hat{\mathbf{a}}_\theta E_r H^*_\phi] \tag{4-21}$$

which by using (4-20a)–(4-20d) reduces to

$$\mathbf{W}_{av} = \frac{1}{2}\mathrm{Re}\left[-\hat{\mathbf{a}}_r j\frac{\eta}{k}\left|\frac{I_0 l}{4\pi}\right|^2 \frac{\sin^2\theta}{r^5} + \hat{\mathbf{a}}_\theta j\frac{\eta}{k}\frac{|I_0 l|^2}{8\pi^2}\frac{\sin\theta\cos\theta}{r^5}\right] = 0 \tag{4-22}$$

The condition of $kr \ll 1$ can be satisfied at moderate distances away from the antenna provided that the frequency of operation is very low. Equations (4-20a) and (4-20b) are similar to those of a static electric dipole and (4-20d) to that of a static current element. Thus we usually refer to (4-20a)–(4-20d) as the *quasistationary fields.*

4.2.5 Intermediate-Field ($kr > 1$) Region

As the values of kr begin to increase and become greater than unity, the terms that were dominant for $kr \ll 1$ become smaller and eventually vanish. For moderate values of kr the E-field components lose their in-phase condition and approach time-phase quadrature. Since their magnitude is not the same, in general, they form a rotating vector whose extremity traces an ellipse. This is analogous to the polarization problem except that the vector rotates in a plane parallel to the direction of propagation and is usually referred to as the *cross field.* At these intermediate values of kr, the E_θ and H_ϕ components approach time-phase, which is an indication of the formation of time-average power flow in the outward (radial) direction (radiation phenomenon).

As the values of kr become moderate ($kr > 1$), the field expressions can be approximated again but in a different form. In contrast to the region where $kr \ll 1$, the first term within the brackets in (4-8b) and (4-10a) becomes more dominant and the second term can be neglected. The same is true for (4-10b) where the second and third terms become less dominant than the first. Thus we can write for $kr > 1$

$$E_r \simeq \eta\frac{I_0 l e^{-jkr}}{2\pi r^2}\cos\theta \tag{4-23a}$$

$$E_\theta \simeq j\eta\frac{kI_0 l e^{-jkr}}{4\pi r}\sin\theta \tag{4-23b}$$

$$E_\phi = H_r = H_\theta = 0 \tag{4-23c}$$

$$H_\phi \simeq j\frac{kI_0 l e^{-jkr}}{4\pi r}\sin\theta \tag{4-23d}$$

$kr > 1$

The total electric field is given by

$$\mathbf{E} = \hat{\mathbf{a}}_r E_r + \hat{\mathbf{a}}_\theta E_\theta \tag{4-24}$$

whose magnitude can be written as

$$|\mathbf{E}| = \sqrt{|E_r|^2 + |E_\theta|^2} \tag{4-25}$$

4.2.6 Far-Field ($kr \gg 1$) Region

Since (4-23a)–(4-23d) are valid only for values of $kr > 1$ ($r > \lambda$), then E_r will be smaller than E_θ because E_r is inversely proportional to r^2 where E_θ is inversely proportional to r. In a region where $kr \gg 1$, (4-23a)–(4-23d) can be simplified and approximated by

$$\left.\begin{aligned} E_\theta &\simeq j\eta \frac{kI_0 le^{-jkr}}{4\pi r} \sin\theta && \text{(4-26a)} \\ E_r \simeq E_\phi &= H_r = H_\theta = 0 && \text{(4-26b)} \\ H_\phi &\simeq j\frac{kI_0 le^{-jkr}}{4\pi r} \sin\theta && \text{(4-26c)} \end{aligned}\right\} \quad kr \gg 1$$

The ratio of E_θ to H_ϕ is equal to

$$Z_w = \frac{E_\theta}{H_\phi} \simeq \eta \tag{4-27}$$

where

Z_w = wave impedance
η = intrinsic impedance (377 $\simeq$ 120π ohms for free-space)

The **E**- and **H**-field components are perpendicular to each other, transverse to the radial direction of propagation, and the r variations are separable from those of θ and ϕ. The shape of the pattern is not a function of the radial distance r, and the fields form a *T*ransverse *E*lectro*M*agnetic (TEM) wave whose wave impedance is equal to the intrinsic impedance of the medium. As it will become even more evident in later chapters, this relationship is applicable in the far-field region of all antennas of finite dimensions. Equations (4-26a)–(4-26c) can also be derived using the procedure outlined and relationships developed in Section 3.6. This is left as an exercise to the reader (Prob. 4.11).

Example 4.2

For an infinitesimal dipole determine and interpret the vector effective length. At what incidence angle does the open-circuit maximum voltage occurs at the output terminals of the dipole if the electric field intensity of the incident wave is 10 mvolts/meter? The length of the dipole is 10 cm.

SOLUTION

Using (4-26a) and the effective length as defined by (2-92), we can write that

$$E_\theta = j\eta \frac{kI_0 le^{-jkr}}{4\pi r} \sin\theta = -\hat{\mathbf{a}}_\theta j\eta \frac{kI_0 e^{-jkr}}{4\pi r} \cdot (-\hat{\mathbf{a}}_\theta l \sin\theta)$$

$$= -\hat{\mathbf{a}}_\theta j\eta \frac{kI_0 e^{-jkr}}{4\pi r} \cdot \ell_e$$

Therefore, the effective length is

$$\ell_e = -\hat{\mathbf{a}}_\theta l \sin\theta$$

whose maximum value occurs when $\theta = 90°$, and it is equal to l. Therefore, to achieve maximum output the wave must be incident upon the dipole at a normal incidence angle ($\theta = 90°$).

The open-circuit maximum voltage is equal to

$$V_{oc}\Big|_{\max} = |\mathbf{E}^i \cdot \ell_e|_{\max} = |\hat{\mathbf{a}}_\theta 10 \times 10^{-3} \cdot (-\hat{\mathbf{a}}_\theta l \sin\theta)|_{\max}$$
$$= 10 \times 10^{-3} l \simeq 10^{-3} \text{ volts}$$

4.2.7 Directivity

The real power P_{rad} radiated by the dipole was found in Section 4.2.2, as given by (4-16). The same expression can be obtained by first forming the average power density, using (4-26a)–(4-26c). That is,

$$\mathbf{W}_{av} = \frac{1}{2}\text{Re}(\mathbf{E} \times \mathbf{H}^*) = \hat{\mathbf{a}}_r \frac{1}{2\eta}|E_\theta|^2 = \hat{\mathbf{a}}_r \frac{\eta}{2}\left|\frac{kI_0 l}{4\pi}\right|^2 \frac{\sin^2\theta}{r^2} \tag{4-28}$$

Integrating (4-28) over a closed sphere of radius r reduces it to (4-16). This is left as an exercise to the reader (Prob. 4.10).

Associated with the average power density of (4-28) is a radiation intensity U which is given by

$$U = r^2 W_{av} = \frac{\eta}{2}\left(\frac{kI_0 l}{4\pi}\right)^2 \sin^2\theta = \frac{r^2}{2\eta}|E_\theta(r, \theta, \phi)|^2 \tag{4-29}$$

and it conforms with (2-12a). The normalized pattern of (4-29) is shown in Figure 4.3. The maximum value occurs at $\theta = \pi/2$ and it is equal to

$$U_{\max} = \frac{\eta}{2}\left(\frac{kI_0 l}{4\pi}\right)^2 \tag{4-30}$$

Using (4-16) and (4-30), the directivity reduces to

$$\boxed{D_0 = 4\pi\frac{U_{\max}}{P_{rad}} = \frac{3}{2}} \tag{4-31}$$

and the maximum effective aperture to

$$\boxed{A_{em} = \left(\frac{\lambda^2}{4\pi}\right)D_0 = \frac{3\lambda^2}{8\pi}} \tag{4-32}$$

The radiation resistance of the dipole can be obtained by the definition of (4-18). Since the radiated power obtained by integrating (4-28) over a closed sphere is the same as that of (4-16), the radiation resistance using it will also be the same as obtained previously and given by (4-19).

Integrating the complex Poynting vector over a closed sphere, as was done in (4-13), results in the power (real and imaginary) directed in the radial direction. Any

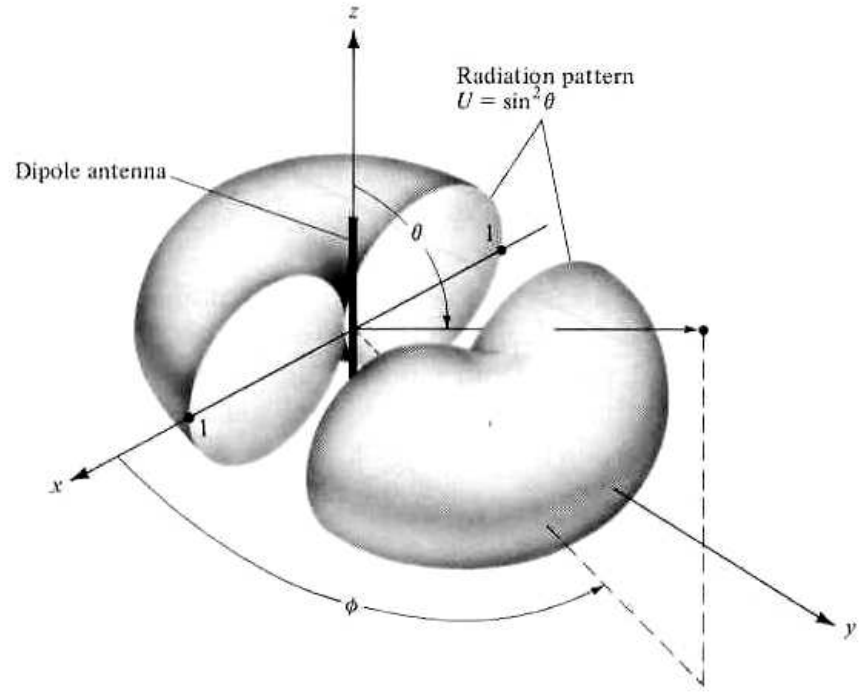

Figure 4.3 Three-dimensional radiation pattern of infinitesimal dipole.

transverse components of power density, as given by (4-12b), will not be captured by the integration even though they are part of the overall power. Because of this limitation, this method cannot be used to derive the input reactance of the antenna.

4.3 SMALL DIPOLE

The creation of the current distribution on a thin wire was discussed in Section 1.4, and it was illustrated with some examples in Figure 1.16. The radiation properties of an infinitesimal dipole, which is usually taken to have a length $l \leq \lambda/50$, were discussed in the previous section. Its current distribution was assumed to be constant. Although a constant current distribution is not realizable (other than top-hat-loaded elements), it is a mathematical quantity that is used to represent actual current distributions of antennas that have been incremented into many small lengths.

A better approximation of the current distribution of wire antennas, whose lengths are usually $\lambda/50 < l \leq \lambda/10$, is the triangular variation of Figure 1.16(a). The sinusoidal variations of Figures 1.16(b)–(c) are more accurate representations of the current distribution of any length wire antenna.

The most convenient geometrical arrangement for the analysis of a dipole is usually to have it positioned symmetrically about the origin with its length directed along the z-axis, as shown in Figure 4.4(a). This is not necessary, but it is usually the most convenient. The current distribution of a small dipole ($\lambda/50 < l \leq \lambda/10$) is shown in Figure 4.4(b), and it is given by

$$\mathbf{I}_e(x', y', z') = \begin{cases} \hat{\mathbf{a}}_z I_0 \left(1 - \dfrac{2}{l} z'\right), & 0 \leq z' \leq l/2 \\ \hat{\mathbf{a}}_z I_0 \left(1 + \dfrac{2}{l} z'\right), & -l/2 \leq z' \leq 0 \end{cases} \tag{4-33}$$

where I_0 = constant.

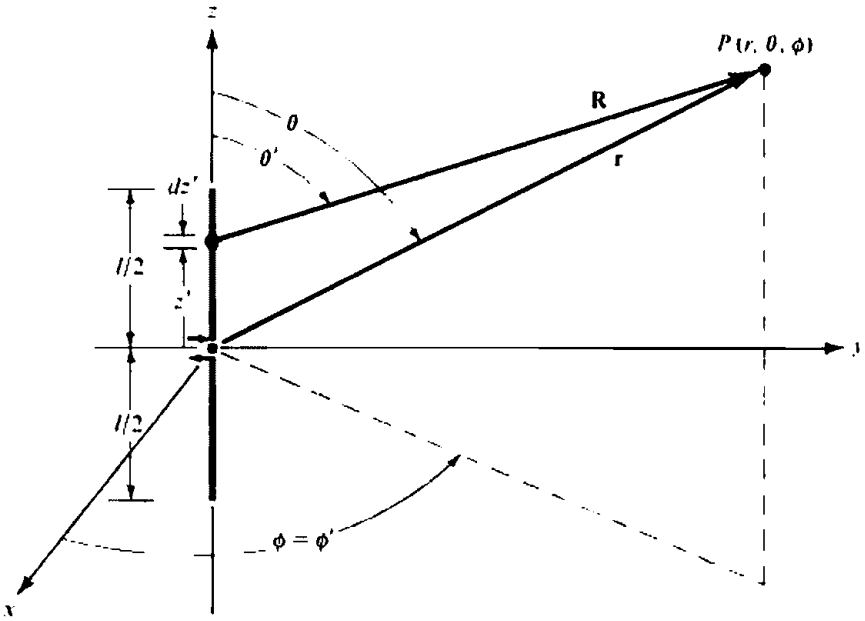

(a) Dipole and geometry

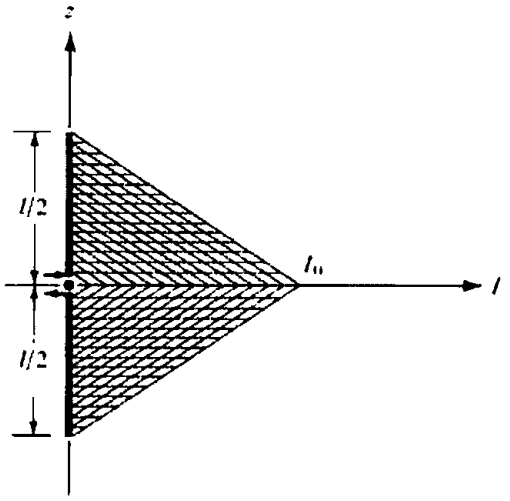

(b) Current distribution

Figure 4.4 Geometrical arrangement of dipole and current distribution.

Following the procedure established in the previous section, the vector potential of (4-2) can be written using (4-33) as

$$\mathbf{A}(x, y, z) = \frac{\mu}{4\pi}\left[\hat{\mathbf{a}}_z \int_{-l/2}^{0} I_0\left(1 + \frac{2}{l}z'\right)\frac{e^{-jkR}}{R}\,dz' + \hat{\mathbf{a}}_z \int_{0}^{l/2} I_0\left(1 - \frac{2}{l}z'\right)\frac{e^{-jkR}}{R}\,dz'\right] \tag{4-34}$$

Because the overall length of the dipole is very small (usually $l \leq \lambda/10$), the values of R for different values of z' along the length of the wire ($-l/2 \leq z' \leq l/2$) are not much different from r. Thus R can be approximated by $R \simeq r$ throughout the integration path. The maximum phase error in (4-34) by allowing $R = r$ for $\lambda/50 < l \leq \lambda/10$, will be $kl/2 = \pi/10$ rad $= 18°$ for $l = \lambda/10$. Smaller values will occur for the other lengths. As it will be shown in the next section, this amount of phase error

is usually considered negligible and has very little effect on the overall radiation characteristics. Performing the integration, (4-34) reduces to

$$\mathbf{A} = \hat{\mathbf{a}}_z A_z = \hat{\mathbf{a}}_z \frac{1}{2}\left[\frac{\mu I_0 l e^{-jkr}}{4\pi r}\right] \tag{4-35}$$

which is one-half of that obtained in the previous section for the infinitesimal dipole and given by (4-4).

The potential function given by (4-35) becomes a more accurate approximation as $kr \to \infty$. This is also the region of most practical interest, and it has been designated as the *far-field* region. Since the potential function for the triangular distribution is one-half of the corresponding one for the constant (uniform) current distribution, the corresponding fields of the former are one-half of the latter. Thus we can write the **E**- and **H**-fields radiated by a small dipole as

$$E_\theta \simeq j\eta \frac{kI_0 l e^{-jkr}}{8\pi r} \sin\theta \tag{4-36a}$$

$$E_r \simeq E_\phi = H_r = H_\theta = 0 \qquad kr \gg 1 \tag{4-36b}$$

$$H_\phi \simeq j \frac{kI_0 l e^{-jkr}}{8\pi r} \sin\theta \tag{4-36c}$$

with the wave impedance equal, as before, to (4-27).

Since the directivity of an antenna is controlled by the relative shape of the field or power pattern, the directivity and maximum effective area of this antenna are the same as the ones with the constant current distribution given by (4-31) and (4-32), respectively.

The radiation resistance of the antenna is strongly dependent upon the current distribution. Using the procedure established for the infinitesimal dipole, it can be shown that for the small dipole its radiated power is one-fourth ($\frac{1}{4}$) of (4-18). Thus the radiation resistance reduces to

$$\boxed{R_r = \frac{2P_{\text{rad}}}{|I_0|^2} = 20\pi^2\left(\frac{l}{\lambda}\right)^2} \tag{4-37}$$

which is also one-fourth ($\frac{1}{4}$) of that obtained for the infinitesimal dipole as given by (4-19). Their relative patterns (shapes) are the same and are shown in Figure 4.3.

4.4 REGION SEPARATION

Before we attempt to solve for the fields radiated by a finite dipole of any length, it would be very desirable to discuss the separation of the space surrounding an antenna into three regions; namely, the *reactive near-field, radiating near-field (Fresnel)* and the *far-field (Fraunhofer)* which were introduced briefly in Section 2.2. This is necessary because for a dipole antenna of any length and any current distribution, it will become increasingly difficult to solve for the fields everywhere. Approximations can be made, especially for the far-field (Fraunhofer) region which is usually the one of most practical interest, to simplify the formulation to yield closed form solutions. The same approximations used to simplify the formulation of the fields radiated by a finite

dipole are also used to formulate the fields radiated by most practical antennas. So it will be very important to introduce them properly and understand their implications upon the solution.

The difficulties in obtaining closed form solutions that are valid everywhere for any practical antenna stem from the inability to perform the integration of

$$\mathbf{A}(x, y, z) = \frac{\mu}{4\pi} \int_C \mathbf{I}_e(x', y', z') \frac{e^{-jkR}}{R} dl' \tag{4-38}$$

where

$$R = \sqrt{(x - x')^2 + (y - y')^2 + (z - z')^2} \tag{4-38a}$$

For a finite dipole with sinusoidal current distribution, the integral of (4-38) can be reduced to a closed form that is valid everywhere! This will be shown in Chapter 8. The length R is defined as the distance from any point on the source to the observation point. The integral of (4-38) was used to solve for the fields of infinitesimal and small dipoles in Sections 4.1 and 4.2. However in the first case (infinitesimal dipole) $R = r$ and in the second case (small dipole) R was approximated by r ($R \simeq r$) because the length of the dipole was restricted to be $l \leq \lambda/10$. The major simplification of (4-38) will be in the approximation of R.

A very thin dipole of finite length l is symmetrically positioned about the origin with its length directed along the z-axis, as shown in Figure 4.5(a). Because the wire is assumed to be very thin ($x' = y' = 0$), we can write (4-38) as

$$R = \sqrt{(x - x')^2 + (y - y')^2 + (z - z')^2} = \sqrt{x^2 + y^2 + (z - z')^2} \tag{4-39}$$

which when expanded can be written as

$$R = \sqrt{(x^2 + y^2 + z^2) + (-2zz' + z'^2)} = \sqrt{r^2 + (-2rz' \cos\theta + z'^2)} \tag{4-40}$$

where

$$r^2 = x^2 + y^2 + z^2 \tag{4-40a}$$

$$z = r\cos\theta \tag{4-40b}$$

Using the binomial expansion, we can write (4-40) in a series

$$R = r - z'\cos\theta + \frac{1}{r}\left(\frac{z'^2}{2}\sin^2\theta\right) + \frac{1}{r^2}\left(\frac{z'^3}{2}\cos\theta\sin^2\theta\right) + \cdots \tag{4-41}$$

whose higher order terms become less significant provided $r \gg z'$.

4.4.1 Far-Field (Fraunhofer) Region

The most convenient simplification of (4-41), other than $R \simeq r$, will be to approximate it by its first two terms, or

$$R \simeq r - z'\cos\theta \tag{4-42}$$

The most significant neglected term of (4-41) is the third whose maximum value is

$$\frac{1}{r}\left(\frac{z'^2}{2}\sin^2\theta\right)_{\max} = \frac{z'^2}{2r} \qquad \text{when } \theta = \pi/2 \tag{4-43}$$

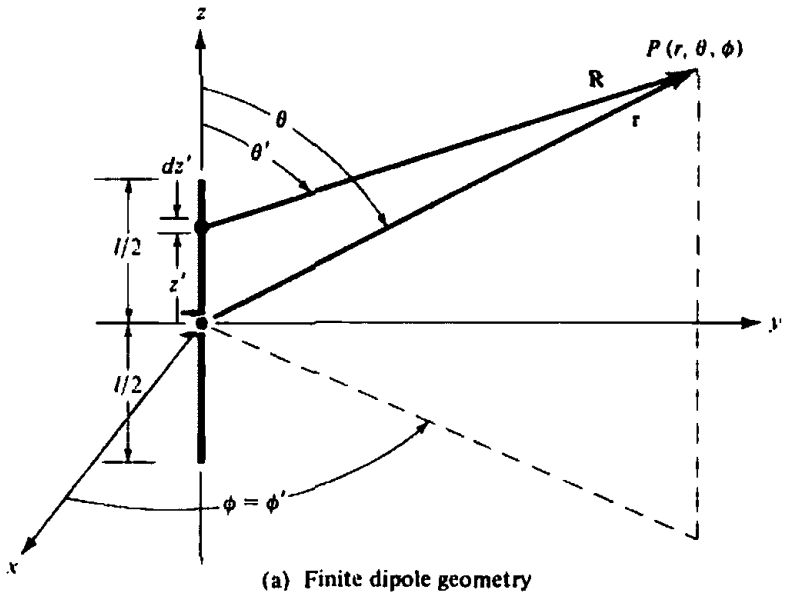

(a) Finite dipole geometry

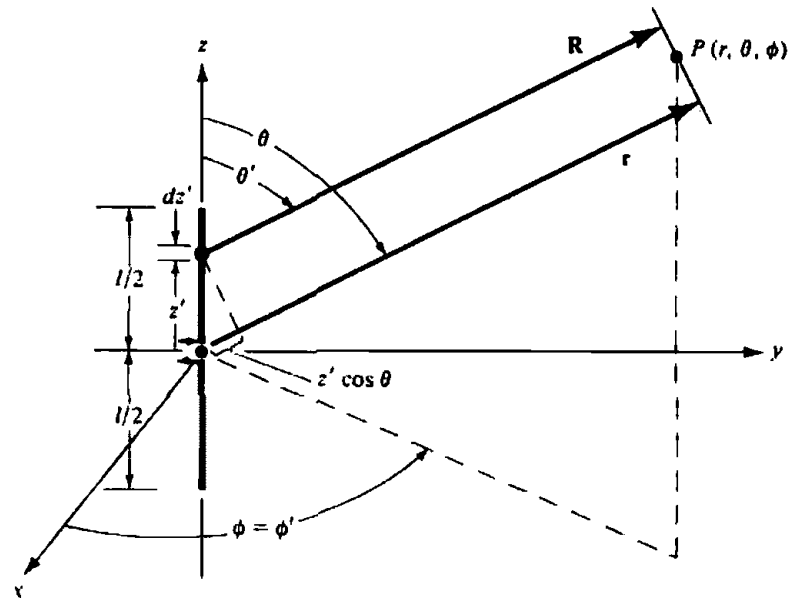

(b) Geometrical arrangement for far-field approximations

Figure 4.5 Finite dipole geometry and far-field approximations.

When (4-43) attains its maximum value, the fourth term of (4-41) vanishes because $\theta = \pi/2$. It can be shown that the higher order terms not shown in (4-41) also vanish. Therefore approximating (4-41) by (4-42) introduces a *maximum* error given by (4-43).

It has been shown by many investigators through numerous examples that for most practical antennas, *with overall lengths greater than a wavelength* ($l > \lambda$), a maximum total phase error of $\pi/8$ rad (22.5°) is not very detrimental in their analytical formulation. Using that as a criterion we can write, using (4-43), that the maximum phase error should always be

$$\frac{k(z')^2}{2r} \leq \frac{\pi}{8} \tag{4-44}$$

which for $-l/2 \leq z' \leq l/2$ reduces to

$$r \geq 2\left(\frac{l^2}{\lambda}\right) \tag{4-45}$$

Equation (4-45) simply states that to maintain the maximum phase error of an antenna equal to or less than $\pi/8$ rad (22.5°), the observation distance r must equal or be greater than $2l^2/\lambda$ where l is the largest* dimension of the antenna structure. The usual simplification for the far-field region is to approximate the R in the exponential (e^{-jkR}) of (4-38) by (4-42) and the R in the denominator of (4-38) by $R \simeq r$. These simplifications are designated as the far-field approximations and are usually denoted in the literature as

Far-field Approximations

$$\begin{aligned} R &\simeq r - z' \cos\theta \quad && \text{for phase terms} \\ R &\simeq r && \text{for amplitude terms} \end{aligned} \tag{4-46}$$

provided r satisfies (4-45).

It may be advisable to illustrate the approximation (4-46) geometrically. For $R \simeq r - z' \cos\theta$, where θ is the angle measured from the z-axis, the radial vectors $\mathbf{R}$ and $\mathbf{r}$ must be parallel to each other, as shown in Figure 4.5(b). For any other antenna whose maximum dimension is D, the approximation of (4-46) is valid provided the observations are made at a distance

$$r \geq 2D^2/\lambda \tag{4-47}$$

For an aperture antenna the maximum dimension is taken to be its diagonal.

For most practical antennas, whose overall length is large compared to the wavelength, these are adequate approximations which have been shown by many investigators through numerous examples to give valid results in pattern predictions. Some discrepancies are evident in regions of low intensity (usually below -25 dB). This is illustrated in Figure 2.6 where the patterns of a paraboloidal antenna for $R = \infty$ and $R = 2D^2/\lambda$ differ at levels below -25 dB. Allowing R to have a value of $R = 4D^2/\lambda$ gives better results.

It would seem that the approximation of R in (4-46) for the amplitude is more severe than that for the phase. However a close observation reveals this is not the case. Since the observations are made at a distance where r is very large, any small error in the approximation of the denominator (amplitude) will not make much difference in the answer. However, because of the periodic nature of the phase (repeats every 2π rad), it can be a major fraction of a period. The best way to illustrate it will be to consider an example.

Example 4.3

For an antenna with an overall length $l = 5\lambda$, the observations are made at $r = 60\lambda$. Find the errors in phase and amplitude using (4-46).

*Provided the overall length (l) of the antenna is large compared to the wavelength [see IEEE Standard Definitions of Terms for Antennas, IEEE Std (145-1983)].

SOLUTION

For $\theta = 90°$, $z' = 2.5\lambda$, and $r = 60\lambda$, (4-40) reduces to

$$R_1 = \lambda\sqrt{(60)^2 + (2.5)^2} = 60.052\lambda$$

and (4-46) to

$$R_2 = r = 60\lambda$$

Therefore the phase difference is

$$\Delta\phi = k\Delta R = \frac{2\pi}{\lambda}(R_1 - R_2) = 2\pi(0.052) = 0.327 \text{ rad} = 18.74°$$

which in an appreciable fraction ($\simeq \frac{1}{20}$) of a full period (360°).

The difference of the inverse values of R is

$$\frac{1}{R_2} - \frac{1}{R_1} = \frac{1}{\lambda}\left(\frac{1}{60} - \frac{1}{60.052}\right) = \frac{1.44 \times 10^{-5}}{\lambda}$$

which should always be a very small value.

4.4.2 Radiating Near-Field (Fresnel) Region

If the observation point is chosen to be smaller than $r = 2l^2/\lambda$, the maximum phase error by the approximation of (4-46) is greater than $\pi/8$ rad (22.5°) which may be undesirable in many applications. If it is necessary to choose observation distances smaller than (4-45), another term (the third) in the series solution of (4-41) must be retained to maintain a maximum phase error of $\pi/8$ rad (22.5°). Doing this, the infinite series of (4-41) can be approximated by

$$R \simeq r - z' \cos\theta + \frac{1}{r}\left(\frac{z'^2}{2}\sin^2\theta\right) \tag{4-48}$$

The most significant term that we are neglecting from the infinite series of (4-41) is the fourth. To find the maximum phase error introduced by the omission of the next most significant term, the angle θ at which this occurs must be found. To do this, the neglected term is differentiated with respect to θ and the result is set equal to zero. Thus

$$\frac{\partial}{\partial\theta}\left[\frac{1}{r^2}\left(\frac{z'^3}{2}\cos\theta\sin^2\theta\right)\right] = \frac{z'^3}{2r^2}\sin\theta[-\sin^2\theta + 2\cos^2\theta] = 0 \tag{4-49}$$

The angle $\theta = 0$ is not chosen as a solution because for that value the fourth term is equal to zero. In other words, $\theta = 0$ gives the minimum error. The maximum error occurs when the second term of (4-49) vanishes; that is when

$$[-\sin^2\theta + 2\cos^2\theta]_{\theta=\theta_1} = 0 \tag{4-50}$$

or

$$\theta_1 = \tan^{-1}(\pm\sqrt{2}) \tag{4-50a}$$

If the maximum phase error is allowed to be equal or less than $\pi/8$ rad, the distance r at which this occurs can be found from

$$\frac{kz'^3}{2r^2}\cos\theta\sin^2\theta\Big|_{\substack{z'=l/2\\ \theta=\tan^{-1}\sqrt{2}}} = \frac{\pi}{\lambda}\frac{l^3}{8r^2}\left(\frac{1}{\sqrt{3}}\right)\left(\frac{2}{3}\right) = \frac{\pi}{12\sqrt{3}}\left(\frac{l^3}{\lambda r^2}\right) \le \frac{\pi}{8} \tag{4-51}$$

which reduces to

$$r^2 \ge \frac{2}{3\sqrt{3}}\left(\frac{l^3}{\lambda}\right) = 0.385\left(\frac{l^3}{\lambda}\right) \tag{4-52}$$

or

$$r \ge 0.62\sqrt{l^3/\lambda} \tag{4-52a}$$

A value of r greater than that of (4-52a) will lead to an error less than $\pi/8$ rad (22.5°). Thus the region where the first three terms of (4-41) are significant, and the omission of the fourth introduces a maximum phase error of $\pi/8$ rad (22.5°), is defined by

$$2l^2/\lambda > r \ge 0.62\sqrt{l^3/\lambda} \tag{4-53}$$

where l is the length of the antenna. This region is designated as *radiating near-field* because the radiating power density is greater than the reactive power density and the field pattern (its shape) is a function of the radial distance r. This region is also called the *Fresnel region* because the field expressions in this region reduce to Fresnel integrals.

The discussion has centered around the finite length antenna of length l with the observation considered to be a point source. If the antenna is not a line source, l in (4-53) must represent the largest dimension of the antenna (which for an aperture is the diagonal). Also if the transmitting antenna has maximum length l_t and the receiving antenna has maximum length l_r, then the *sum of* l_t *and* l_r must be used in place of l in (4-53).

The boundaries for separating the far-field (Fraunhofer), the radiating near-field (Fresnel), and the reactive near-field regions are not very rigid. Other criteria have also been established [4] but the ones introduced here are the most "popular." Also the fields, as the boundaries from one region to the other are crossed, do not change abruptly but undergo a very gradual transition.

4.4.3 Reactive Near-Field Region

If the distance of observation is smaller than the inner boundary of the Fresnel region, this region is usually designated as *reactive near-field* with inner and outer boundaries defined by

$$0.62\sqrt{l^3/\lambda} > r > 0 \tag{4-54}$$

where l is the length of the antenna. In this region the reactive power density predominates, as was demonstrated in Section 4.1 for the infinitesimal dipole.

In summary, the space surrounding an antenna is divided into three regions whose boundaries are determined by

$$\boxed{\begin{array}{ll} \text{reactive near-field } [0.62\sqrt{D^3/\lambda} > r > 0] & \text{(4-55a)} \\ \text{radiating near-field (Fresnel) } [2D^2/\lambda > r \geq 0.62\sqrt{D^3/\lambda}] & \text{(4-55b)} \\ \text{far-field (Fraunhofer) } [\infty \geq r \geq 2D^2/\lambda] & \text{(4-55c)} \end{array}}$$

where D is the largest dimension of the antenna ($D = l$ for a wire antenna).

4.5 FINITE LENGTH DIPOLE

The techniques that were developed previously can also be used to analyze the radiation characteristics of a linear dipole of any length. To reduce the mathematical complexities, it will be assumed in this chapter that the dipole has a negligible diameter (ideally zero). This is a good approximation provided the diameter is considerably smaller than the operating wavelength. Finite radii dipoles will be analyzed in Chapters 8 and 9.

4.5.1 Current Distribution

For a very thin dipole (ideally zero diameter), the current distribution can be written, to a good approximation, as

$$\mathbf{I}_e(x' = 0, y' = 0, z') = \begin{cases} \hat{\mathbf{a}}_z I_0 \sin\left[k\left(\frac{l}{2} - z'\right)\right], & 0 \leq z' \leq l/2 \\ \hat{\mathbf{a}}_z I_0 \sin\left[k\left(\frac{l}{2} + z'\right)\right], & -l/2 \leq z' \leq 0 \end{cases} \tag{4-56}$$

This distribution assumes that the antenna is *center-fed and the current vanishes at the end points* ($z' = \pm l/2$). Experimentally it has been verified that the current in a center-fed wire antenna has sinusoidal form with nulls at the end points. For $l = \lambda/2$ and $\lambda/2 < l < \lambda$ the current distribution of (4-56) is shown plotted in Figures 1.16(b) and 1.12(c), respectively. The geometry of the antenna is that shown in Figure 4.5.

4.5.2 Radiated Fields: Element Factor, Space Factor, and Pattern Multiplication

For the current distribution of (4-56) it will be shown in Chapter 8 that closed form expressions for the **E**- and **H**-fields can be obtained which are valid in all regions (any observation point except on the source itself). In general, however, this is not the case. Usually we are limited to the far-field region, because of the mathematical complications provided in the integration of the vector potential **A** of (4-2). Since closed form solutions, which are valid everywhere, cannot be obtained for many antennas, the observations will be restricted to the far-field region. This will be done first in order to illustrate the procedure. In some cases, even in that region it may become impossible to obtain closed form solutions.

The finite dipole antenna of Figure 4.5 is subdivided into a number of infinitesimal

dipoles of length $\Delta z'$. As the number of subdivisions is increased, each infinitesimal dipole approaches a length dz'. For an infinitesimal dipole of length dz' positioned along the z-axis at z', the electric and magnetic field components in the far-field are given, using (4-26a)–(4-26c), as

$$dE_\theta \simeq j\eta \frac{kI_e(x', y', z')e^{-jkR}}{4\pi R} \sin\theta\, dz' \tag{4-57a}$$

$$dE_r \simeq dE_\phi = dH_r = dH_\theta = 0 \tag{4-57b}$$

$$dH_\phi \simeq j \frac{kI_e(x', y', z')e^{-jkR}}{4\pi R} \sin\theta\, dz' \tag{4-57c}$$

where R is given by (4-39) or (4-40).

Using the far-field approximations given by (4-46), (4-57a) can be written as

$$dE_\theta \simeq j\eta \frac{kI_e(x', y', z')e^{-jkr}}{4\pi r} \sin\theta e^{+jkz'\cos\theta} dz' \tag{4-58}$$

Summing the contributions from all the infinitesimal elements, the summation reduces, in the limit, to an integration. Thus

$$\boxed{E_\theta = \int_{-l/2}^{+l/2} dE_\theta = j\eta \frac{ke^{-jkr}}{4\pi r} \sin\theta \left[\int_{-l/2}^{+l/2} I_e(x', y', z') e^{jkz'\cos\theta} dz' \right]} \tag{4-58a}$$

The factor outside the brackets is designated as the *element factor* and that within the brackets as the *space factor*. For this antenna, the element factor is equal to the field of a unit length infinitesimal dipole located at a reference point (the origin). In general, the element factor depends on the type of current and its direction of flow while the space factor is a function of the current distribution along the source.

The total field of the antenna is equal to the product of the element and space factors. This is referred to as *pattern multiplication* for continuously distributed sources, and it can be written as

$$\boxed{\text{total field} = (\text{element factor}) \times (\text{space factor})} \tag{4-59}$$

The pattern multiplication for continuous sources is analogous to the pattern multiplication of (6-5) for discrete-element antennas (arrays).

For the current distribution of (4-56), (4-58a) can be written as

$$E_\theta \simeq j\eta \frac{kI_0 e^{-jkr}}{4\pi r} \sin\theta \left\{ \int_{-l/2}^{0} \sin\left[k\left(\frac{l}{2} + z'\right)\right] e^{+jkz'\cos\theta} dz' + \int_{0}^{+l/2} \sin\left[k\left(\frac{l}{2} - z'\right)\right] e^{+jkz'\cos\theta} dz' \right\} \tag{4-60}$$

Each one of the integrals in (4-60) can be integrated using

$$\int e^{\alpha x} \sin(\beta x + \gamma)\, dx = \frac{e^{\alpha x}}{\alpha^2 + \beta^2} [\alpha \sin(\beta x + \gamma) - \beta \cos(\beta x + \gamma)] \tag{4-61}$$

where

$$\alpha = \pm jk \cos\theta \tag{4-61a}$$

$$\beta = \pm k \tag{4-61b}$$

$$\gamma = kl/2 \tag{4-61c}$$

After some mathematical manipulations, (4-60) takes the form of

$$\boxed{E_\theta \simeq j\eta \frac{I_0 e^{-jkr}}{2\pi r}\left[\frac{\cos\left(\frac{kl}{2}\cos\theta\right) - \cos\left(\frac{kl}{2}\right)}{\sin\theta}\right]} \tag{4-62a}$$

In a similar manner, or by using the established relationship between the E_θ and H_ϕ in the far-field as given by (3-58b) or (4-27), the total H_ϕ component can be written as

$$\boxed{H_\phi \simeq \frac{E_\theta}{\eta} \simeq j\frac{I_0 e^{-jkr}}{2\pi r}\left[\frac{\cos\left(\frac{kl}{2}\cos\theta\right) - \cos\left(\frac{kl}{2}\right)}{\sin\theta}\right]} \tag{4-62b}$$

4.5.3 Power Density, Radiation Intensity, and Radiation Resistance

For the dipole, the average Poynting vector can be written as

$$\mathbf{W}_{av} = \frac{1}{2}\text{Re}[\mathbf{E} \times \mathbf{H}^*] = \frac{1}{2}\text{Re}[\hat{\mathbf{a}}_\theta E_\theta \times \hat{\mathbf{a}}_\phi H_\phi^*] = \frac{1}{2}\text{Re}\left[\hat{\mathbf{a}}_\theta E_\theta \times \hat{\mathbf{a}}_\phi \frac{E_\theta^*}{\eta}\right]$$

$$\mathbf{W}_{av} = \hat{\mathbf{a}}_r W_{av} = \hat{\mathbf{a}}_r \frac{1}{2\eta}|E_\theta|^2 = \eta\frac{|I_0|^2}{8\pi^2 r^2}\left[\frac{\cos\left(\frac{kl}{2}\cos\theta\right) - \cos\left(\frac{kl}{2}\right)}{\sin\theta}\right]^2 \tag{4-63}$$

and the radiation intensity as

$$U = r^2 W_{av} = \eta\frac{|I_0|^2}{8\pi^2}\left[\frac{\cos\left(\frac{kl}{2}\cos\theta\right) - \cos\left(\frac{kl}{2}\right)}{\sin\theta}\right]^2 \tag{4-64}$$

The normalized (to 0 dB) elevation power patterns, as given by (4-64) for $l = \lambda/4$, $\lambda/2$, $3\lambda/4$, and λ are shown plotted in Figure 4.6. The current distribution of each is given by (4-56). The power patterns for an infinitesimal dipole $l \ll \lambda$ ($U \sim \sin^2\theta$) is also included for comparison. As the length of the antenna increases, the beam becomes narrower. Because of that, the directivity should also increase with length. It is found that the 3-dB beamwidth of each is equal to

$$\begin{aligned}
&l \ll \lambda && \text{3-db beamwidth} = 90^\circ \\
&l = \lambda/4 && \text{3-dB beamwidth} = 87^\circ \\
&l = \lambda/2 && \text{3-dB beamwidth} = 78^\circ \\
&l = 3\lambda/4 && \text{3-dB beamwidth} = 64^\circ \\
&l = \lambda && \text{3-dB beamwidth} = 47.8^\circ
\end{aligned} \tag{4-65}$$

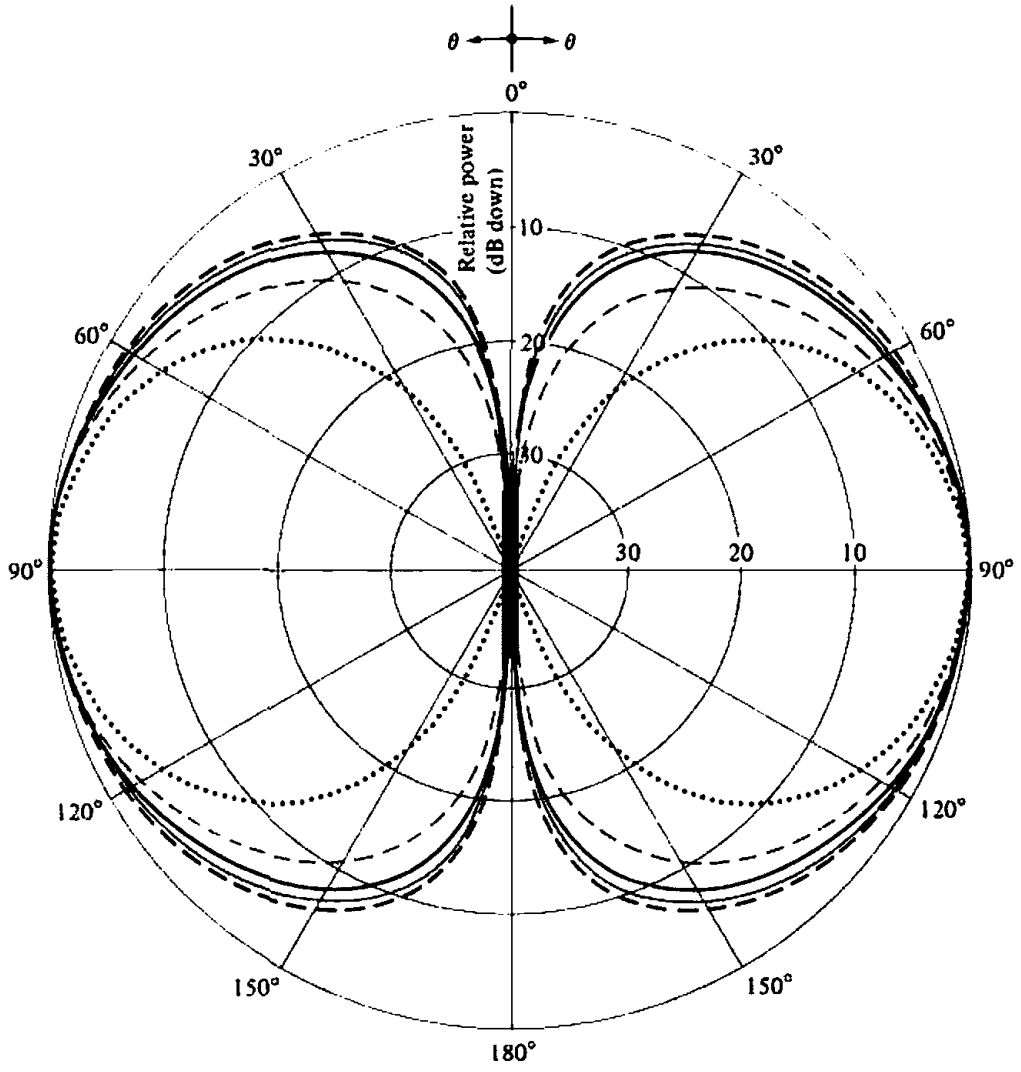

Figure 4.6 *Elevation plane amplitude patterns for a thin dipole with sinusoidal current distribution ($l = \lambda/4, \lambda/2, 3\lambda/4, \lambda$).*

As the length of the dipole increases beyond one wavelength ($l > \lambda$), the number of lobes begin to increase. The normalized power pattern for a dipole with $l = 1.25\lambda$ is shown in Figure 4.7. In Figure 4.7(a) the three-dimensional pattern is illustrated using the software from [5], while in Figure 4.7(b) the two-dimensional (elevation pattern) is depicted. For the three-dimensional illustration a 90° angular section of the pattern has been omitted to illustrate the elevation plane directional pattern variations. The current distribution for the dipoles with $l = \lambda/4, \lambda/2, \lambda, 3\lambda/2$, and 2λ, as given by (4-56), is shown in Figure 4.8.

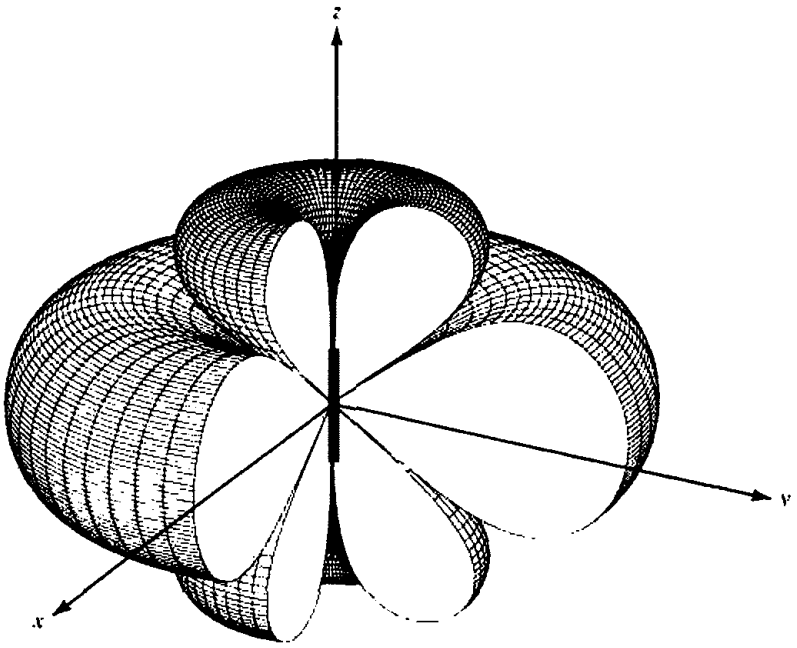

(a) Three-dimensional

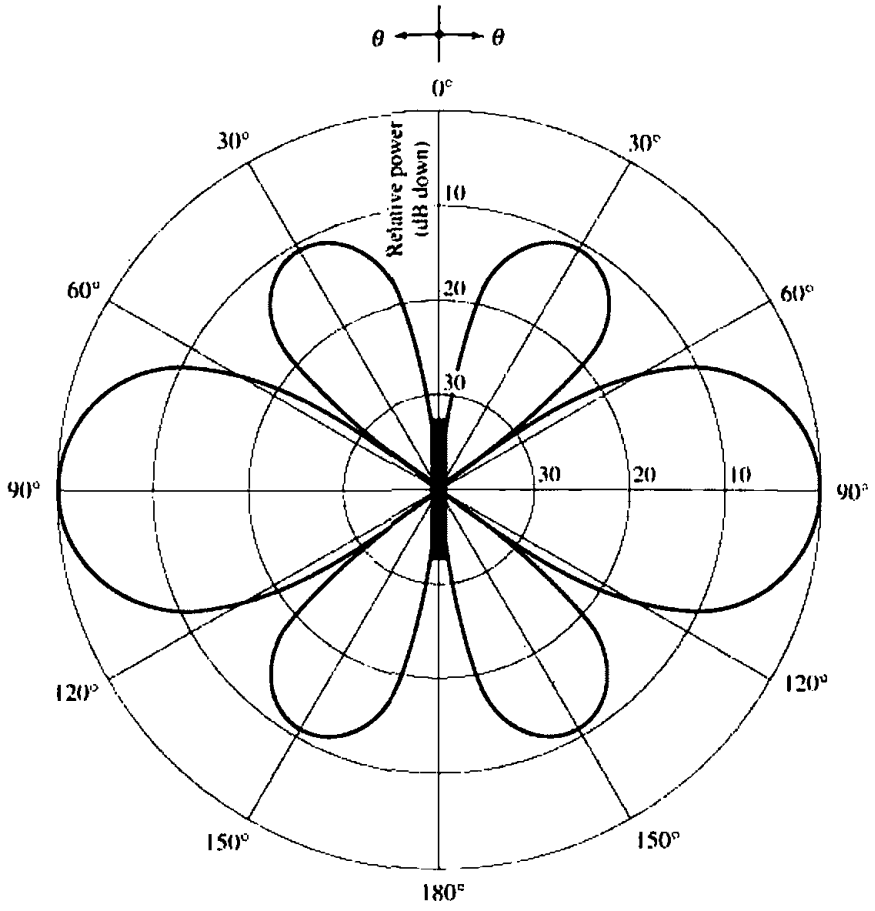

(b) Two-dimensional

Figure 4.7 Three- and two-dimensional amplitude patterns for a thin dipole of $l = 1.25\lambda$ and sinusoidal current distribution.

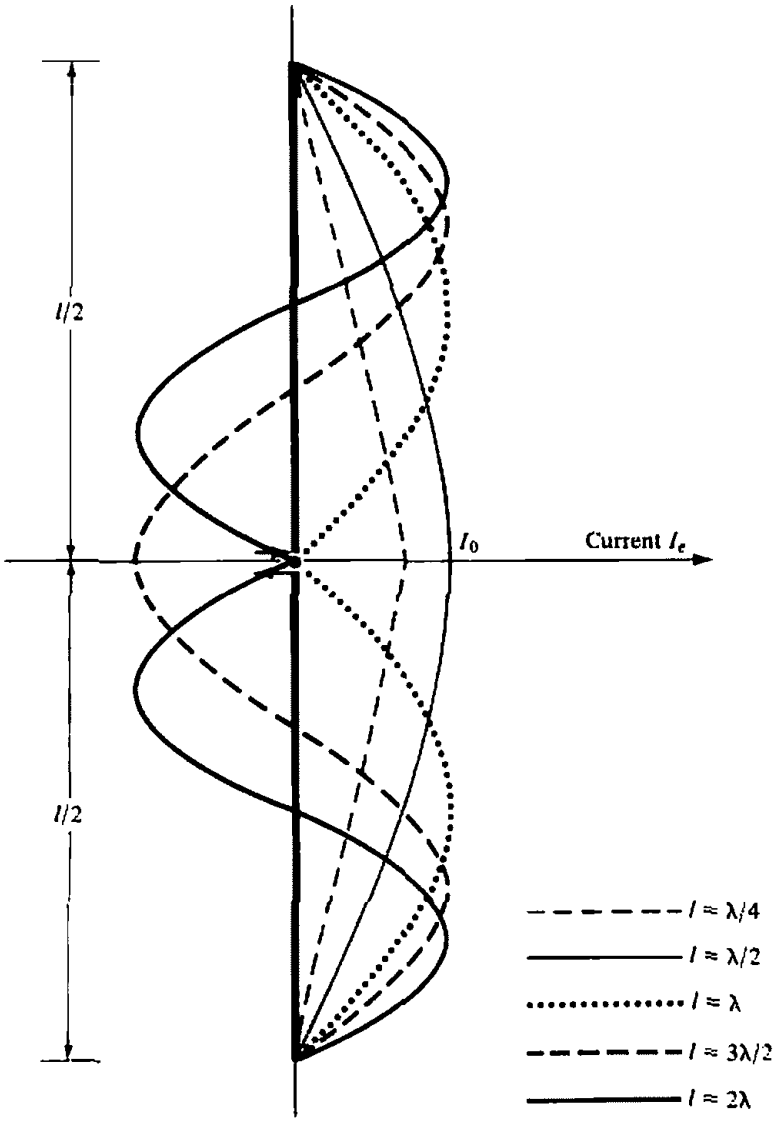

Figure 4.8 Current distributions along the length of a linear wire antenna.

To find the total power radiated, the average Poynting vector of (4-63) is integrated over a sphere of radius r. Thus

$$P_{\text{rad}} = \oiint_S \mathbf{W}_{\text{av}} \cdot d\mathbf{s} = \int_0^{2\pi} \int_0^{\pi} \hat{\mathbf{a}}_r W_{\text{av}} \cdot \hat{\mathbf{a}}_r r^2 \sin\theta \, d\theta \, d\phi$$

$$= \int_0^{2\pi} \int_0^{\pi} W_{\text{av}} r^2 \sin\theta \, d\theta \, d\phi \tag{4-66}$$

Using (4-63), we can write (4-66) as

$$P_{\text{rad}} = \int_0^{2\pi} \int_0^{\pi} W_{\text{av}} r^2 \sin\theta \, d\theta \, d\phi$$

$$= \eta \frac{|I_0|^2}{4\pi} \int_0^{\pi} \frac{\left[\cos\left(\frac{kl}{2}\cos\theta\right) - \cos\left(\frac{kl}{2}\right)\right]^2}{\sin\theta} d\theta \tag{4-67}$$

After some extensive mathematical manipulations, it can be shown that (4-67) reduces to

$$P_{\text{rad}} = \eta\frac{|I_0|^2}{4\pi}\{C + \ln(kl) - C_i(kl) + \tfrac{1}{2}\sin(kl)[S_i(2kl) - 2S_i(kl)] + \tfrac{1}{2}\cos(kl)[C + \ln(kl/2) + C_i(2kl) - 2C_i(kl)]\} \tag{4-68}$$

where $C = 0.5772$ (Euler's constant) and $C_i(x)$ and $S_i(x)$ are the cosine and sine integrals (see Appendix III) given by

$$C_i(x) = -\int_x^\infty \frac{\cos y}{y}dy = \int_\infty^x \frac{\cos y}{y}dy \tag{4-68a}$$

$$S_i(x) = \int_0^x \frac{\sin y}{y}dy \tag{4-68b}$$

The derivation of (4-68) from (4-67) is assigned as a problem at the end of the chapter (Prob. 4.17). $C_i(x)$ is related to $C_{in}(x)$ by

$$C_{in}(x) = \ln(\gamma x) - C_i(x) = \ln(\gamma) + \ln(x) - C_i(x) = 0.5772 + \ln(x) - C_i(x) \tag{4-69}$$

where

$$C_{in}(x) = \int_0^x \left(\frac{1 - \cos y}{y}\right)dy \tag{4-69a}$$

$C_i(x)$, $S_i(x)$ and $C_{in}(x)$ are tabulated in Appendix III.

The radiation resistance can be obtained using (4-18) and (4-68) and can be written as

$$R_r = \frac{2P_{\text{rad}}}{|I_0|^2} = \frac{\eta}{2\pi}\{C + \ln(kl) - C_i(kl) + \tfrac{1}{2}\sin(kl) \times |S_i(2kl) - 2S_i(kl)| + \tfrac{1}{2}\cos(kl) \times [C + \ln(kl/2) + C_i(2kl) - 2C_i(kl)]\} \tag{4-70}$$

Shown in Figure 4.9 is a plot of R_r as a function of l (in wavelengths) when the antenna is radiating into free-space ($\eta \simeq 120\pi$).

4.5.4 Directivity

As was illustrated in Figure 4.6, the radiation pattern of a dipole becomes more directional as its length increases. When the overall length is greater than about one wavelength, the number of lobes increases and the antenna loses its directional properties. The parameter that is used as a "figure-of-merit" for the directional properties of the antenna is the directivity which was defined in Section 2.5.

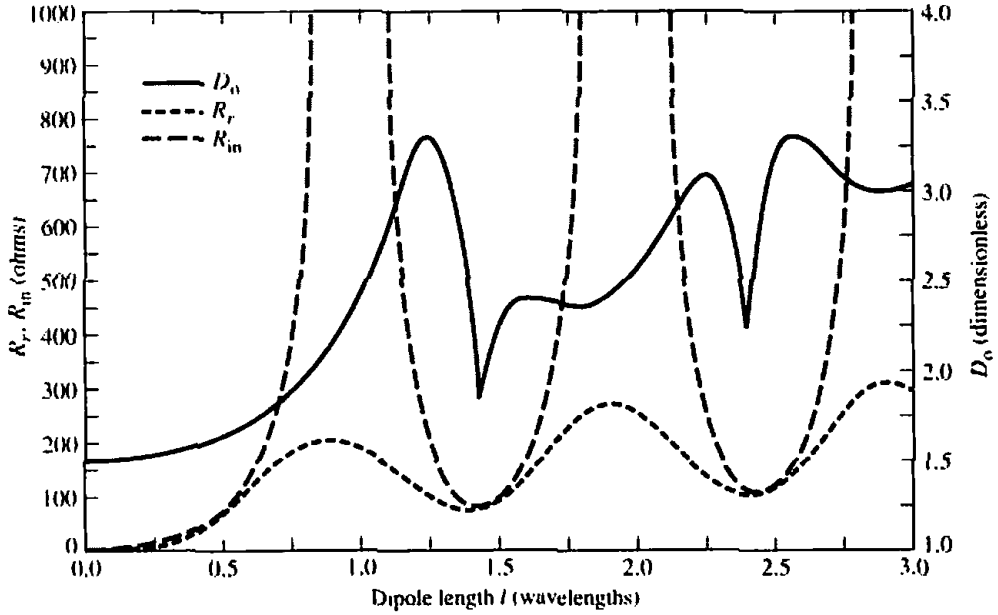

Figure 4.9 Radiation resistance, input resistance and directivity of a thin dipole with sinusoidal current distribution.

The directivity was defined mathematically by (2-22), or

$$D_0 = 4\pi \frac{F(\theta, \phi)|_{\max}}{\int_0^{2\pi} \int_0^{\pi} F(\theta, \phi) \sin\theta \, d\theta \, d\phi} \tag{4-71}$$

where $F(\theta, \phi)$ is related to the radiation intensity U by (2-19), or

$$U = B_0 F(\theta, \phi) \tag{4-72}$$

From (4-64), the dipole antenna of length l has

$$F(\theta, \phi) = F(\theta) = \left[\frac{\cos\left(\frac{kl}{2}\cos\theta\right) - \cos\left(\frac{kl}{2}\right)}{\sin\theta} \right]^2 \tag{4-73}$$

and

$$B_0 = \eta \frac{|I_0|^2}{8\pi^2} \tag{4-73a}$$

Because the pattern is not a function of ϕ, (4-71) reduces to

$$D_0 = \frac{2F(\theta)|_{\max}}{\int_0^{\pi} F(\theta) \sin\theta \, d\theta} \tag{4-74}$$

Equation (4-74) can be written, using (4-67), (4-68), and (4-73), as

$$D_0 = \frac{2F(\theta)|_{\max}}{Q} \tag{4-75}$$

where

$$Q = \{C + \ln(kl) - C_i(kl) + \tfrac{1}{2}\sin(kl)[S_i(2kl) - 2S_i(kl)] + \tfrac{1}{2}\cos(kl)[C + \ln(kl/2) + C_i(2kl) - 2C_i(kl)]\} \quad (4\text{-}75a)$$

The maximum value of $F(\theta)$ varies and depends upon the length of the dipole.

Values of the directivity, as given by (4-75) and (4-75a), have been obtained for $0 < l \leq 3\lambda$ and are shown plotted in Figure 4.9. The corresponding values of the maximum effective aperture are related to the directivity by

$$A_{em} = \frac{\lambda^2}{4\pi} D_0 \quad (4\text{-}76)$$

4.5.5 Input Resistance

In Section 2.13 the input impedance was defined as "the ratio of the voltage to current at a pair of terminals or the ratio of the appropriate components of the electric to magnetic fields at a point." The real part of the input impedance was defined as the input resistance which for a lossless antenna reduces to the radiation resistance, a result of the radiation of real power.

In Section 4.2.2, the radiation resistance of an infinitesimal dipole was derived using the definition of (4-18). The radiation resistance of a dipole of length l with sinusoidal current distribution, of the form given by (4-56), is expressed by (4-70). By this definition, the radiation resistance is referred to the maximum current which for some lengths ($l = \lambda/4, 3\lambda/4, \lambda$, etc.) does not occur at the input terminals of the antenna (see Figure 4.8). To refer the radiation resistance to the input terminals of the antenna, the antenna itself is first assumed to be lossless ($R_l = 0$). Then the power at the input terminals is equated to the power at the current maximum.

Referring to Figure 4.10, we can write

$$\frac{|I_{in}|^2}{2} R_{in} = \frac{|I_0|^2}{2} R_r \quad (4\text{-}77)$$

or

$$R_{in} = \left[\frac{I_0}{I_{in}}\right]^2 R_r \quad (4\text{-}77a)$$

where

R_{in} = radiation resistance at input (feed) terminals
R_r = radiation resistance at current maximum Eq. (4-70)
I_0 = current maximum
I_{in} = current at input terminals

For a dipole of length l, the current at the input terminals (I_{in}) is related to the current maximum (I_0) referring to Figure 4.10, by

$$I_{in} = I_0 \sin\left(\frac{kl}{2}\right) \quad (4\text{-}78)$$

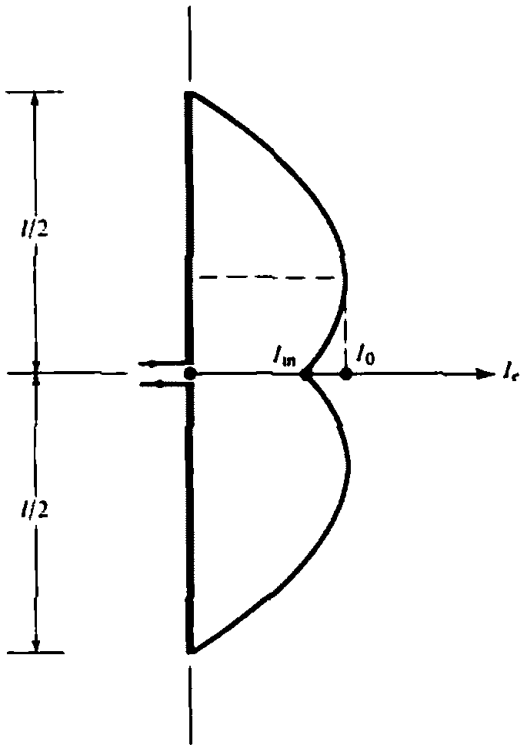

Figure 4.10 Current distribution of a linear wire antenna when current maximum does not occur at the input terminals.

Thus the input radiation resistance of (4-77a) can be written as

$$R_{in} = \frac{R_r}{\sin^2\left(\frac{kl}{2}\right)} \tag{4-79}$$

Values of R_{in} for $0 < l \leq 3\lambda$ are shown in Figure 4.9.

To compute the radiation resistance (in ohms), directivity (dimensionless and in dB), and input resistance (in ohms) for a dipole of length l, a FORTRAN computer program has been developed. The program is based on the definitions of each as given by (4-70), (4-71), and (4-79). The radiated power P_{rad} is computed by numerically integrating (over a closed sphere) the radiation intensity of (4-72)–(4-73a). The program is included at the end of this chapter and in the computer disc made available with the book. The length of the dipole (in wavelengths) must be inserted as an input.

When the overall length of the antenna is a multiple of λ (i.e., $l = n\lambda$, $n = 1, 2, 3, \ldots$), it is apparent from (4-56) and from Figure 4.8 that $I_{in} = 0$. That is,

$$I_{in} = I_0 \sin\left[k\left(\frac{l}{2} \pm z'\right)\right]\Big|_{\substack{z'=0 \\ l=n\lambda,\, n=0,1,2,\ldots}} = 0 \tag{4-80}$$

which indicates that the radiation resistance at the input terminals, as given by (4-77a) or (4-79) is infinite. In practice this is not the case because the current distribution does not follow an exact sinusoidal distribution, especially at the feed point. It has, however, very high values. Two of the primary factors which contribute

to the nonsinusoidal current distribution on an actual wire antenna are the nonzero radius of the wire and finite gap spacing at the terminals.

The radiation resistance and input resistance, as predicted, respectively, by (4-70) and (4-79), are based on the ideal current distribution of (4-56) and do not account for the finite radius of the wire or the gap spacing at the feed. Although the radius of the wire does not strongly influence the resistances, the gap spacing at the feed does play a significant role especially when the current at and near the feed point is small.

4.5.6 Finite Feed Gap

To analytically account for a nonzero current at the feed point for antennas with a finite gap at the terminals, Schelkunoff and Friis [6] have changed the current of (4-56) by including a quadrature term in the distribution. The additional term is inserted to take into account the effects of radiation on the antenna current distribution. In other words, once the antenna is excited by the "ideal" current distribution of (4-56), electric and magnetic fields are generated which in turn disturb the "ideal" current distribution. This reaction is included by modifying (4-56) to

$$\mathbf{I}_e(x', y', z') = \begin{cases} \hat{\mathbf{a}}_z \left\{ I_0 \sin\left[k\left(\frac{l}{2} - z'\right)\right] + jpI_0\left[\cos(kz') - \cos\left(\frac{k}{2}l\right)\right]\right\}, & 0 \le z' \le l/2 \\ \hat{\mathbf{a}}_z \left\{ I_0 \sin\left[k\left(\frac{l}{2} + z'\right)\right] + jpI_0\left[\cos(kz') - \cos\left(\frac{k}{2}l\right)\right]\right\}, & -l/2 \le z' \le 0 \end{cases} \tag{4-81}$$

where p is a coefficient that is dependent upon the overall length of the antenna and the gap spacing at the terminals. The values of p become smaller as the radius of the wire and the gap decrease.

When $l = \lambda/2$,

$$\mathbf{I}_e(x', y', z') = \hat{\mathbf{a}}_z I_0(1 + jp)\cos(kz') \qquad 0 \le |z'| \le \lambda/4 \tag{4-82}$$

and for $l = \lambda$

$$\mathbf{I}_e(x', y', z') = \begin{cases} \hat{\mathbf{a}}_z I_0\{\sin(kz') + jp[1 + \cos(kz')]\} & 0 \le z' \le \lambda/2 \\ \hat{\mathbf{a}}_z I_0\{-\sin(kz') + jp[1 + \cos(kz')]\} & -\lambda/2 \le z' \le 0 \end{cases} \tag{4-83}$$

Thus for $l = \lambda/2$ the shape of the current is not changed while for $l = \lambda$ it is modified by the second term which is more dominant for small values of z'.

The variations of the current distribution and impedances, especially of wire-type antennas, as a function of the radius of the wire and feed gap spacing can be easily taken into account by using advanced computational methods and numerical techniques, especially Integral Equations and Moment Method [7]–[12], which are introduced in Chapter 8.

To illustrate the point, the current distribution of an $l = \lambda/2$ and $l = \lambda$ dipole has been computed using an integral equation formulation with a moment method

numerical solution, and it is shown in Figure 8.13(b) where it is compared with the ideal distribution of (4-56) and other available data. For the moment method solution, a gap at the feed has been inserted. As expected and illustrated in Figure 8.13(b), the current distribution for the $l = \lambda/2$ dipole based on (4-56) is not that different from that based on the moment method. This is also illustrated by (4-82). Therefore the input resistance based on these two methods will not be that different. However, for the $l = \lambda$ dipole, the current distribution based on (4-56) is quite different, especially at and near the feed point, compared to that based on the moment method, as shown in Figure 8.13(b). This is expected since the current distribution based on the ideal current distribution is zero at the feed point; for practical antennas it is very small. Therefore the gap at the feed plays an important role on the current distribution at and near the feed point. In turn, the values of the input resistance based on the two methods will be quite different, since there is a significant difference in the current between the two methods. This is discussed further in Chapter 8.

4.6 HALF-WAVELENGTH DIPOLE

One of the most commonly used antennas is the half-wavelength ($l = \lambda/2$) dipole. Because its radiation resistance is 73 ohms, which is very near the 75-ohm characteristic impedance of some transmission lines, its matching to the line is simplified especially at resonance. Because of its wide acceptance in practice, we will examine in a little more detail its radiation characteristics.

The electric and magnetic field components of a half-wavelength dipole can be obtained from (4-62a) and (4-62b) by letting $l = \lambda/2$. Doing this, they reduce to

$$E_\theta \simeq j\eta \frac{I_0 e^{-jkr}}{2\pi r}\left[\frac{\cos\left(\frac{\pi}{2}\cos\theta\right)}{\sin\theta}\right] \tag{4-84}$$

$$H_\phi \simeq j\frac{I_0 e^{-jkr}}{2\pi r}\left[\frac{\cos\left(\frac{\pi}{2}\cos\theta\right)}{\sin\theta}\right] \tag{4-85}$$

In turn, the time-average power density and radiation intensity can be written, respectively, as

$$W_{av} = \eta\frac{|I_0|^2}{8\pi^2 r^2}\left[\frac{\cos\left(\frac{\pi}{2}\cos\theta\right)}{\sin\theta}\right]^2 \simeq \eta\frac{|I_0|^2}{8\pi^2 r^2}\sin^3\theta \tag{4-86}$$

and

$$U \simeq r^2 W_{av} = \eta\frac{|I_0|^2}{8\pi^2}\left[\frac{\cos\left(\frac{\pi}{2}\cos\theta\right)}{\sin\theta}\right]^2 \simeq \eta\frac{|I_0|^2}{8\pi^2}\sin^3\theta \tag{4-87}$$

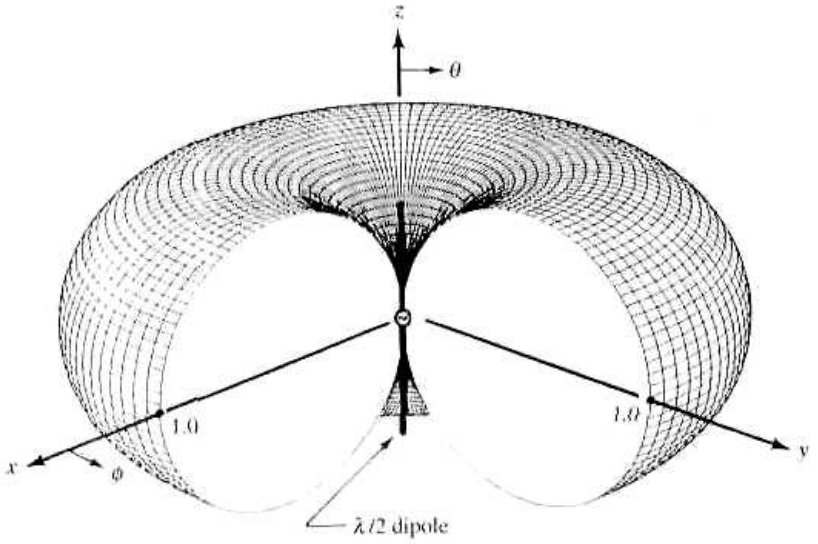

Figure 4.11 Three-dimensional pattern of a $\lambda/2$ dipole. (SOURCE: C. A. Balanis, "Antenna Theory: A Review" *Proc. IEEE*, Vol. 80, No 1. Jan. 1992. © 1992 IEEE.)

whose two-dimensional pattern is shown plotted in Figure 4.6 while the three-dimensional pattern is depicted in Figure 4.11. For the three-dimensional pattern of Figure 4.11, a 90° angular sector has been removed to illustrate the figure-eight elevation plane pattern variations.

The total power radiated can be obtained as a special case of (4-67), or

$$P_{\text{rad}} = \eta \frac{|I_0|^2}{4\pi} \int_0^{\pi} \frac{\cos^2\left(\frac{\pi}{2}\cos\theta\right)}{\sin\theta} d\theta \tag{4-88}$$

which when integrated reduces, as a special case of (4-68), to

$$P_{\text{rad}} = \eta \frac{|I_0|^2}{8\pi} \int_0^{2\pi} \left(\frac{1-\cos y}{y}\right) dy = \eta \frac{|I_0|^2}{8\pi} C_{\text{in}}(2\pi) \tag{4-89}$$

By the definition of $C_{\text{in}}(x)$, as given by (4-69), $C_{\text{in}}(2\pi)$ is equal to

$$C_{\text{in}}(2\pi) = 0.5772 + \ln(2\pi) - C_i(2\pi) = 0.5772 + 1.838 - (-0.02) \simeq 2.435 \tag{4-90}$$

where $C_i(2\pi)$ is obtained from the tables in Appendix III.

Using (4-87), (4-89), and (4-90), the directivity of the half-wavelength dipole reduces to

$$\boxed{D_0 = 4\pi \frac{U_{max}}{P_{\text{rad}}} = 4\pi \frac{U|_{\theta=\pi/2}}{P_{\text{rad}}} = \frac{4}{C_{\text{in}}(2\pi)} = \frac{4}{2.435} \simeq 1.643} \tag{4-91}$$

The corresponding maximum effective area is equal to

$$\boxed{A_{em} = \frac{\lambda^2}{4\pi} D_0 = \frac{\lambda^2}{4\pi}(1.643) \simeq 0.13\lambda^2} \tag{4-92}$$

and the radiation resistance, for a free-space medium ($\eta = 120\pi$), is given by

$$R_r = \frac{2P_{\text{rad}}}{|I_0|^2} = \frac{\eta}{4\pi} C_{\text{in}}(2\pi) = 30(2.435) \simeq 73 \tag{4-93}$$

The radiation resistance of (4-93) is also the radiation resistance at the input terminals (input resistance) since the current maximum for a dipole of $l = \lambda/2$ occurs at the input terminals (see Figure 4.8). As it will be shown in Chapter 8, the imaginary part (reactance) associated with the input impedance of a dipole is a function of its length (for $l \simeq \lambda/2$, it is equal to $j42.5$). Thus the total input impedance for $l = \lambda/2$ is equal to $Z_{\text{in}} = 73 + j42.5$. To reduce the imaginary part of the input impedance to zero, the antenna is matched or reduced in length until the reactance vanishes. The latter is most commonly used in practice for half-wavelength dipoles.

Depending on the radius of the wire, the length of the dipole for first resonance is about $l = 0.47\lambda$ to 0.48λ; the thinner the wire, the closer the length is to 0.48λ. Thus, for thicker wires, a larger segment of the wire has to be removed from $\lambda/2$ to achieve resonance.

4.7 LINEAR ELEMENTS NEAR OR ON INFINITE PERFECT CONDUCTORS

Thus far we have considered the radiation characteristics of antennas radiating into an unbounded medium. The presence of an obstacle, especially when it is near the radiating element, can significantly alter the overall radiation properties of the antenna system. In practice the most common obstacle that is always present, even in the absence of anything else, is the ground. Any energy from the radiating element directed toward the ground undergoes a reflection. The amount of reflected energy and its direction are controlled by the geometry and constitutive parameters of the ground.

In general, the ground is a lossy medium ($\sigma \neq 0$) whose effective conductivity increases with frequency. Therefore it should be expected to act as a very good conductor above a certain frequency, depending primarily upon its moisture content. To simplify the analysis, it will first be assumed that the ground is a perfect electric conductor, flat, and infinite in extent. The effects of finite conductivity and earth curvature will be incorporated later. The same procedure can also be used to investigate the characteristics of any radiating element near any other infinite, flat, perfect electric conductor. Although infinite structures are not realistic, the developed procedures can be used to simulate very large (electrically) obstacles. The effects that finite dimensions have on the radiation properties of a radiating element can be conveniently accounted for by the use of the Geometrical Theory of Diffraction (Chapter 12, Section 12.10) and/or the Moment Method (Chapter 8, Section 8.4).

4.7.1 Image Theory

To analyze the performance of an antenna near an infinite plane conductor, virtual sources (images) will be introduced to account for the reflections. As the name implies, these are not real sources but imaginary ones, which when combined with the real

sources, form an equivalent system. For analysis purposes only, the equivalent system gives the same radiated field on and above the conductor as the actual system itself. Below the conductor, the equivalent system does not give the correct field. However, in this region the field is zero and there is no need for the equivalent.

To begin the discussion, let us assume that a vertical electric dipole is placed a distance h above an infinite, flat, perfect electric conductor as shown in Figure 4.12(a). The arrow indicates the polarity of the source. Energy from the actual source is radiated in all directions in a manner determined by its unbounded medium directional properties. For an observation point P_1, there is a direct wave. In addition, a wave from the actual source radiated toward point R_1 of the interface undergoes a reflection. The direction is determined by the law of reflection ($\theta_1^i = \theta_1^r$) which assures that the energy in homogeneous media travels in straight lines along the shortest paths. This wave will pass through the observation point P_1. By extending its actual path below the interface, it will seem to originate from a virtual source positioned a distance h below the boundary. For another observation point P_2 the point of reflection is R_2, but the virtual source is the same as before. The same is concluded for all other observation points above the interface.

The amount of reflection is generally determined by the respective constitutive parameters of the media below and above the interface. For a perfect electric conductor below the interface, the incident wave is completely reflected and the field below the boundary is zero. According to the boundary conditions, the tangential components of the electric field must vanish at all points along the interface. Thus for an incident electric field with vertical polarization shown by the arrows, the polarization of the reflected waves must be as indicated in the figure to satisfy the boundary conditions. To excite the polarization of the reflected waves, the virtual source must also be vertical and with a polarity in the same direction as that of the actual source (thus a reflection coefficient of $+1$).

Another orientation of the source will be to have the radiating element in a horizontal position, as shown in Figure 4.21. Following a procedure similar to that of the vertical dipole, the virtual source (image) is also placed a distance h below the interface but with a 180° polarity difference relative to the actual source (thus a reflection coefficient of -1).

In addition to electric sources, artificial equivalent "magnetic" sources and magnetic conductors have been introduced to aid in the analyses of electromagnetic boundary value problems. Figure 4.13(a) displays the sources and their images for an electric plane conductor. The single arrow indicates an electric element and the double a magnetic one. The direction of the arrow identifies the polarity. Since many problems can be solved using duality, Figure 4.13(b) illustrates the sources and their images when the obstacle is an infinite, flat, perfect "magnetic" conductor.

4.7.2 Vertical Electric Dipole

The analysis procedure for vertical and horizontal electric and magnetic elements near infinite electric and magnetic plane conductors, using image theory, was illustrated graphically in the previous section. Based on the graphical model of Figure 4.12, the mathematical expressions for the fields of a vertical linear element near a perfect electric conductor will now be developed. For simplicity, only far-field observations will be considered.

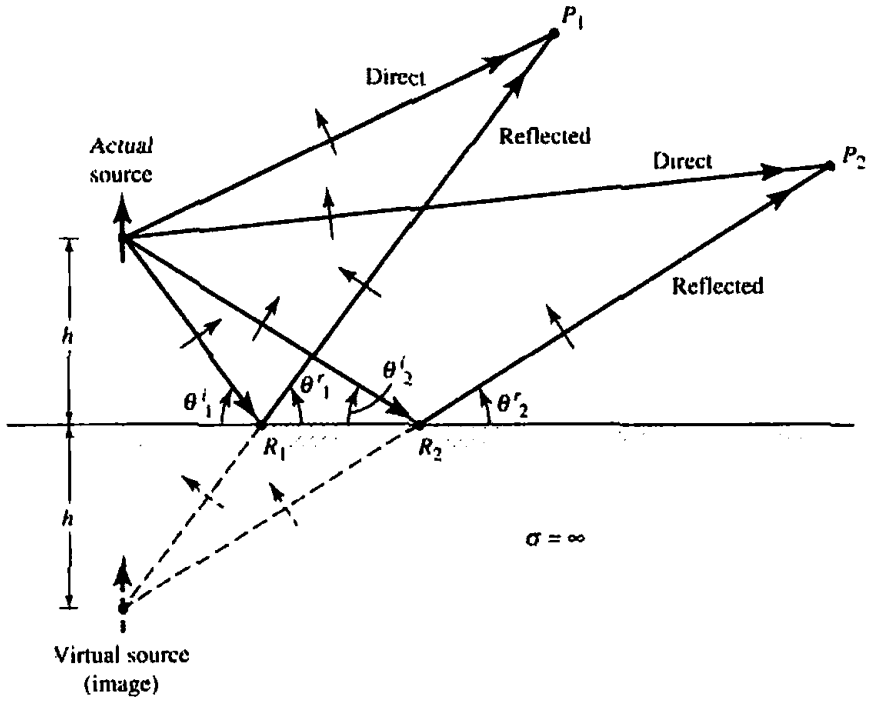

(a) Vertical electric dipole

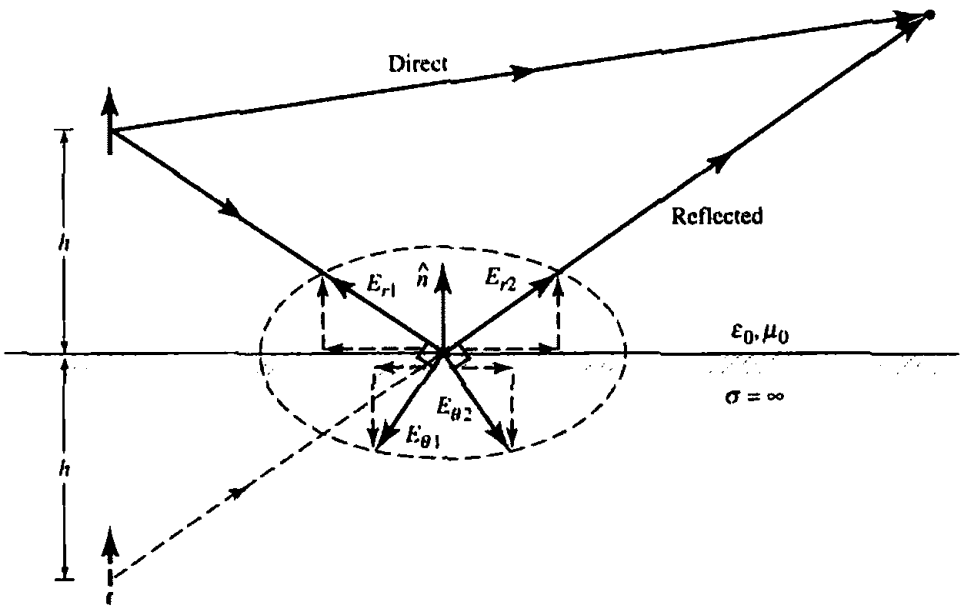

(b) Field components at point of reflection

Figure 4.12 Vertical electric dipole above an infinite, flat, perfect electric conductor.

Referring to the geometry of Figure 4.14(a), the far-zone direct component of the electric field of the infinitesimal dipole of length l, constant current I_0, and observation point P is given according to (4-26a) by

$$E_\theta^d = j\eta \frac{kI_0 l e^{-jkr_1}}{4\pi r_1} \sin \theta_1 \tag{4-94}$$

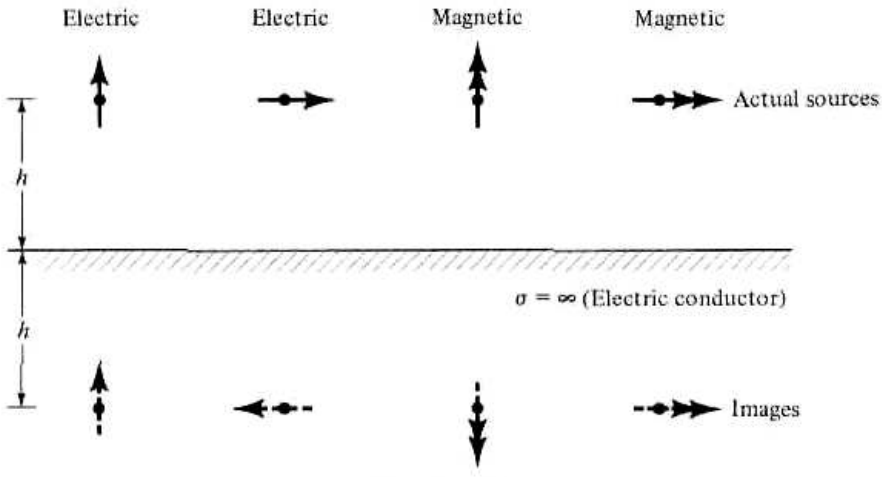

(a) Electric conductor

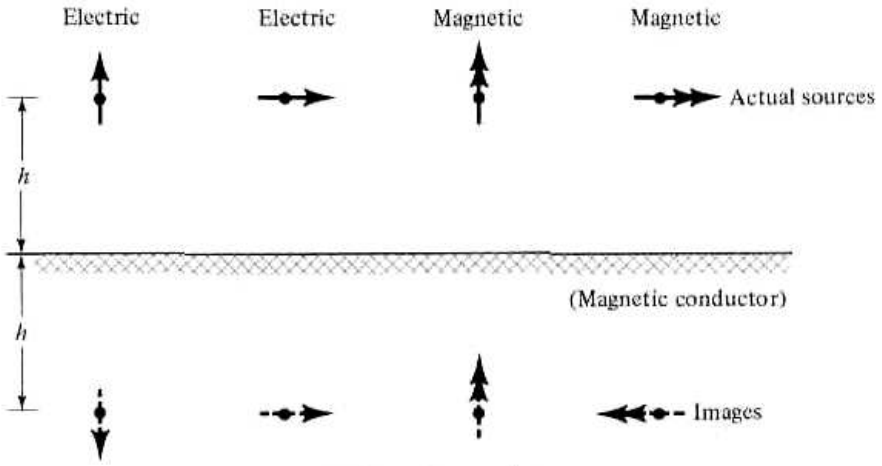

(b) Magnetic conductor

Figure 4.13 Electric and magnetic sources and their images near electric and magnetic conductors.

The reflected component can be accounted for by the introduction of the virtual source (image), as shown in Figure 4.14(a), and it can be written as

$$E_\theta^r = jR_v\eta\frac{kI_0le^{-jkr_2}}{4\pi r_2}\sin\theta_2 \tag{4-95}$$

or

$$E_\theta^r = j\eta\frac{kI_0le^{-jkr_2}}{4\pi r_2}\sin\theta_2 \tag{4-95a}$$

since the reflection coefficient R_v is equal to unity.

The total field above the interface ($z \geq 0$) is equal to the sum of the direct and reflected components as given by (4-94) and (4-95a). Since a field cannot exist inside a perfect electric conductor, it is equal to zero below the interface. To simplify the expression for the total electric field, it is referred to the origin of the coordinate system ($z = 0$).

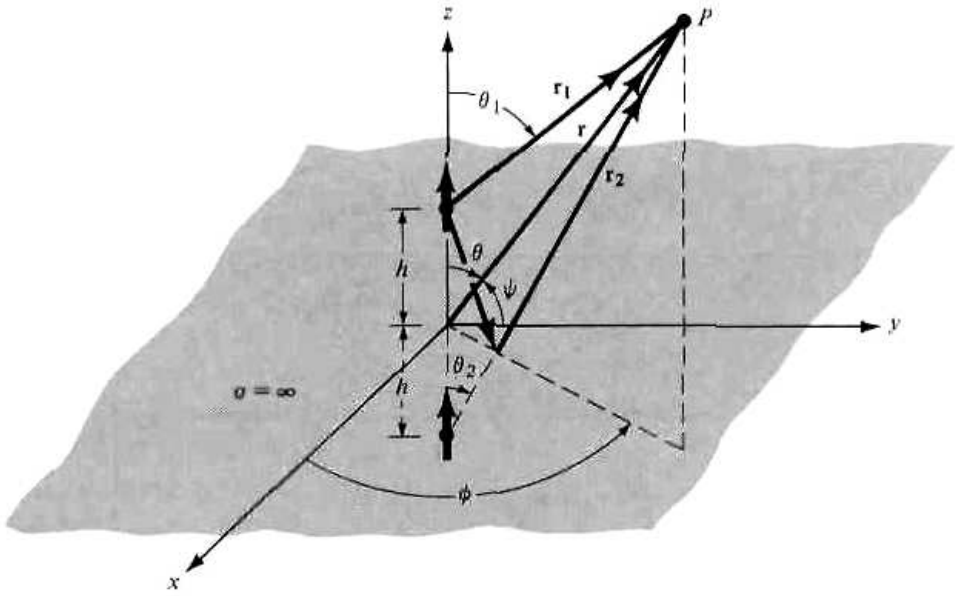

(a) Vertical electric dipole above ground plane

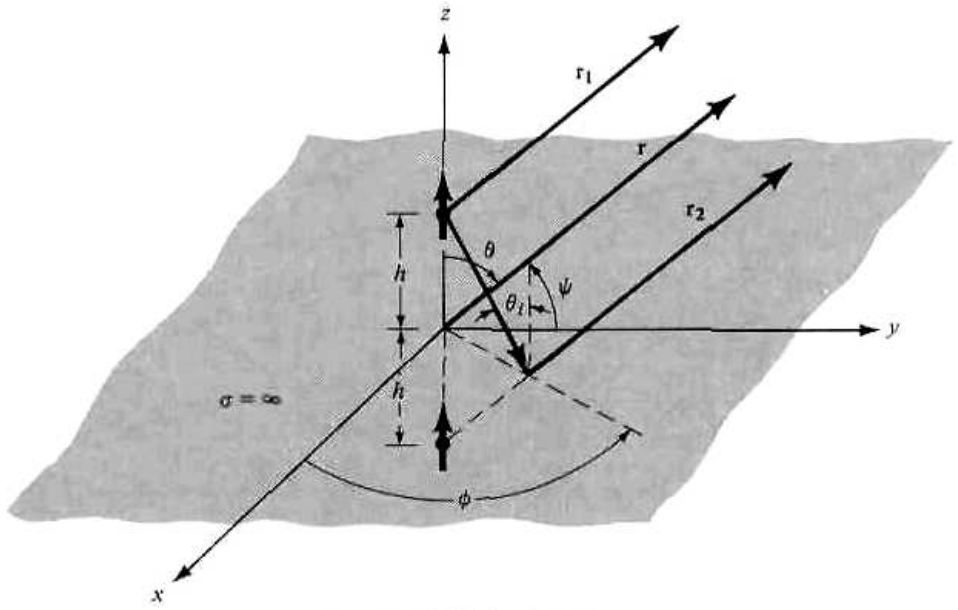

(b) Far-field observations

Figure 4.14 Vertical electric dipole above infinite perfect electric conductor.

In general, we can write that

$$r_1 = [r^2 + h^2 - 2rh\cos\theta]^{1/2} \tag{4-96a}$$

$$r_2 = [r^2 + h^2 - 2rh\cos(\pi - \theta)]^{1/2} \tag{4-96b}$$

For far-field observations ($r \gg h$), (4-96a) and (4-96b) reduce using the binomial expansion to

$$r_1 \simeq r - h\cos\theta \tag{4-97a}$$

$$r_2 \simeq r + h\cos\theta \tag{4-97b}$$

As shown in Figure 4.14(b), geometrically (4-97a) and (4-97b) represent parallel lines. Since the amplitude variations are not as critical

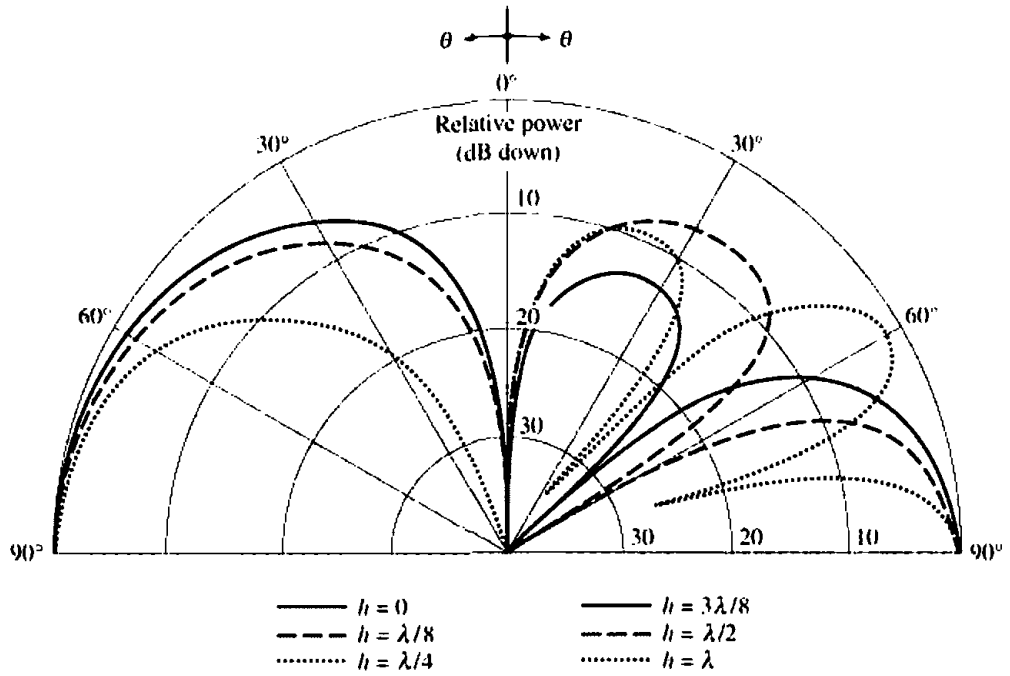

Figure 4.15 Elevation plane amplitude patterns of a vertical infinitesimal electric dipole for different heights above an infinite perfect electric conductor.

$$r_1 \simeq r_2 \simeq r \qquad \text{for amplitude variations} \tag{4-98}$$

Using (4-97a)–(4-98), the sum of (4-94) and (4-95a) can be written as

$$\left.\begin{aligned} E_\theta &\simeq j\eta \frac{kI_0 l e^{-jkr}}{4\pi r} \sin\theta |2\cos(kh\cos\theta)| \qquad z \geq 0 \\ E_\theta &= 0 \qquad\qquad\qquad\qquad\qquad\qquad\qquad\qquad z < 0 \end{aligned}\right\} \tag{4-99}$$

It is evident that the total electric field is equal to the product of the field of a single source positioned symmetrically about the origin and a factor [within the brackets in (4-99)] which is a function of the antenna height (h) and the observation angle (θ). This is referred to as *pattern multiplication* and the factor is known as the *array factor*. This will be developed and discussed in more detail and for more complex configurations in Chapter 6.

The shape and amplitude of the field is not only controlled by the field of the single element but also by the positioning of the element relative to the ground. To examine the field variations as a function of the height h, the normalized (to 0 dB) power patterns for $h = 0, \lambda/8, \lambda/4, 3\lambda/8, \lambda/2$, and λ have been plotted in Figure 4.15. Because of symmetry, only half of each pattern is shown. For $h > \lambda/4$ more minor lobes, in addition to the major ones, are formed. As h attains values greater than λ, an even greater number of minor lobes is introduced. These are shown in Figure 4.16 for $h = 2\lambda$ and 5λ. The introduction of the additional lobes in Figure 4.16 is usually called *scalloping*. In general, the total number of lobes is equal to the integer that is closest to

$$\boxed{\text{number of lobes} \simeq \frac{2h}{\lambda} + 1} \tag{4-100}$$

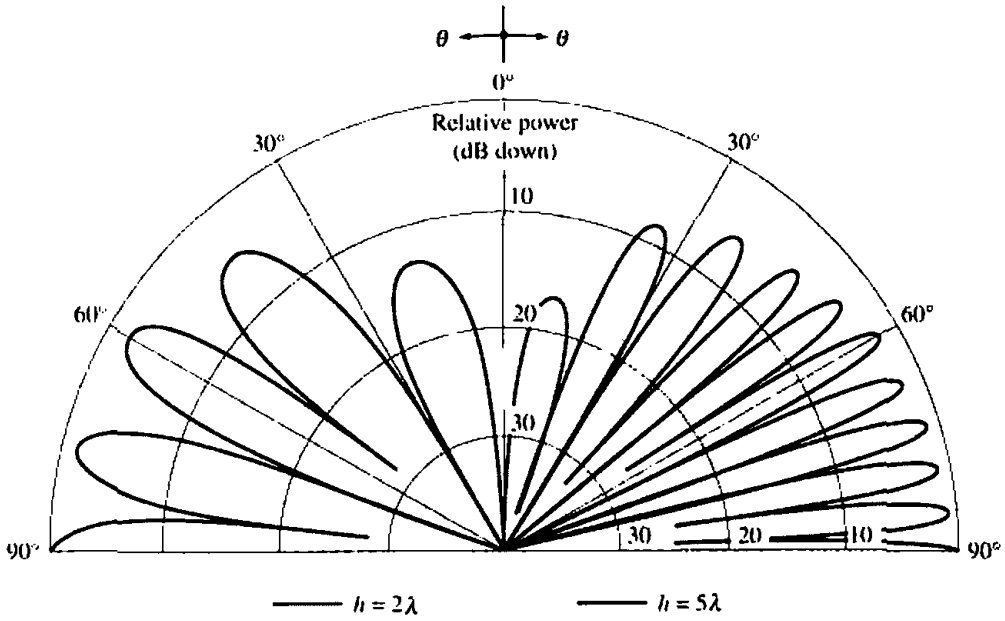

Figure 4.16 Elevation plane amplitude patterns of a vertical infinitesimal electric dipole for heights of 2λ and 5λ above an infinite perfect electric conductor.

Since the total field of the antenna system is different from that of a single element, the directivity and radiation resistance are also different. To derive expressions for them, we first find the total radiated power over the upper hemisphere of radius r using

$$P_{\text{rad}} = \oiint_S \mathbf{W}_{\text{av}} \cdot d\mathbf{s} = \frac{1}{2\eta} \int_0^{2\pi} \int_0^{\pi/2} |E_\theta|^2 r^2 \sin\theta \, d\theta \, d\phi$$

$$= \frac{\pi}{\eta} \int_0^{\pi/2} |E_\theta|^2 r^2 \sin\theta \, d\theta \tag{4-101}$$

which simplifies, with the aid of (4-99), to

$$P_{\text{rad}} = \pi\eta \left| \frac{I_0 l}{\lambda} \right|^2 \left[\frac{1}{3} - \frac{\cos(2kh)}{(2kh)^2} + \frac{\sin(2kh)}{(2kh)^3} \right] \tag{4-102}$$

As $kh \to \infty$ the radiated power, as given by (4-102), is equal to that of an isolated element. However, for $kh \to 0$, it can be shown by expanding the sine and cosine functions into series that the power is twice that of an isolated element. Using (4-99), the radiation intensity can be written as

$$U = r^2 W_{\text{av}} = r^2 \left(\frac{1}{2\eta} |E_\theta|^2 \right) = \frac{\eta}{2} \left| \frac{I_0 l}{\lambda} \right|^2 \sin^2\theta \cos^2(kh \cos\theta) \tag{4-103}$$

The maximum value of (4-103) occurs at $\theta = \pi/2$ and is given, excluding $kh \to \infty$, by

$$U_{\max} = U|_{\theta = \pi/2} = \frac{\eta}{2} \left| \frac{I_0 l}{\lambda} \right|^2 \tag{4-103a}$$

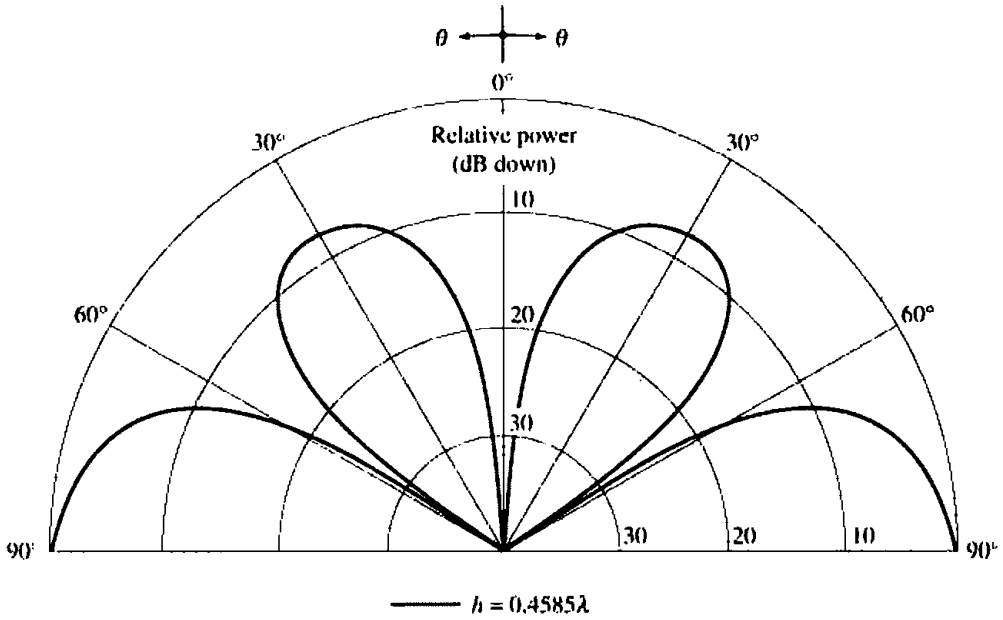

Figure 4.17 Elevation plane amplitude pattern of a vertical infinitesimal electric dipole at a height of 0.4585λ above an infinite perfect electric conductor.

which is four times greater than that of an isolated element. With (4-102) and (4-103a), the directivity can be written as

$$D_0 = \frac{4\pi U_{\max}}{P_{\text{rad}}} = \frac{2}{\left[\frac{1}{3} - \frac{\cos(2kh)}{(2kh)^2} + \frac{\sin(2kh)}{(2kh)^3}\right]} \tag{4-104}$$

whose value for $kh = 0$ is 3. The maximum value occurs when $kh = 2.881$ ($h = 0.4585\lambda$), and it is equal to 6.566 which is greater than four times that of an isolated element (1.5). The pattern for $h = 0.4585\lambda$ is shown plotted in Figure 4.17 while the directivity, as given by (4-104), is displayed in Figure 4.18 for $0 \le h \le 5\lambda$.

Using (4-102), the radiation resistance can be written as

$$R_r = \frac{2P_{\text{rad}}}{|I_0|^2} = 2\pi\eta\left(\frac{l}{\lambda}\right)^2\left[\frac{1}{3} - \frac{\cos(2kh)}{(2kh)^2} + \frac{\sin(2kh)}{(2kh)^3}\right] \tag{4-105}$$

whose value for $kh \to \infty$ is the same and for $kh = 0$ is twice that of the isolated element as given by (4-19). When $kh = 0$, the value of R_r as given by (4-105) is only one-half the value of an $l' = 2l$ isolated element according to (4-19). The radiation resistance, as given by (4-105), is plotted in Figure 4.18 for $0 \le h \le 5\lambda$ when $l = \lambda/50$ and the element is radiating into free-space ($\eta \simeq 120\pi$). It can be compared to the value of $R_r = 0.316$ ohms for the isolated element of Example 4.1.

In practice, a wide use has been made of a quarter-wavelength monopole ($l = \lambda/4$) mounted above a ground plane, as shown in Figure 4.19(a). For analysis purposes, a $\lambda/4$ image is introduced and it forms the $\lambda/2$ equivalent of Figure 4.19(b). It should be emphasized that the $\lambda/2$ equivalent of Figure 4.19(b) gives the correct field values for the actual system of Figure 4.19(a) only above the interface ($z \ge 0$, $0 \le \theta \le \pi/2$). Thus, the far-zone electric and magnetic fields for the $\lambda/4$ monopole above the ground plane are given, respectively, by (4-84) and (4-85).

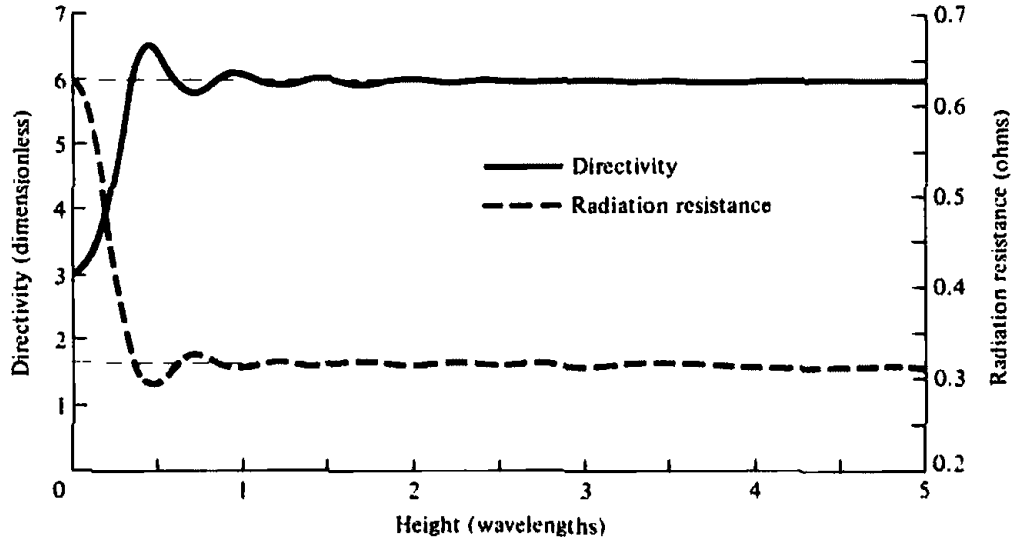

Figure 4.18 Directivity and radiation resistance of a vertical infinitesimal electric dipole as a function of its height above an infinite perfect electric conductor.

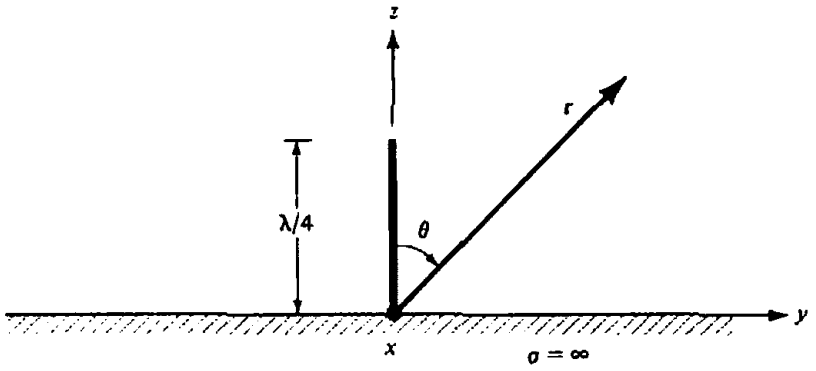

(a) λ/4 monopole on infinite electric conductor

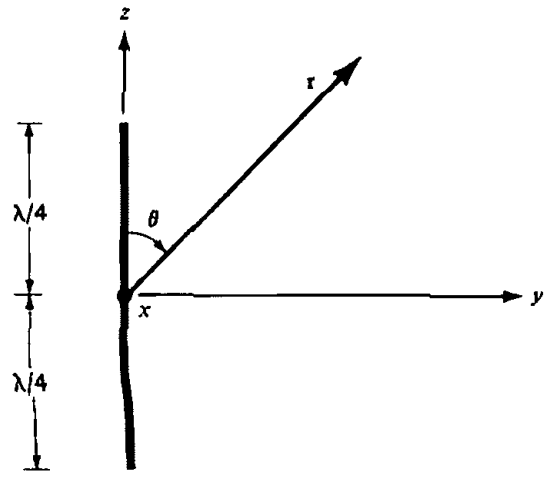

(b) Equivalent of λ/4 monopole on infinite electric conductor

Figure 4.19 Quarter-wavelength monopole on an infinite perfect electric conductor.

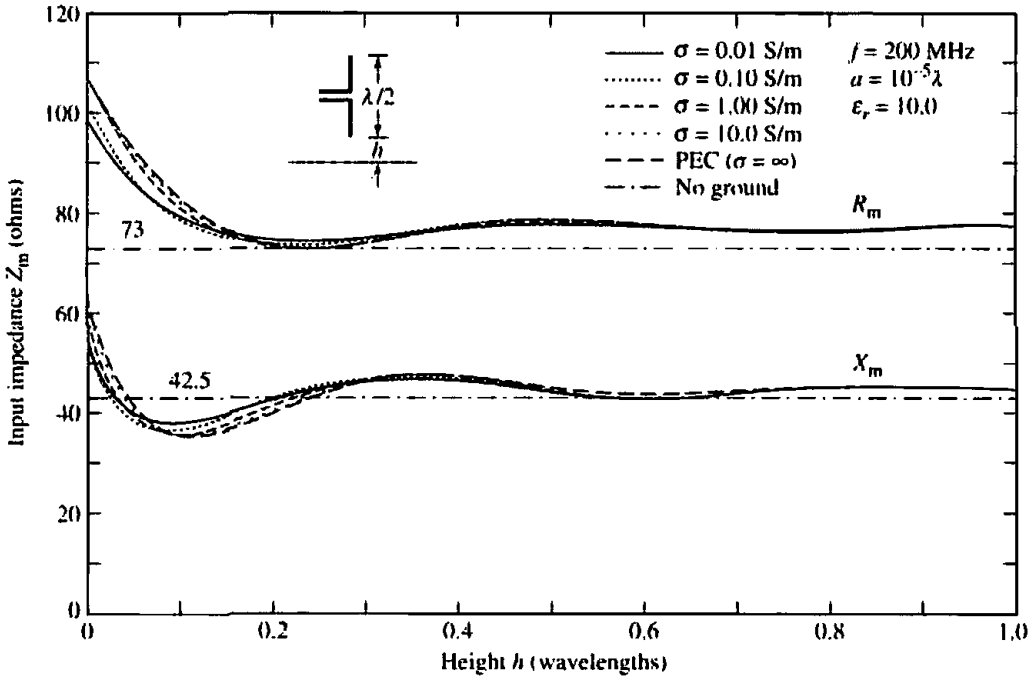

Figure 4.20 Input impedance of a vertical $\lambda/2$ dipole above a flat lossy electric conducting surface.

From the discussions of the resistance of an infinitesimal dipole above a ground plane for $kh = 0$, it follows that the input impedance of a $\lambda/4$ monopole above a ground plane is equal to one-half that of an isolated $\lambda/2$ dipole. Thus, referred to the current maximum, the input impedance Z_{in} is given by

$$Z_{in}\,(\text{monopole}) = \tfrac{1}{2} Z_{in}\,(\text{dipole}) = \tfrac{1}{2}[73 + j42.5] = 36.5 + j21.25 \quad (4\text{-}106)$$

where $73 + j42.5$ is the input impedance (and also the impedance referred to the current maximum) of a $\lambda/2$ dipole.

The same procedure can be followed for any other length. The input impedance $Z_{in} = R_{in} + jX_{in}$ (referred to the current maximum) of a vertical $\lambda/2$ dipole placed near a flat lossy electric conductor, as a function of height above the ground plane, is plotted in Figure 4.20, for $0 \leq h \leq \lambda$. Conductivity values considered were 10^{-2}, 10^{-1}, 1, 10 S/m, and infinity (PEC). It is apparent that the conductivity does not strongly influence the impedance values. The conductivity values used are representative of dry to wet earth. It is observed that the values of the resistance and reactance approach, as the height increases, the corresponding ones of the isolated element (73 ohms for the resistance and 42.5 ohms for the reactance).

4.7.3 Approximate Formulas for Rapid Calculations and Design

Although the input resistance of a dipole of any length can be computed using (4-70) and (4-79), while that of the corresponding monopole using (4-106), very good answers can be obtained using simpler but approximate expressions. Defining G as

$$G = kl/2 \text{ for dipole} \quad (4\text{-}107a)$$

$$G = kl \text{ for monopole} \quad (4\text{-}107b)$$

where l is the total length of each respective element, it has been shown that the input resistance of the dipole and monopole can be computed approximately using [10]

$$\underline{0 < G < \pi/4}$$

(*maximum input resistance of dipole is less than 12.337 ohms*)

$$R_{in}\text{ (dipole)} = 20G^2 \qquad 0 < l < \lambda/4 \tag{4-108a}$$

$$R_{in}\text{ (monopole)} = 10G^2 \qquad 0 < l < \lambda/8 \tag{4-108b}$$

$$\underline{\pi/4 \leq G < \pi/2}$$

(*maximum input resistance of dipole is less than 76.383 ohms*)

$$R_{in}\text{ (dipole)} = 24.7G^{2.5} \qquad \lambda/4 \leq l < \lambda/2 \tag{4-109a}$$

$$R_{in}\text{ (monopole)} = 12.35G^{2.5} \qquad \lambda/8 \leq l < \lambda/4 \tag{4-109b}$$

$$\underline{\pi/2 \leq G < 2}$$

(*maximum input resistance of dipole is less than 200.53 ohms*)

$$R_{in}\text{ (dipole)} = 11.14G^{4.17} \qquad \lambda/2 \leq l < 0.6366\lambda \tag{4-110a}$$

$$R_{in}\text{ (monopole)} = 5.57G^{4.17} \qquad \lambda/4 \leq l < 0.3183\lambda \tag{4-110b}$$

Besides being much simpler in form, these formulas are much more convenient in design (synthesis) problems where the input resistance is given and it is desired to determine the length of the element. These formulas can be verified by plotting the actual resistance versus length on a log–log scale and observe the slope of the line [13]. For example, the slope of the line for values of G up to about $\pi/4 \simeq 0.75$ is 2.

Example 4.4

Determine the length of the dipole whose input resistance is 50 ohms. Verify the answer.

SOLUTION

Using (4-109a)

$$50 \simeq 24.7G^{2.5}$$

or

$$G = 1.3259 = kl/2$$

Therefore

$$l = 0.422\lambda$$

Using (4-70) and (4-79) R_{in} for 0.422λ is 45.816 ohms, which closely agrees with the desired value of 50 ohms. To obtain 50 ohms using (4-70) and (4-79), $l = 0.4363\lambda$.

4.7.4 Antennas for Mobile Communication Systems

The dipole and monopole are two of the most widely used antennas for wireless mobile communication systems [14]–[17]. An array of dipole elements is extensively used as an antenna at the base station of a land mobile system while the monopole, because of its broadband characteristics and simple construction, is perhaps to most common antenna element for portable equipments, such as cellular telephones, cordless telephones, automobiles, trains, etc. The radiation efficiency and gain characteristics of both of these elements are strongly influenced by their electrical length which is related to the frequency of operation. In a hand-held unit, such as a cellular telephone, the position of the monopole element on the unit influences the pattern while it does not strongly affect the input impedance and resonant frequency. In addition to its use in mobile communication systems, the quarter-wavelength monopole is very popular in many other applications. An alternative to the monopole for the hand-held unit is the loop, which is discussed in Chapter 5. Other elements include the inverted F, planar inverted F antenna (PIFA), microstrip (patch), spiral, and others [14]–[17].

4.7.5 Horizontal Electric Dipole

Another dipole configuration is when the linear element is placed horizontally relative to the infinite electric ground plane, as shown in Figure 4.21. The analysis procedure of this is identical to the one of the vertical dipole. Introducing an image and assuming far-field observations, as shown in Figure 4.22(a,b), the direct component can be written as

$$E_{\psi}^{d} = j\eta \frac{kI_0 le^{-jkr_1}}{4\pi r_1} \sin\psi \tag{4-111}$$

and the reflected one by

$$E_{\psi}^{r} = jR_h \eta \frac{kI_0 le^{-jkr_2}}{4\pi r_2} \sin\psi \tag{4-112}$$

or

$$E_{\psi}^{r} = -j\eta \frac{kI_0 le^{-jkr_2}}{4\pi r_2} \sin\psi \tag{4-112a}$$

since the reflection coefficient is equal to $R_h = -1$.

To find the angle ψ, which is measured from the y-axis toward the observation point, we first form

$$\cos\psi = \hat{\mathbf{a}}_y \cdot \hat{\mathbf{a}}_r = \hat{\mathbf{a}}_y \cdot (\hat{\mathbf{a}}_x \sin\theta\cos\phi + \hat{\mathbf{a}}_y \sin\theta\sin\phi + \hat{\mathbf{a}}_z \cos\theta) = \sin\theta\sin\phi \tag{4-113}$$

from which we find

$$\sin\psi = \sqrt{1 - \cos^2\psi} = \sqrt{1 - \sin^2\theta\sin^2\phi} \tag{4-114}$$

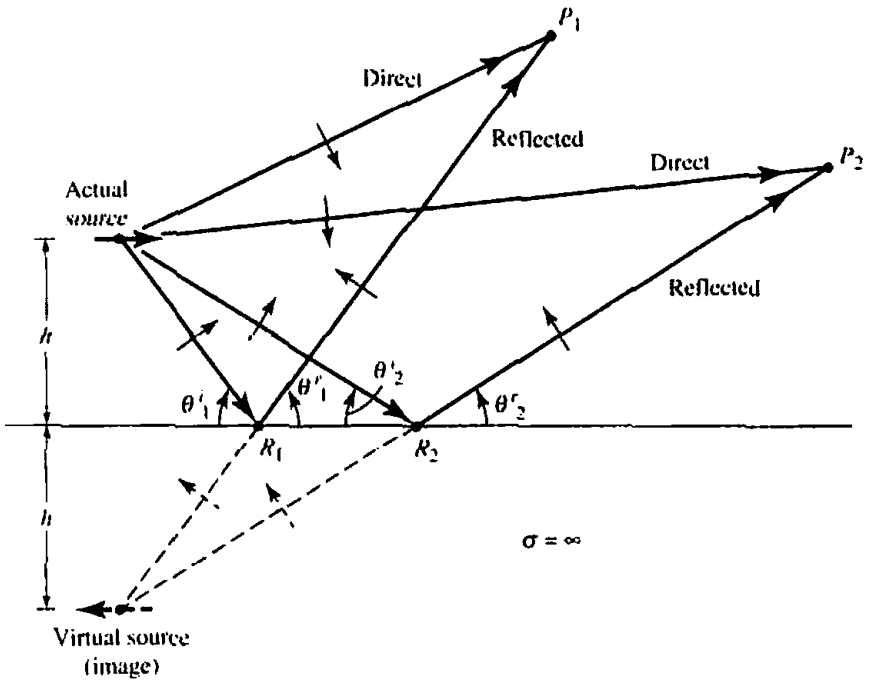

Figure 4.21 Horizontal electric dipole, and its associated image, above an infinite, flat, perfect electric conductor.

Since for far-field observations

$$\left.\begin{aligned} r_1 &\simeq r - h\cos\theta \\ r_2 &\simeq r + h\cos\theta \end{aligned}\right\} \quad \text{for phase variations} \tag{4-115a}$$

$$r_1 \simeq r_2 \simeq r \quad \text{for amplitude variations} \tag{4-115b}$$

the total field, which is valid only above the ground plane ($z \geq h$; $0 \leq \theta \leq \pi/2$, $0 \leq \phi \leq 2\pi$), can be written as

$$E_\phi = E_\phi^i + E_\phi^r = j\eta\frac{kI_0le^{-jkr}}{4\pi r}\sqrt{1 - \sin^2\theta\sin^2\phi}\,[2j\sin(kh\cos\theta)] \tag{4-116}$$

Equation (4-116) again consists of the product of the field of a single isolated element placed symmetrically at the origin and a factor (within the brackets) known as the *array factor*. This again is the pattern multiplication rule which is discussed in more detail in Chapter 6.

To examine the variations of the total field as a function of the element height above the ground plane, the two-dimensional elevation plane patterns (normalized to 0 dB) for $\phi = 90°$ (y-z plane) when $h = 0$, $\lambda/8$, $\lambda/4$, $3\lambda/8$, $\lambda/2$, and λ are plotted in Figure 4.23. Since this antenna system is not symmetric, the azimuthal plane (x-y plane) pattern will not be isotropic.

To obtain a better visualization of the radiation intensity in all directions above the interface, the three-dimensional pattern for $h = \lambda$ is shown plotted in Figure 4.24. The radial distance on the x-y plane represents the elevation angle θ from 0° to 90°, and the z-axis represents the normalized amplitude of the radiation field intensity from

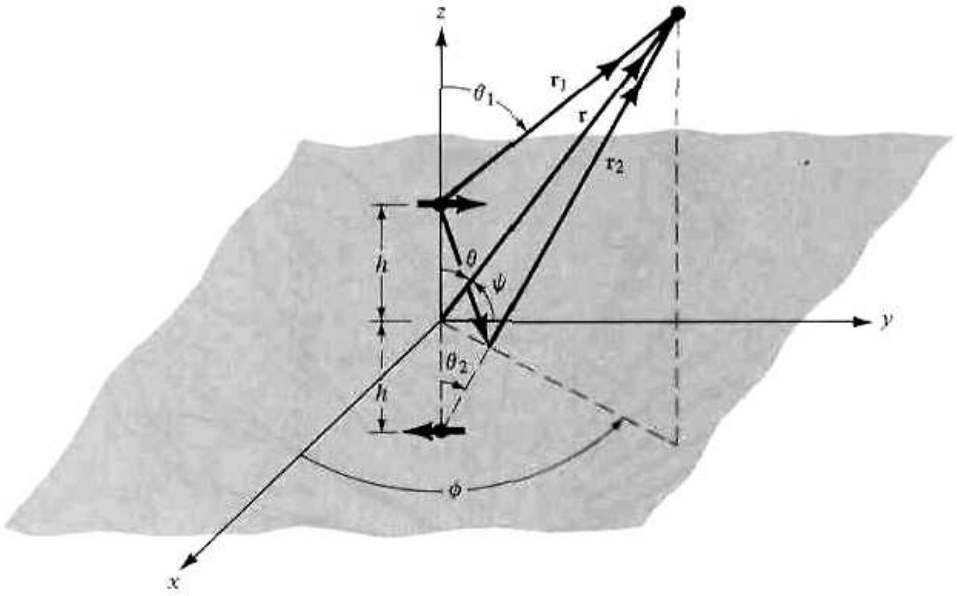

(a) Horizontal electric dipole above ground plane

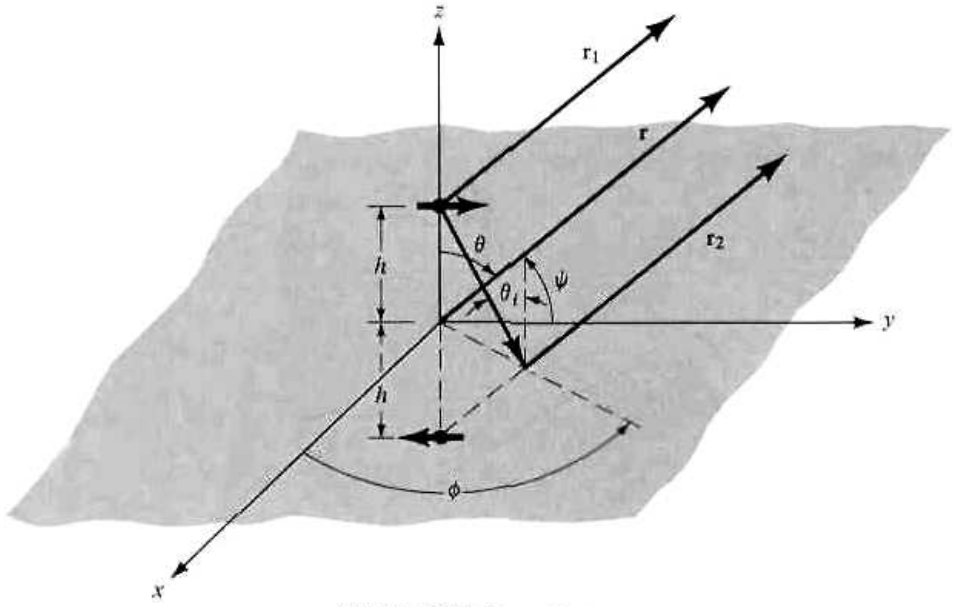

(b) Far-field observations

Figure 4.22 Horizontal electric dipole above an infinite perfect electric conductor.

0 to 1. The azimuthal angle ϕ ($0 \leq \phi \leq 2\pi$) is measured from the x- toward the y-axis on the x-y plane.

As the height increases beyond one wavelength ($h > \lambda$), a larger number of lobes is again formed. This is illustrated in Figure 4.25 for $h = 2\lambda$ and 5λ. The scalloping effect is evident here, as in Figure 4-16 for the vertical dipole. The total number of lobes is equal to the integer that most closely is equal to

$$\boxed{\text{number of lobes} \simeq 2\left(\frac{h}{\lambda}\right)} \tag{4-117}$$

with unity being the smallest number.

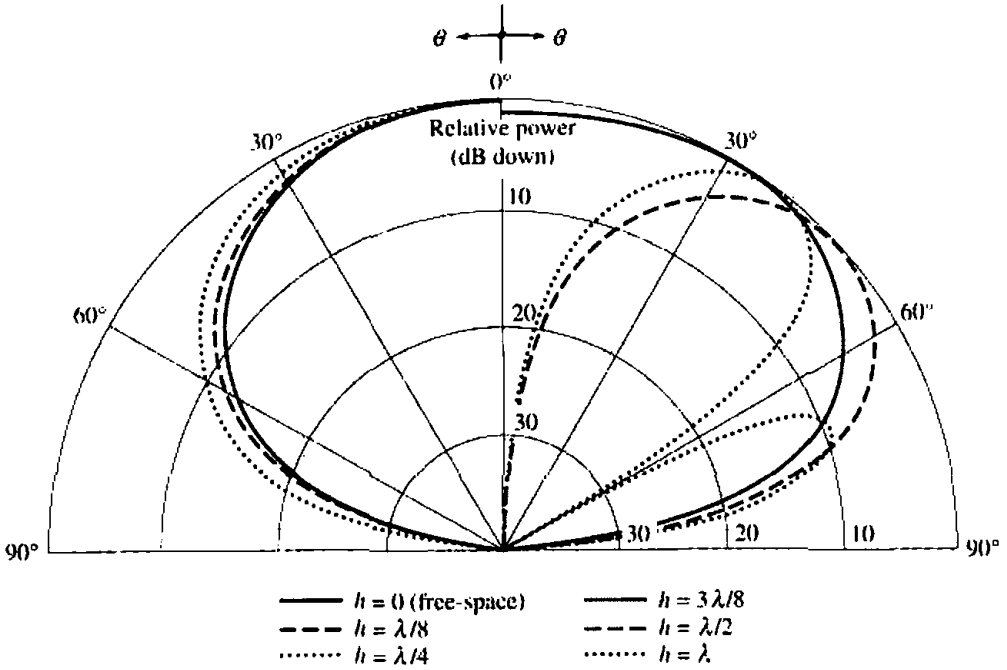

Figure 4.23 Elevation plane ($\phi = 90°$) amplitude patterns of a horizontal infinitesimal electric dipole for different heights above an infinite perfect electric conductor.

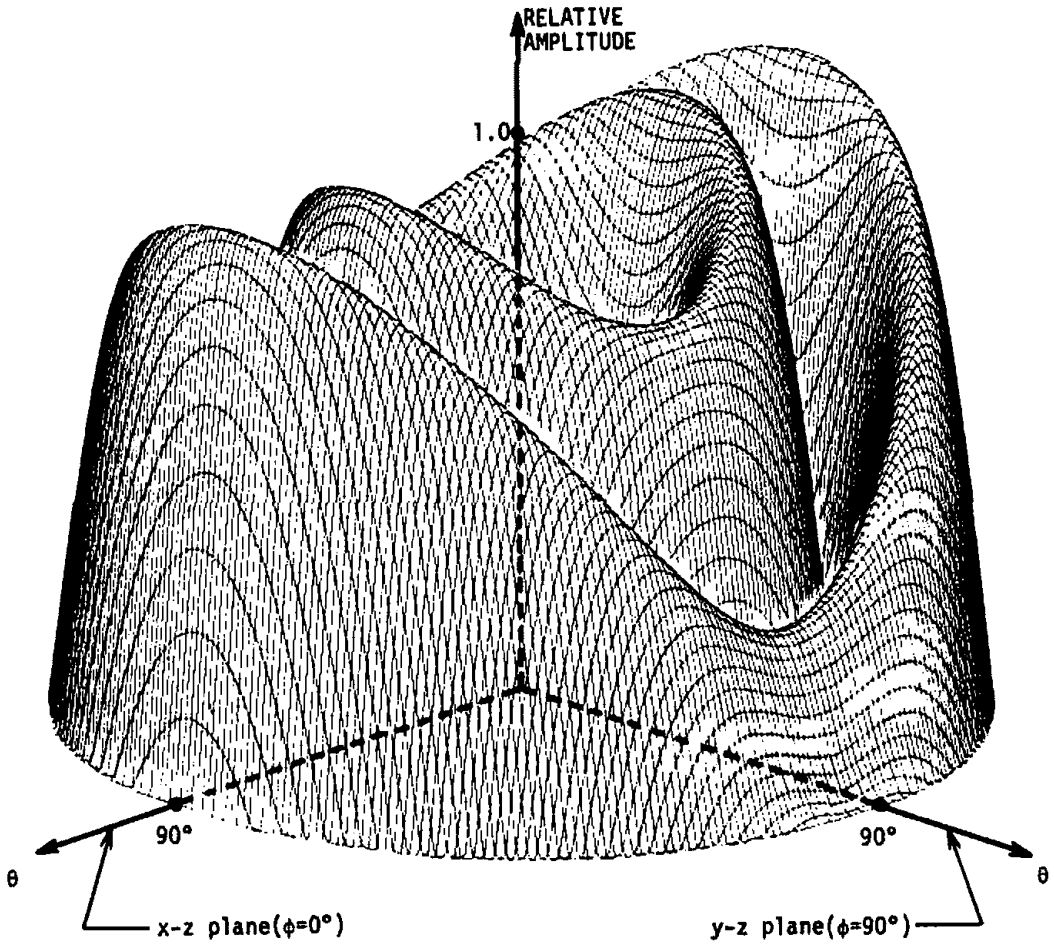

Figure 4.24 Three-dimensional amplitude pattern of an infinitesimal horizontal dipole a distance $h = \lambda$ above an infinite perfect electric conductor.

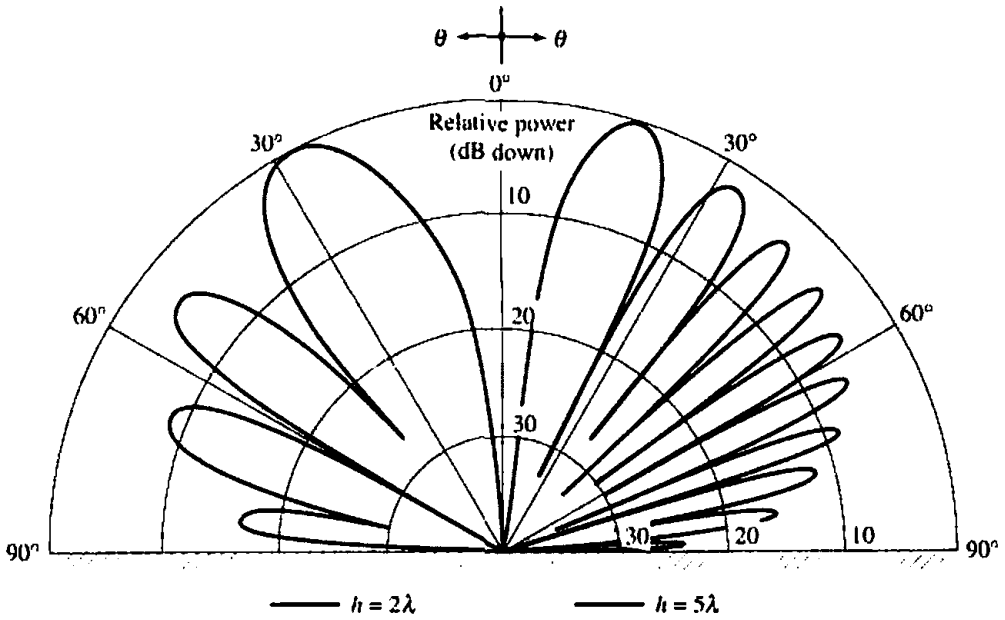

Figure 4.25 Elevation plane ($\phi = 90°$) amplitude patterns of a horizontal infinitesimal electric dipole for heights 2λ and 5λ above an infinite perfect electric conductor.

Following a procedure similar to the one performed for the vertical dipole, the radiated power can be written as

$$P_{rad} = \eta \frac{\pi}{2} \left| \frac{I_0 l}{\lambda} \right|^2 \left[\frac{2}{3} - \frac{\sin(2kh)}{2kh} - \frac{\cos(2kh)}{(2kh)^2} + \frac{\sin(2kh)}{(2kh)^3} \right] \tag{4-118}$$

and the radiation resistance as

$$R_r = \eta\pi \left(\frac{l}{\lambda} \right)^2 \left[\frac{2}{3} - \frac{\sin(2kh)}{2kh} - \frac{\cos(2kh)}{(2kh)^2} + \frac{\sin(2kh)}{(2kh)^3} \right] \tag{4-119}$$

By expanding the sine and cosine functions into series, it can be shown that (4-119) reduces for small values of kh to

$$R_r \overset{kh \to 0}{=} \eta\pi \left(\frac{l}{\lambda} \right)^2 \left[\frac{2}{3} - \frac{2}{3} + \frac{8}{15} \left(\frac{2\pi h}{\lambda} \right)^2 \right] = \eta \frac{32\pi^3}{15} \left(\frac{l}{\lambda} \right)^2 \left(\frac{h}{\lambda} \right)^2 \tag{4-120}$$

For $kh \to \infty$, (4-119) reduces to that of an isolated element. The radiation resistance, as given by (4-119), is plotted in Figure 4.26 for $0 \le h \le 5\lambda$ when $l = \lambda/50$ and the antenna is radiating into free space ($\eta \simeq 120\pi$).

The radiation intensity is given by

$$U \simeq \frac{r^2}{2\eta} |E_\phi|^2 = \frac{\eta}{2} \left| \frac{I_0 l}{\lambda} \right|^2 (1 - \sin^2\theta \sin^2\phi) \sin^2(kh \cos\theta) \tag{4-121}$$

The maximum value of (4-121) depends on the value of kh (whether $kh \le \pi/2$, $h \le \lambda/4$ or $kh > \pi/2$, $h > \lambda/4$). It can be shown that the maximum of (4-121) is:

$$U_{max} = \begin{cases} \dfrac{\eta}{2} \left| \dfrac{I_0 l}{\lambda} \right|^2 \sin^2(kh) & kh \le \pi/2 \ (h \le \lambda/4) \\ & (\theta = 0°) \end{cases} \tag{4-122a}$$

$$\begin{cases} \dfrac{\eta}{2} \left| \dfrac{I_0 l}{\lambda} \right|^2 & kh > \pi/2 \ (h > \lambda/4) \\ & [\phi = 0° \text{ and } \sin(kh \cos\theta_{max}) = 1 \\ & \text{or } \theta_{max} = \cos^{-1}(\pi/2kh)] \end{cases} \tag{4-122b}$$

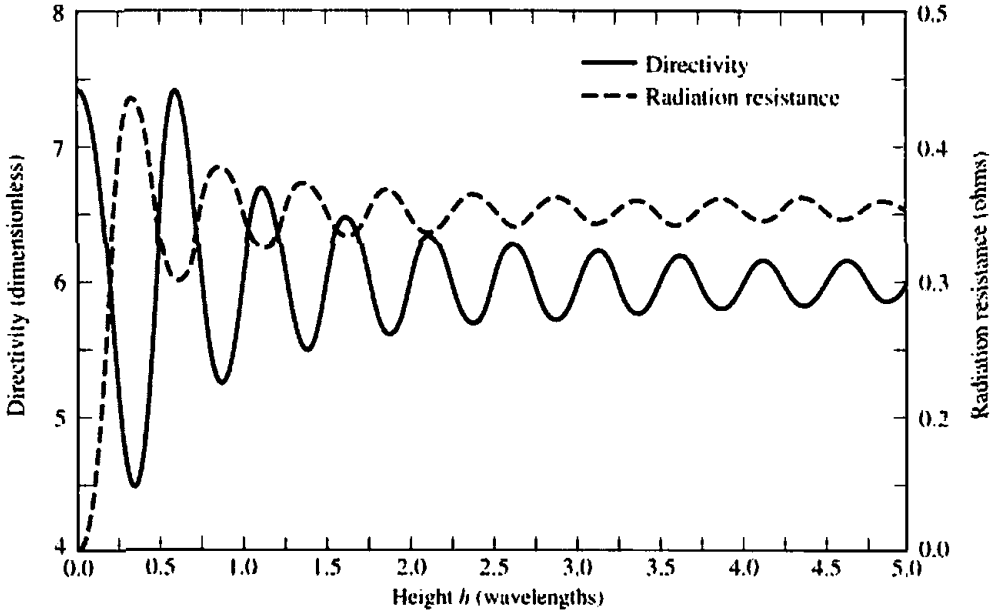

Figure 4.26 Radiation resistance and directivity gain of a horizontal infinitesimal electric dipole as a function of its height above an infinite perfect electric conductor.

Using (4-118) and (4-122a), (4-122b), the directivity can be written as

$$D_0 = \frac{4\pi U_{\max}}{P_{\text{rad}}} = \begin{cases} \dfrac{4\sin^2(kh)}{R(kh)} & kh \le \pi/2 \ (h \le \lambda/4) \qquad \text{(4-123a)} \\ \dfrac{4}{R(kh)} & kh > \pi/2 \ (h > \lambda/4) \qquad \text{(4-123b)} \end{cases}$$

where

$$R(kh) = \left[\frac{2}{3} - \frac{\sin(2kh)}{2kh} - \frac{\cos(2kh)}{(2kh)^2} + \frac{\sin(2kh)}{(2kh)^3}\right] \qquad \text{(4-123c)}$$

For small values of kh ($kh \to 0$), (4-123a) reduces to

$$D_0 \overset{kh\to 0}{=} \frac{4\sin^2(kh)}{\left[\frac{2}{3} - \frac{2}{3} + \frac{8}{15}(kh)^2\right]} = 7.5\left(\frac{\sin kh}{kh}\right)^2 \qquad \text{(4-124)}$$

For $h = 0$ the element is shorted and it does not radiate. The directivity, as given by (4-123a), (4-123b) is plotted for $0 \le h \le 5\lambda$ in Figure 4.26. It exhibits a maximum value of 7.5 for small values of h. Maximum values of 6 occur when $h = (0.725 + n/2)\lambda$, $n = 0, 1, 2, 3, \ldots$.

The input impedance $Z_{\text{in}} = R_{\text{in}} + jX_{\text{in}}$ (referred to the current maximum) of a horizontal $\lambda/2$ dipole above a flat lossy electric conductor is shown plotted in Figure 4.27 for $0 \le h \le \lambda$. Conductivities of 10^{-2}, 10^{-1}, 1, 10 S/m, and infinity (PEC) were considered. It is apparent that the conductivity does have a more pronounced effect on the impedance values, compared to those of the vertical dipole shown in Figure 4.20. The conductivity values used are representative of those of the dry to wet earth. The values of the resistance and reactance approach, as the height increases, the

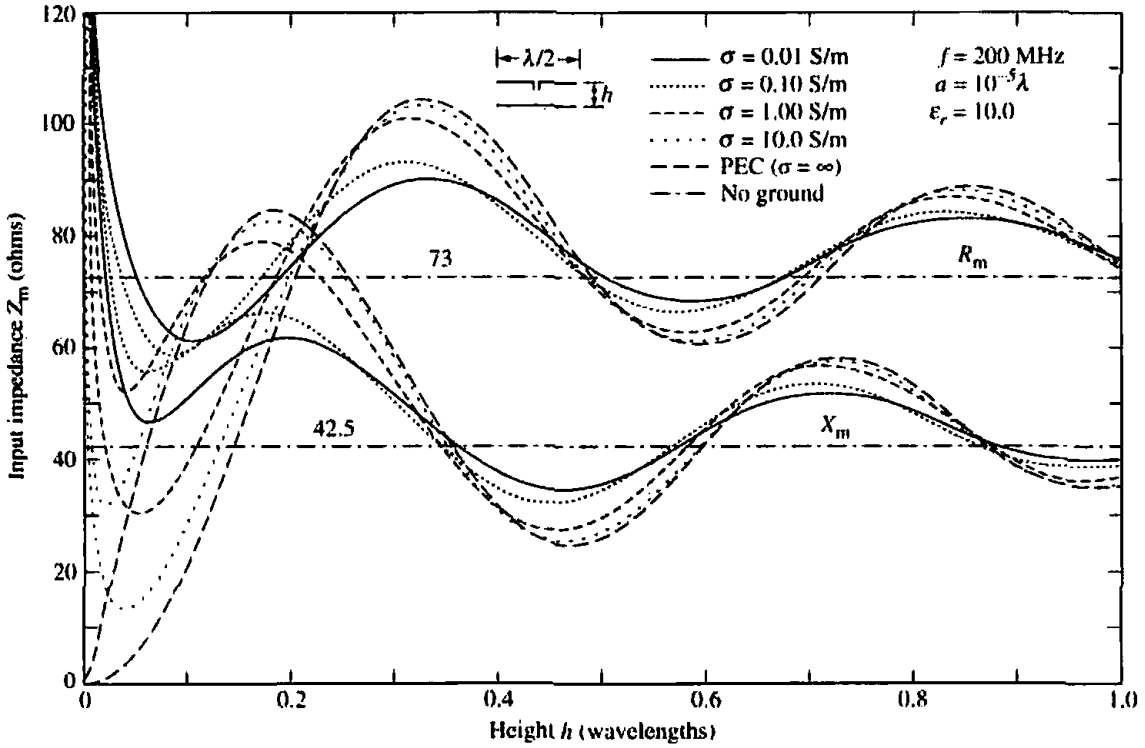

Figure 4.27 Input impedance of a horizontal $\lambda/2$ above a flat lossy electric conducting surface.

corresponding values of the isolated element (73 ohms for the resistance and 42.5 ohms for the reactance).

4.8 GROUND EFFECTS

In the previous two sections the variations of the radiation characteristics (pattern, radiation resistance, directivity) of infinitesimal vertical and horizontal linear elements were examined when they were placed above plane perfect electric conductors. Although ideal electric conductors ($\sigma = \infty$) are not realizable, their effects can be used as guidelines for good conductors ($\sigma \gg \omega\epsilon$, where ϵ is the permittivity of the medium).

One obstacle that is not an ideal conductor, and it is always present in any antenna system, is the ground (earth). In addition, the earth is not a plane surface. To simplify the analysis, however, the earth will initially be assumed to be flat. For pattern analysis, this is a very good engineering approximation provided the radius of the earth is large compared to the wavelength and the observation angles are greater than about $57.3/(ka)^{1/3}$ degrees from grazing (a is the earth radius) [18]. Usually these angles are greater than about 3°.

In general, the characteristics of an antenna at low (LF) and medium (MF) frequencies are profoundly influenced by the lossy earth. This is particularly evident in the input resistance. When the antenna is located at a height that is small compared to the skin depth of the conducting earth, the input resistance may even be greater than its free-space values [18]. This leads to antennas with very low efficiencies. Improvements in the efficiency can be obtained by placing radial wires or metallic disks on the ground.

The analytical procedures that are introduced to examine the ground effects are

based on the geometrical optics models of the previous sections. The image (virtual) source is again placed a distance h below the interface to account for the reflection. However, for each polarization nonunity reflection coefficients are introduced which, in general, will be a function of the angles of incidence and the constitutive parameters of the two media. Although plane wave reflection coefficients are used, even though spherical waves are radiated by the source, the error is small for conducting media [19]. The spherical nature of the wavefront begins to dominate the reflection phenomenon at grazing angles (i.e., as the point of reflection approaches the horizon) [20]. If the height (h) of the antenna above the interface is much less than the skin depth $\delta[\delta = \sqrt{2/(\omega\mu\sigma)}]$ of the ground, the image depth h below the interface should be increased [19] by a complex distance $\delta(1 - j)$.

The geometrical optics formulations are valid provided the sources are located inside the lossless medium. When the sources are placed within the ground, the formulations should include possible surface-wave contributions. Exact boundary-value solutions, based on Sommerfeld integral formulations, are available [18]. However they are too complex to be included in an introductory chapter.

4.8.1 Vertical Electric Dipole

The field radiated by an electric infinitesimal dipole when placed above the ground can be obtained by referring to the geometry of Figures 4.14(a) and (b). Assuming the earth is flat and the observations are made in the far-field, the direct component of the field is given by (4-94) and the reflected by (4-95) where the reflection coefficient $R_{\perp}$ is given by

$$R_{\perp} = \frac{\eta_0 \cos\theta_i - \eta_1 \cos\theta_t}{\eta_0 \cos\theta_i + \eta_1 \cos\theta_t} = -R_{\parallel} \tag{4-125}$$

where $R_{\parallel}$ is the reflection coefficient for parallel polarization [7] and

$\eta_0 = \sqrt{\dfrac{\mu_0}{\epsilon_0}}$ = intrinsic impedance of free-space (air)

$\eta_1 = \sqrt{\dfrac{j\omega\mu_1}{\sigma_1 + j\omega\epsilon_1}}$ = intrinsic impedance of the ground

θ_i = angle of incidence (relative to the normal)

θ_t = angle of refraction (relative to the normal)

The angles θ_i and θ_t are related by Snell's law of refraction

$$\gamma_0 \sin\theta_i = \gamma_1 \sin\theta_t \tag{4-126}$$

where

$\gamma_0 = jk_0$ = propagation constant for free-space (air)

k_0 = phase constant for free-space (air)

$\gamma_1 = (\alpha_1 + jk_1)$ = propagation constant for the ground

α_1 = attenuation constant for the ground

k_1 = phase constant for the ground

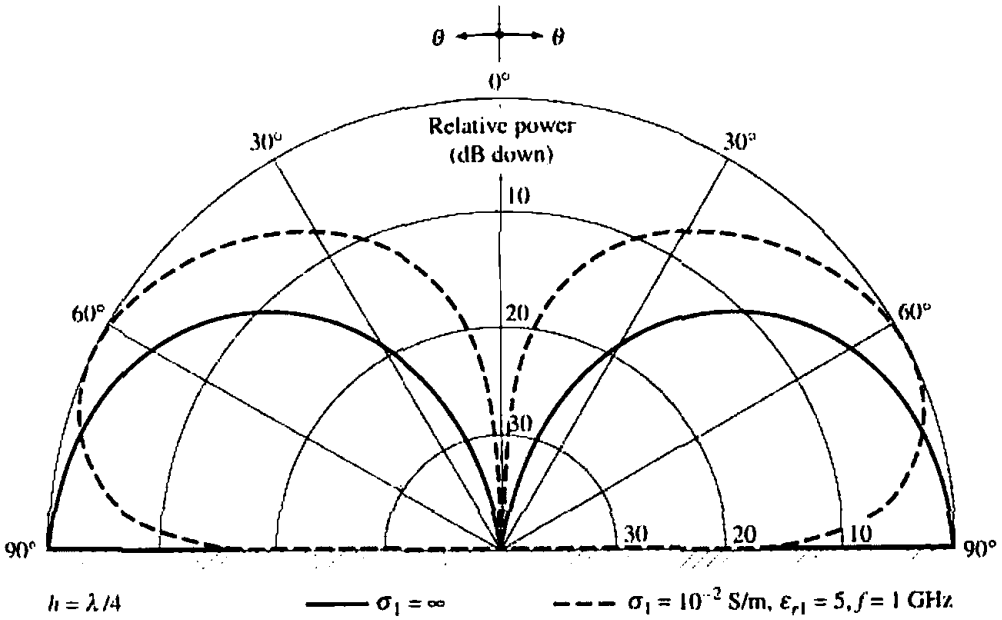

Figure 4.28 Elevation plane amplitude patterns of an infinitesimal verticle dipole above a perfect electric conductor ($\sigma_1 = \infty$) and a flat earth ($\sigma_1 = 0.01$ S/m, $\epsilon_{r1} = 5, f = 1$ GHz).

Using the far-field approximations of (4-97a)–(4-98), the total electric field above the ground ($z \geq 0$) can be written as

$$E_\theta = j\eta \frac{kI_0 l e^{-jkr}}{4\pi r} \sin\theta [e^{jkh\cos\theta} + R_v e^{-jkh\cos\theta}] \qquad z \geq 0 \qquad (4\text{-}127)$$

where R_v is given by (4-125).

The permittivity and conductivity of the earth are strong functions of the ground's geological constituents, especially its moisture. Typical values for the relative permittivity ϵ_r (dielectric constant) are in the range of 5–100 and for the conductivity σ in the range of $10^{-4} - 1$ S/m.

A normalized (to 0 dB) pattern for an infinitesimal dipole above the ground with $h = \lambda/4$, $\epsilon_{r1} = 5$, $f = 1$ GHz, $\sigma_1 = 10^{-2}$ S/m is shown plotted in Figure 4.28 (dashed curves) where it is compared with that (solid curve) of a perfect conductor ($\sigma_1 = \infty$). In the presence of the ground, the radiation toward the vertical direction ($60° > \theta > 0°$) is more intense that for the perfect electric conductor, but it vanishes for grazing angles ($\theta = 90°$). The null field toward the horizon ($\theta = 90°$) is formed because the reflection coefficient R_v approaches -1 as $\theta_i \to 90°$. Thus the ground effects on the pattern of a vertically polarized antenna are significantly different from those of a perfect conductor.

Significant changes also occur in the impedance. Because the formulation for the impedance is much more complex [18], it will not be presented here. Graphical illustrations for the impedance change of a vertical dipole placed a height h above a homogeneous lossy half-space, as compared to those in free-space, are shown in Figure 4.29. They are based on numerical results obtained by Vogler and Noble [21]. The variations in impedance are expressed in terms of changes in resistance ($\Delta R/R_0$) and in reactance ($\Delta X/R_0$), where R_0 is the radiation resistance of an infinitesimal

dipole radiating in an infinite free-space [as given by (4-19)]. The parameter N_1 is defined by

$$N_1 = \sqrt{\frac{\sigma_1 + j\omega\epsilon_1}{j\omega\epsilon_0}} = |N_1|e^{-j\left(\frac{\pi}{4} - \psi\right)} \tag{4-128}$$

where σ_1, ϵ_1 are the conductivity and permittivity, respectively, of the homogeneous lossy half-space, ϵ_0 is the free-space permittivity, and ψ is phase angle of N_1.

The curve in Figure 4.29(a) represents the data for a perfectly conducting ($|N_1| = \infty$) half-space. As expected, the magnitude of $\Delta R/R_0$ approaches unity as $2k_0h \rightarrow 0$, which corresponds to doubling the radiation resistance, while the magnitude of ΔX approaches infinity as $2k_0h \rightarrow 0$. The curves for both ΔR and ΔX become oscillatory as $2k_0h$ exceeds approximately π or the height h exceeds $\lambda_0/4$.

For the finite conductivity half-space, the $\psi = \pi/4$ curves correspond to a perfect dielectric half-space ($\sigma_1 = 0$) while the $\psi = 0$ curves represent negligible displacement currents in the lossy half-space. The curves for $|N_1^2| = 100$ are not too different from that of a perfectly conducting half-space ($|N_1| = \infty$). Significant changes are evident as the values of $|N_1^2|$ decrease particularly in the resistive portion of the $\psi = 0$ curves.

The curves of Figure 4.29 can be used as design data to determine the changes in the input impedance of an infinitesimal vertical dipole when it is placed above a lossy medium. To demonstrate the procedure, let us consider the following example.

Example 4.5

An infinitesimal vertical dipole of length $l = \lambda_0/50$ is placed a height $h = \lambda_0/10$ above the earth. Assume the earth is locally flat with a dielectric constant of 4 and conductivity of 10^{-3} S/m at a frequency of 100 MHz. Determine the changes in input resistance and reactance of the dipole.

SOLUTION

For a frequency of 100 MHz

$$\frac{\sigma_1}{\omega\epsilon_1} = \frac{10^{-3}}{2\pi \times 10^8 \times 4 \times 8.854 \times 10^{-12}} = 1.99 \times 10^{-3} \ll 1$$

Therefore according to (4-125)

$$N_1 \simeq \sqrt{\frac{\epsilon_1}{\epsilon_0}} = \sqrt{4} = 2$$

or

$$|N_1|^2 = 4$$

$$\frac{\pi}{4} - \psi = 0$$

For a height of $\lambda_0/10$

$$2k_0h = 2\left(\frac{2\pi}{\lambda_0}\right)\left(\frac{\lambda_0}{10}\right) = 1.257$$

Using Figure 4.29(d) and the curve for $\pi/4 - \psi = 0$ at $2k_0h = 1.257$, the relative changes in resistance and reactance are, respectively, equal to

$$\frac{\Delta R}{R_0} \simeq 0.767$$

$$\frac{\Delta X}{R_0} \simeq 1.2$$

Since for a $\lambda_0/50$ dipole the radiation resistance according to (4-19) and Example 4.1 is equal to

$$R_r = R_0 = 0.316 \text{ ohms}$$

then the changes in resistance and reactance are, respectively, equal to

$$\Delta R = 0.767(0.316) = 0.242 \text{ ohms}$$
$$\Delta X = 1.2(0.316) = 0.379 \text{ ohms}$$

4.8.2 Horizontal Electric Dipole

The analytical formulation of the horizontal dipole above the ground can also be obtained in a similar manner as for the vertical electric dipole. Referring to Figure 4.22(a) and (b), the direct component is given by (4-111) and the reflected by (4-112) where the reflection coefficient R_h is given by

$$R_h = \begin{cases} R_\perp \text{ for } \phi = 0°, 180° \text{ plane} \\ R_\parallel \text{ for } \phi = 90°, 270° \text{ plane} \end{cases} \tag{4-129}$$

where $R_\parallel$ is the reflection coefficient for parallel polarization, as given by (4-125), and $\perp$ is the reflection coefficient for perpendicular polarization given by [7].

$$R_\perp = \frac{\eta_1 \cos\theta_i - \eta_0 \cos\theta_t}{\eta_1 \cos\theta_i + \eta_0 \cos\theta_t} \tag{4-129a}$$

The angles θ_i and θ_t are again related by Snell's law of refraction as given by (4-126).

Using the far-field approximations of (4-115a) and 4-115b), the total field above the ground ($z \geq h$) can be written as

$$E_\psi = j\eta \frac{kI_0 e^{-jkr}}{4\pi r} \sqrt{1 - \sin^2\theta \sin^2\phi}\,[e^{jkh\cos\theta} + R_h e^{-jkh\cos\theta}],\ z \geq h \tag{4-130}$$

where R_h is given by (4-129).

The normalized (to 0 dB) pattern in the y-z plane ($\phi = 90°$) for $h = \lambda/4$ is shown plotted in Figure 4.30 (dashed curve) where it is compared with that (solid curve) of a perfect conductor ($\sigma_1 = \infty$). In the space above the interface, the relative

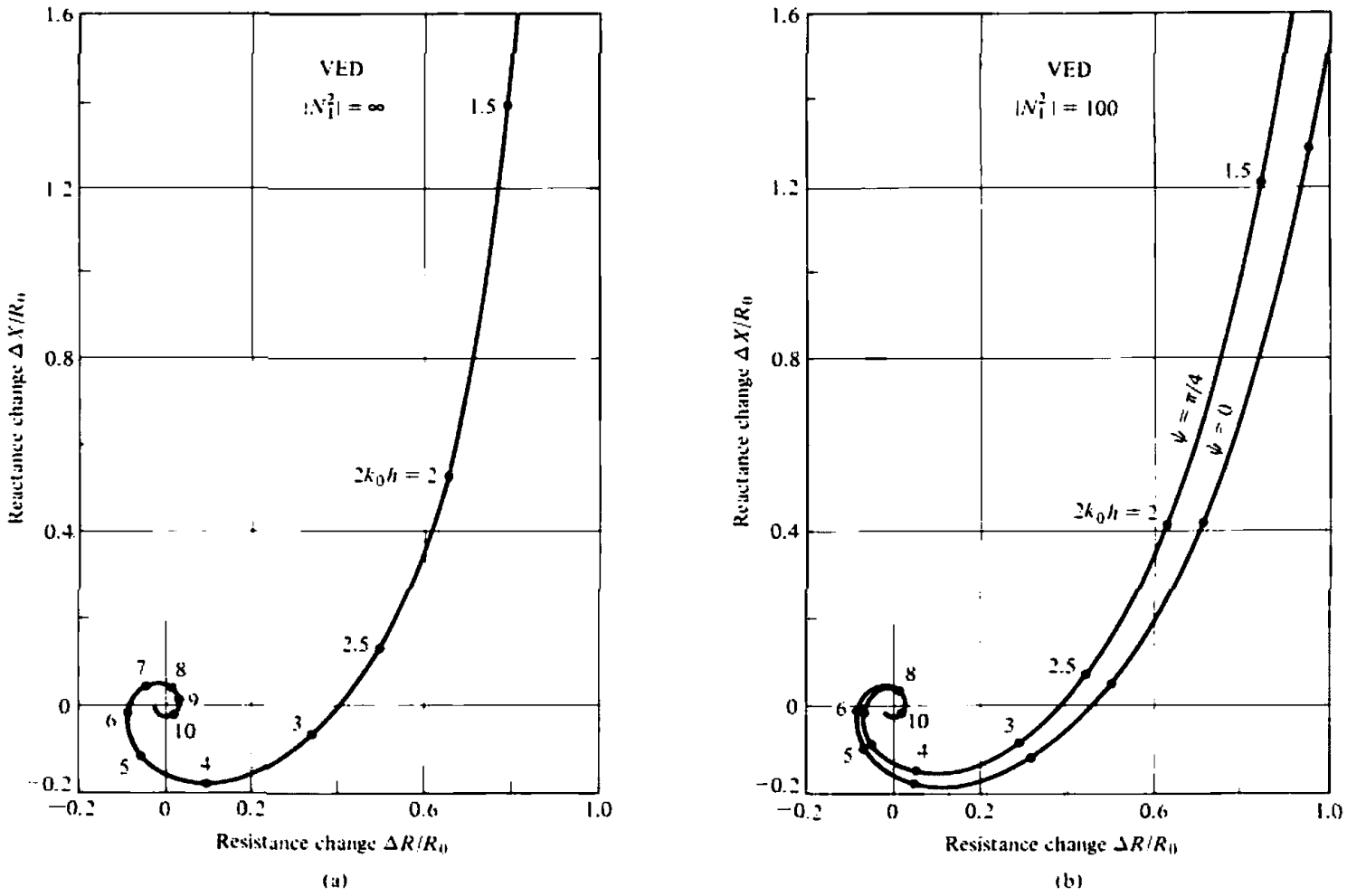

Figure 4.29 Vertical electric dipole (VED) impedance as a function of height above a homogeneous lossy half-space. (SOURCE: R. E. Collin and F. J. Zucker (eds.), *Antenna Theory Part 2*, McGraw-Hill, New York, 1969).

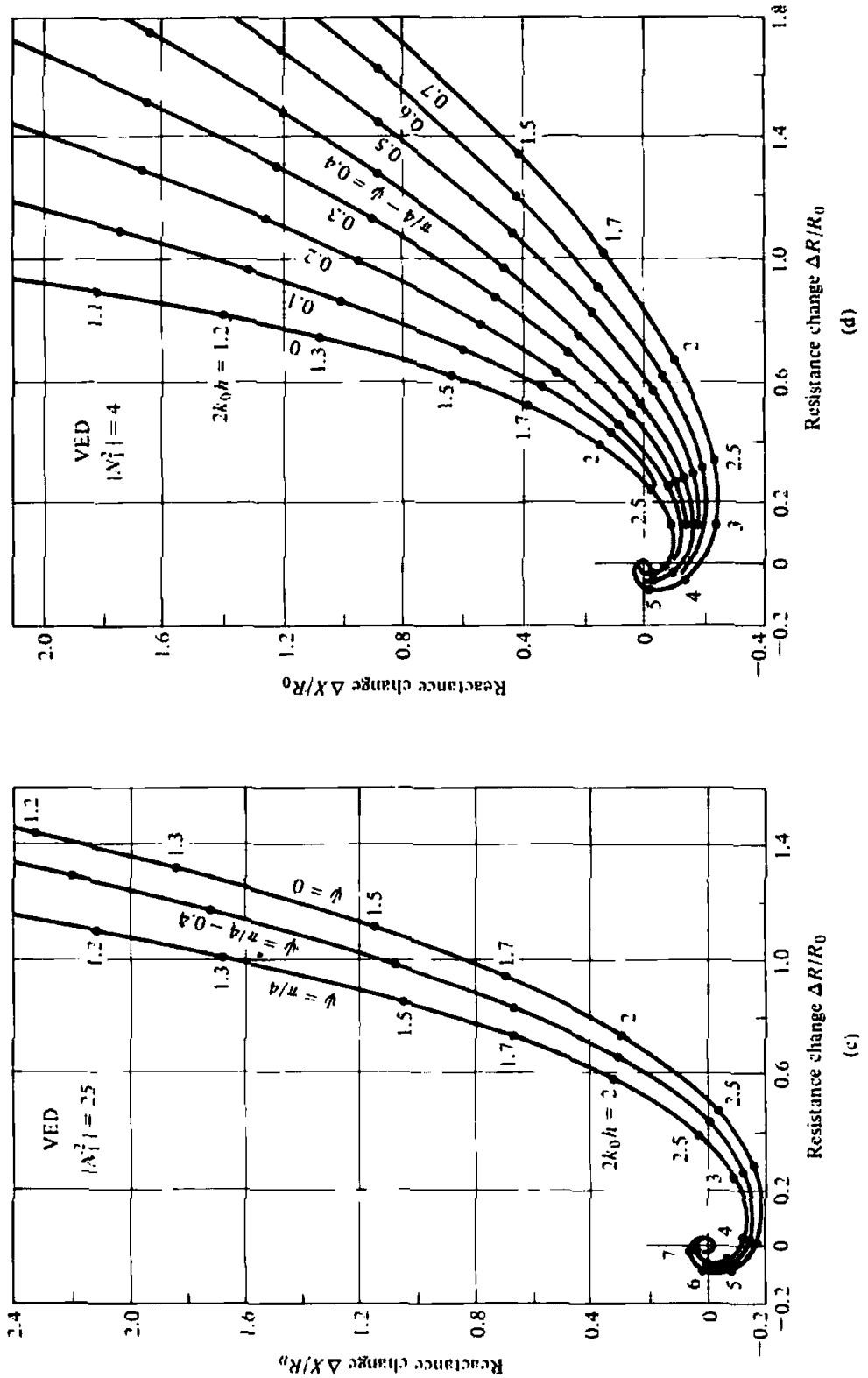

Figure 4.29 (continued)

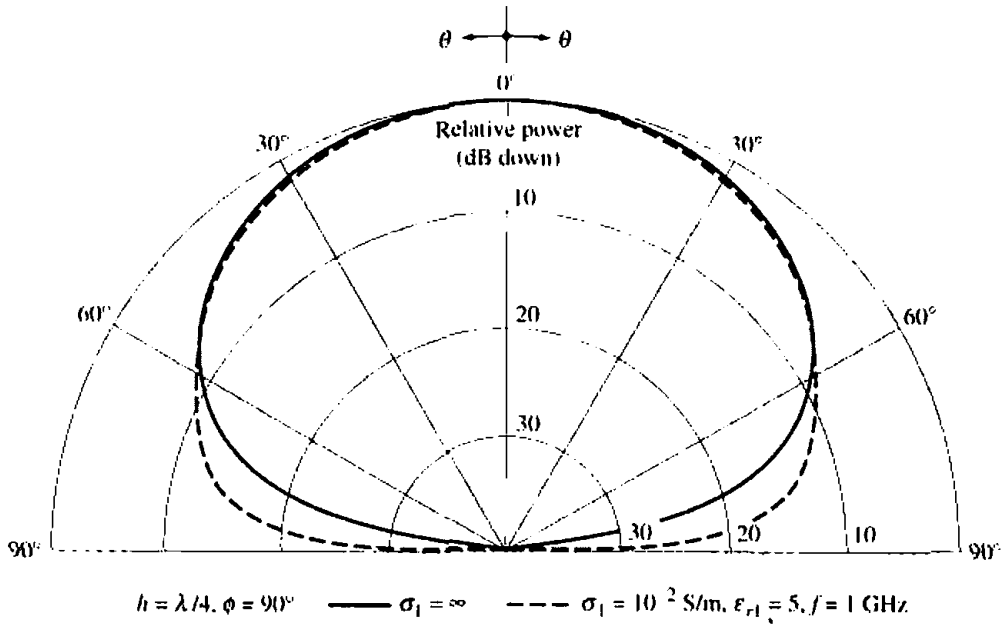

Figure 4.30 Elevation plane ($\phi = 90°$) amplitude patterns of an infinitesimal horizontal dipole above a perfect electric conductor ($\sigma_1 = \infty$) and a flat earth ($\sigma_1 = 0.01$ S/m, $\epsilon_{r1} = 5$, $f = 1$ GHz).

pattern in the presence of the ground is not significantly different from that of a perfect conductor. This becomes more evident by examining $R_{\parallel}$ as given by (4-129). For a ground medium, the values of $R_{\parallel}$ for most observation angles are not much different from -1 (the value of $R_{\parallel}$ for a perfect conductor). For grazing angles ($\theta_i \rightarrow 90°$), the values of $R_{\parallel}$ for the lossy ground approach -1 very rapidly. Thus the relative pattern of a horizontal dipole above a lossy surface is not significantly different from that above a perfect conductor.

4.8.3 Earth Curvature

Antenna pattern measurements on aircraft can be made using either scale models or full scale in-flight. Scale model measurements usually are made indoors using electromagnetic anechoic chambers, as described in Chapter 16. The indoor facilities provide a controlled environment, and all-weather capability, security, and minimize electromagnetic interference. However, scale model measurements may not always simulate real-life outdoor conditions, such as the reflecting surface of sea water. Therefore full-scale model measurements may be necessary. For in-flight measurements, reflecting surfaces, such as sea water, introduce reflections, which usually interfere with the direct signal. These unwanted signals are usually referred to as *multipath*. Therefore the total measured signal in an outdoor system configuration is the combination of the direct signal and that due to multipath, and usually it cannot be easily separated in its parts using measuring techniques. Since the desired signal is that due to the direct path, it is necessary to be able to subtract from the total response the contributions due to multipath. This can be accomplished by developing analytical models to predict the contributions due to multipath, which can then be subtracted from the total signal in order to be left with the desired direct path signal. In this section we will briefly describe techniques that have been used to accomplish this [22], [23].

The analytical formulations of Sections 4.8.1 and 4.8.2 for the patterns of vertical and horizontal dipoles assume that the earth is flat. This is a good approximation provided the curvature of the earth is large compared to the wavelength and the angle of observation is greater than about 3° from grazing [or more accurately greater than about $57.3/(ka)^{1/3}$ degrees, where a is the radius of the earth] from grazing [24]. The curvature of the earth has a tendency to spread out (weaken, diffuse, diverge) the reflected energy more than a corresponding flat surface. The spreading of the reflected energy from a curved surface as compared to that from a flat surface is taken into account by introducing a divergence factor D [20], [22], [23], defined as

$$D = \text{divergence factor} = \frac{\text{reflected field from curved surface}}{\text{reflected field from flat surface}} \tag{4-131}$$

The formula for D can be derived using purely geometrical considerations. It is accomplished by comparing the ray energy density in a small cone reflected from a sphere near the principal point of reflection with the energy density the rays (within the same cone) would have if they were reflected from a plane surface. Based on the geometrical optics energy conservation law for a bundle of rays within a cone, the reflected rays within the cone will subtend a circle on a perpendicular plane for reflections from a flat surface, as shown in Figure 4.31(a). However, according to the geometry of Figure 4.31(b), it will subtend an ellipse for a spherical reflecting surface. Therefore the divergence factor of (4-131) can also be defined as

$$D = \frac{E_s^r}{E_f^r} \approx \left[\frac{\text{area contained in circle}}{\text{area contained in ellipse}}\right]^{1/2} \tag{4-132}$$

where

E_s^r = reflected field from spherical surface

E_f^r = reflected field from flat surface

Using the geometry of Figure 4.32, the divergence factor can be written as [7] and [23]

$$D = \frac{\sqrt{\dfrac{\rho_1^r \rho_2^r}{(\rho_1^r + s)(\rho_2^r + s)}}}{\dfrac{s'}{s' + s}} \tag{4-133}$$

where ρ_1^r and ρ_2^r are the principal radii of curvature of the reflected wavefront at the point of reflection and are given, according to the geometry of Figure 4.32, by

$$\frac{1}{\rho_1^r} = \frac{1}{s'} + \frac{1}{\rho \sin \psi} + \sqrt{\frac{1}{(\rho \sin \psi)^2} - \frac{4}{a^2}} \tag{4-133a}$$

$$\frac{1}{\rho_2^r} = \frac{1}{s'} + \frac{1}{\rho \sin \psi} - \sqrt{\frac{1}{(\rho \sin \psi)^2} - \frac{4}{a^2}} \tag{4-133b}$$

$$\rho = \frac{a}{1 + \sin^2 \psi} \tag{4-133c}$$

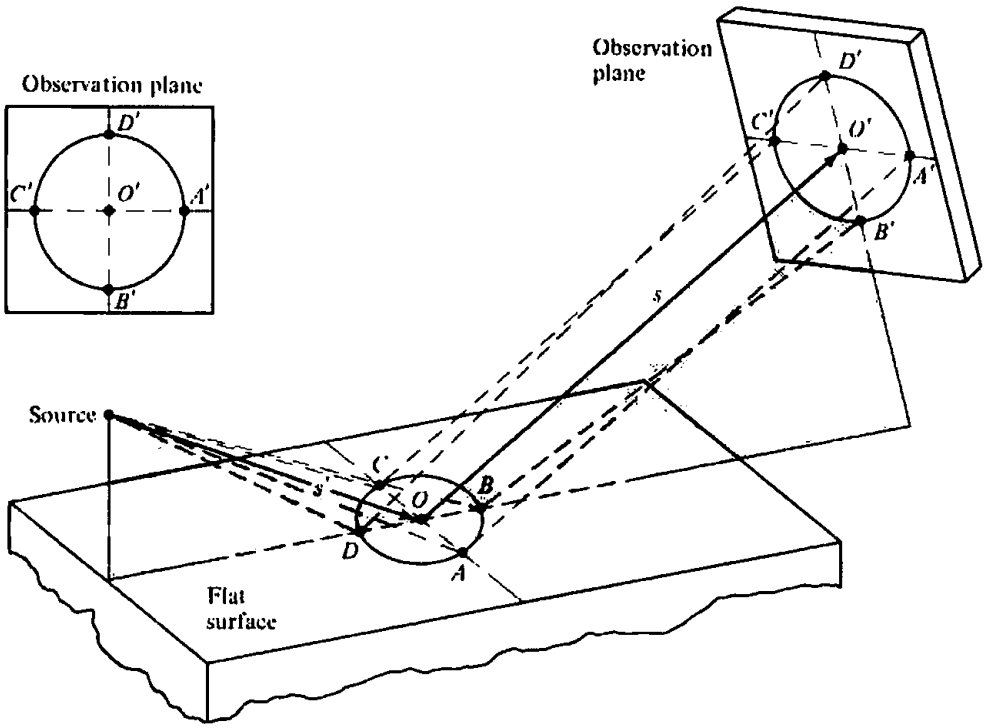

(a) Reflection from a flat surface

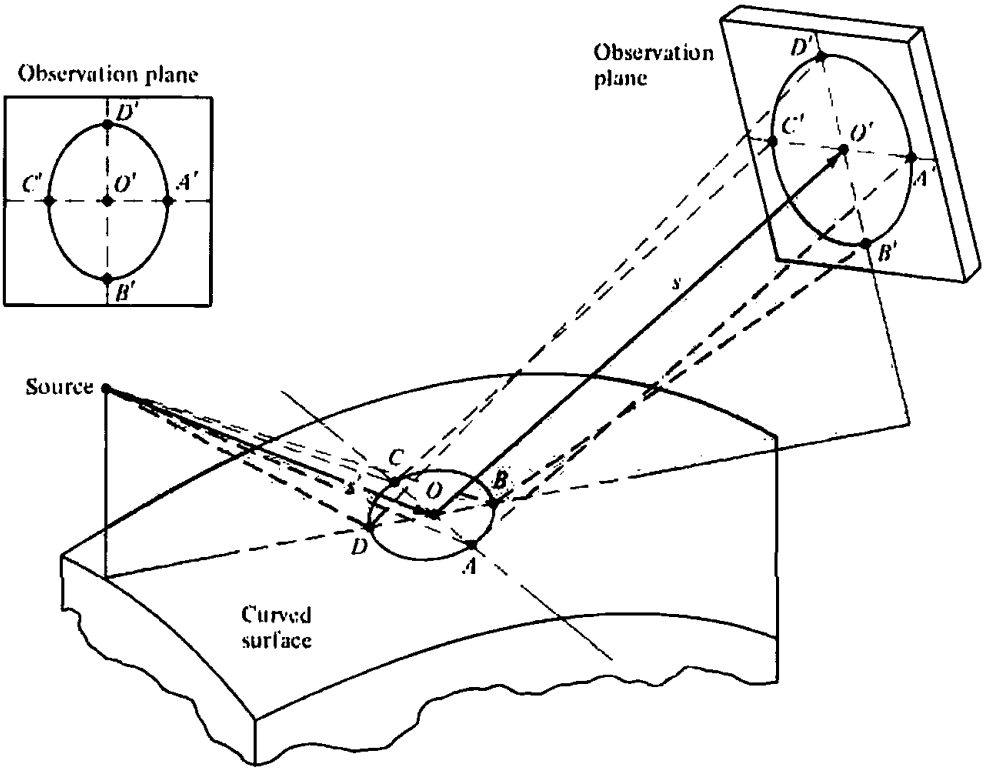

(b) Reflection from a spherical surface

Figure 4.31 Reflection from a flat and spherical surfaces.

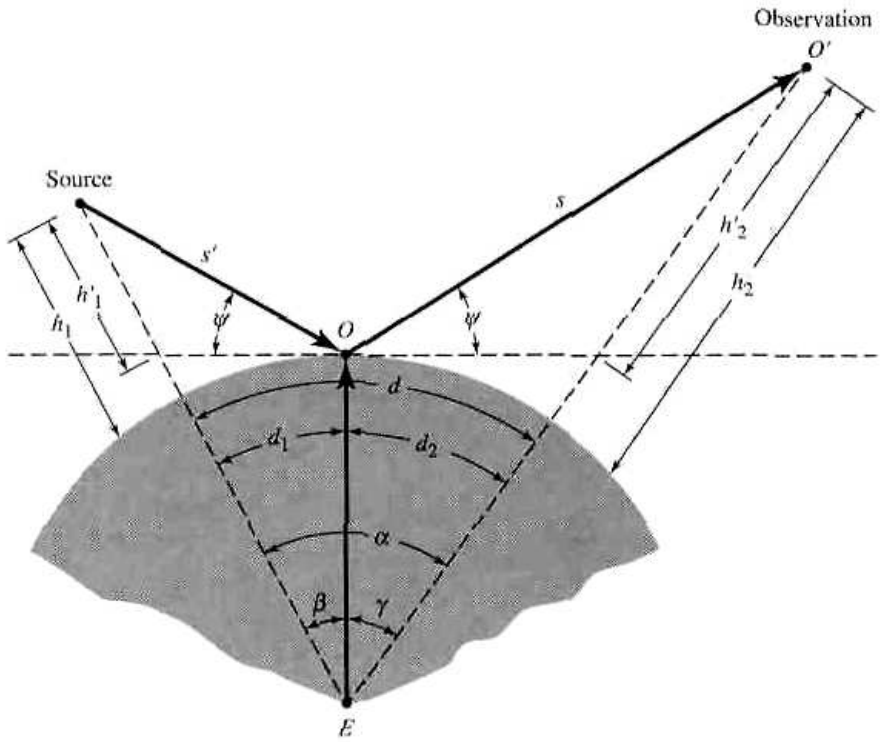

Figure 4.32 Geometry for reflections from a spherical surface.

A simplified form of the divergence factor is that of [25]

$$D \cong \left[1 + \frac{2s's}{a(s' + s)\sin\psi}\right]^{-1/2} \cdot \left[1 + \frac{2s's}{a(s' + s)}\right]^{-1/2} \tag{4-134}$$

Both (4-133) and (4-134) take into account the earth curvature in two orthogonal planes.

Assuming that the divergence of rays in the azimuthal plane (plane vertical to the page) is negligible, the divergence factor can be written as

$$D \simeq \left[1 + 2\frac{ss'}{ad\tan\psi}\right]^{-1/2} \tag{4-135}$$

where ψ is the grazing angle. Thus the divergence factor of (4-135) takes into account energy spreading primarily in the elevation plane. According to Figure 4.32

h_1' = height of the source above the earth (with respect to the tangent at the point of reflection)

h_2' = height of the observation point above the earth (with respect to the tangent at the point of reflection)

d = range (along the surface of the earth) between the source and the observation point

a = radius of the earth (3,959 mi). Usually a $\frac{4}{3}$ radius ($\simeq$ 5,280 mi) is used.

ψ = reflection angle (with respect to the tangent at the point of reflection).

d_1 = distance (along the surface of the earth) from the source to the reflection point

d_2 = distance (along the surface of the earth) from the observation point to the reflection point

The divergence factor can be included in the formulation of the fields radiated by a vertical or a horizontal dipole, in the presence of the earth, by modifying (4-127) and (4-130) and writing them, respectively, as

$$E_\theta = j\eta \frac{kI_0 le^{-jkr}}{4\pi r} \sin\theta [e^{jkh\cos\theta} + DR_v e^{-jkh\cos\theta}] \tag{4-136a}$$

$$E_\psi = j\eta \frac{kI_0 le^{-jkr}}{4\pi r} \sqrt{1 - \sin^2\theta \sin^2\phi}\, [e^{jkh\cos\theta} + DR_h e^{-jkh\cos\theta}] \tag{4-136b}$$

While the previous formulations are valid for smooth surfaces, they can still be used with rough surfaces, provided the surface geometry satisfies the Rayleigh criterion [20] and [25]

$$h_m < \frac{\lambda}{8 \sin\psi} \tag{4-137}$$

where h_m is the maximum height of the surface roughness. Since the dividing line between a smooth and a rough surface is not that well defined, (4-137) should only be used as a guideline.

The *coherent* contributions due to scattering by a surface with Gaussian rough surface statistics can be approximately accounted for by modifying the vertical and horizontal polarization smooth surface reflection coefficients of (4-125) and (4-129) and express them as

$$R^s_{v,h} = R_{v,h} e^{-2(k_0 h_0 \cos\theta_i)^2} \tag{4-138}$$

where

$R^s_{v,h}$ = reflection coefficient of a rough surface for either vertical or horizontal polarization

$R_{v,h}$ = reflection coefficient of a smooth surface for either vertical (4-125) or horizontal (4-129) polarization

h_0^2 = mean-square roughness height

A *slightly rough surface* is defined as one whose rms height is much smaller than the wavelength, while a *very rough surface* is defined as one whose rms height is much greater than the wavelength.

Plots of the divergence factor as a function of the grazing angle ψ (or as a function of the observation point h_2') for different source heights are shown in Figure 4.33. It is observed that the divergence factor is somewhat different and smaller than unity for small grazing angles, and it approaches unity as the grazing angle becomes larger. The variations of D displayed in Figure 4.33 are typical but not unique. For different positions of the source and observation point, the variations will be somewhat different. More detailed information on the variation of the divergence factor and its effect on the overall field pattern is available [23].

The most difficult task usually involves the determination of the reflection point from a knowledge of the heights of the source and observation points, and the range d between them. Procedures to do this have been developed [20], [22]–[26].

However, the one presented here is more accurate and does not require either

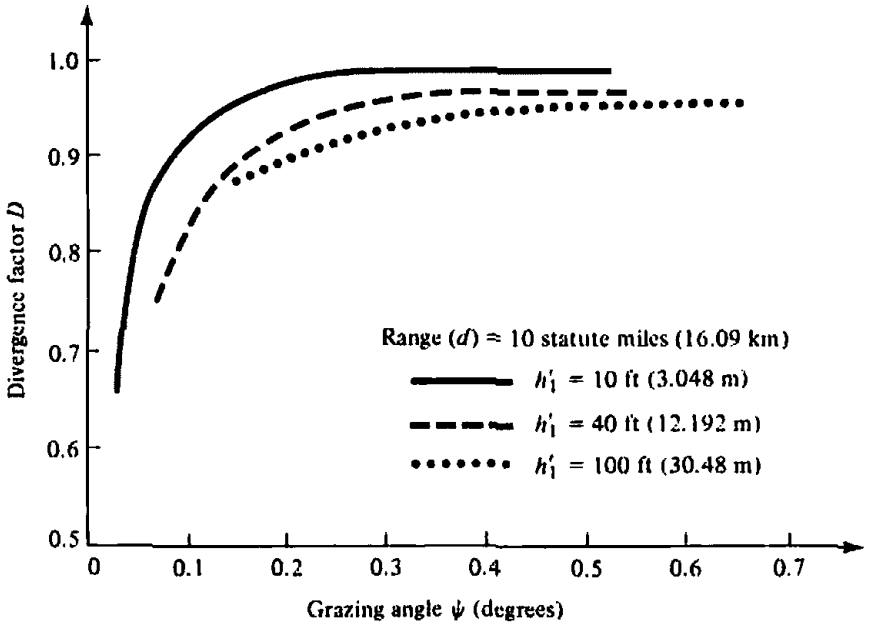

Figure 4.33 Divergence factor for a 4/3 radius earth (a_e = 5,280 mi = 8,497.3 km) as a function of grazing angle ψ.

iterative or graphical solutions. To find d_1 and d_2 (given d, h_1, and h_2), the cubic equation of [20] is utilized

$$2d_1^3 - 3dd_1^2 + [d^2 - 2a(h_1 + h_2)]d_1 + 2ah_1d = 0 \tag{4-139}$$

with solution given by

$$d_1 = \frac{d}{2} + p\cos\left(\frac{\Omega + \pi}{3}\right) \tag{4-139a}$$

$$d_2 = d - d_1 \tag{4-139b}$$

$$p = \frac{2}{\sqrt{3}}\sqrt{a(h_1 + h_2) + \left(\frac{d}{2}\right)^2} \tag{4-139c}$$

$$\Omega = \cos^{-1}\left[\frac{2a(h_1 - h_2)d}{p^3}\right] \tag{4-139d}$$

Equation (4-139) is valid provided that $\alpha - \beta$ is small, such that $\sin(\alpha - \beta) \simeq \alpha - \beta$, $\cos(\alpha - \beta) \simeq 1 - (\alpha - \beta)^2/2$, $\sin\beta \simeq \beta$, and $\cos\beta \simeq 1 - (\beta)^2/2$. Once d_1 and d_2 are found, then successively β, γ, s', s, ψ, r_1, r_2, α_1^r, α_1^d, α_2^r, and α_2^d can be determined using the geometry of Figure 4.31.

Using the analytical model developed here, computations were made to see how well the predictions compared with measurements. For the computations it was assumed that the reflecting surface is sea water possessing a dielectric constant of 81 and a conductivity of 4.64 S/m [22], [23]. To account for atmospheric refraction, a 4/3 earth was assumed [20], [22], [27] so the atmosphere above the earth can be considered homogeneous with propagation occurring along straight lines.

For computations using the earth as the reflecting surface, all three divergence

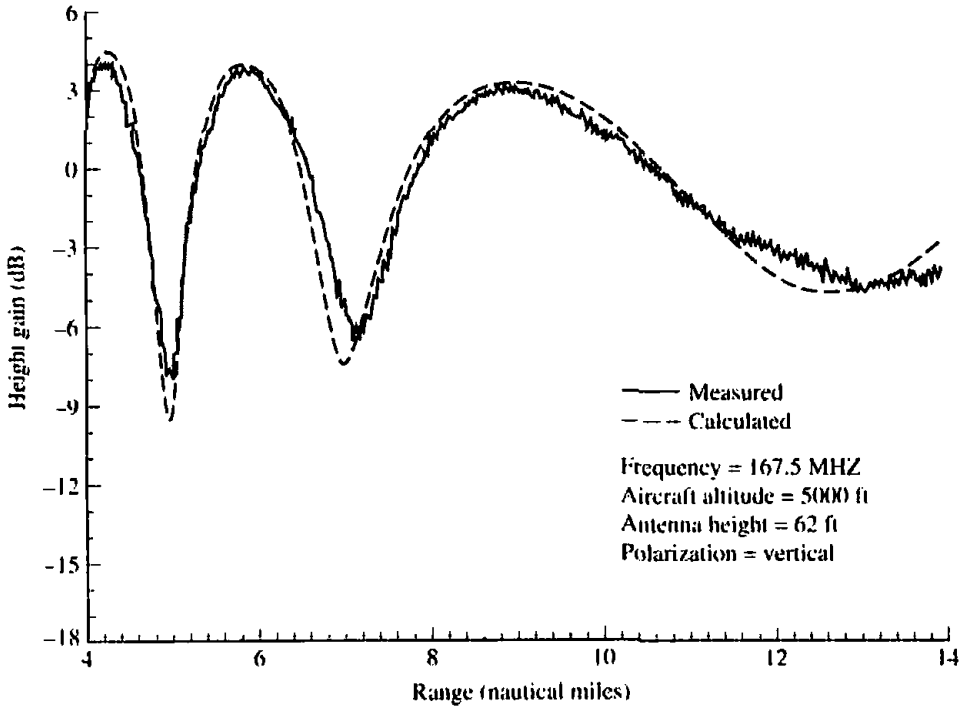

Figure 4.34 Measured and calculated height gain over the ocean (ϵ_r = 81, σ = 4.64 S/m) for vertical polarization.

factors of (4-133)–(4-135) gave the same results. However, for nonspherical reflecting surfaces and for those with smaller radii of curvature, the divergence factor of (4-133) is slightly superior followed by (4-134) and then by (4-135). In Figure 4.34 we display and compare the predicted and measured *height gain* versus range d ($4 < d < 14$ nautical miles) for a vertical-vertical polarization system configuration at a frequency of 167.5 MHz. The *height gain* is defined as the ratio of the total field in the presence of the earth divided by the total field in the absence of the earth. A good agreement is noted between the two. The peaks and nulls are formed by constructive and destructive interferences between the direct and reflected components. If the reflecting surface were perfectly conducting, the maximum height gain would be 2 (6 dB). Because the modeled reflecting surface of Figure 4.34 was sea water with a dielectric constant of 81 and a conductivity of 4.64 S/m, the maximum height gain is less than 6 dB. The measurements were taken by aircraft and facilities of the Naval Air Warfare Center, Patuxent River, MD. Additional measurements were made but are not included here; they can be found in [28] and [29].

References

1. W. A. Wheeler, "The Spherical Coil as an Inductor, Shield, or Antenna," *Proc. IRE*, Vol. 46, pp. 1595–1602, September 1958 (correction, Vol. 48, p. 328, March 1960).
2. W. A. Wheeler, "The Radiansphere Around a Small Antenna," *Proc. IRE*, Vol. 47, pp. 1325–1331, August 1959.
3. W. A. Wheeler, "Small Antennas," *IEEE Trans. Antennas Propagat.*, Vol. AP-23, No. 4, pp. 462–469, July 1975.
4. C. H. Walter, *Traveling Wave Antennas*, McGraw-Hill, 1965, pp. 32–44.

5. W. R. Scott, Jr., "A General Program for Plotting Three-Dimensional Antenna Patterns," *IEEE Antennas and Propagation Society Newsletter*, pp. 6–11, December 1989.
6. S. K. Schelkunoff and H. T. Friis, *Antennas: Theory and Practice*, Wiley, New York, 1952, pp. 229–244, 351–353.
7. C. A. Balanis, *Advanced Engineering Electromagnetics*, John Wiley & Sons, Inc., New York, 1989.
8. R. F. Harrington, "Matrix Methods for Field Problems," *Proc. IEEE*, Vol. 55, No. 2, pp. 136–149, February 1967.
9. R. F. Harrington, *Field Computation by Moment Methods*, Macmillan, New York, 1968.
10. R. Mittra (Ed.), *Computer Techniques for Electromagnetics*, Pergamon, New York, 1973.
11. J. Moore and P. Pizer (Eds.), *Moment Methods in Electromagnetics: Techniques and Applications*, Letchworth, UK: Research Studies Press, 1984.
12. J. J. Wang, *Generalized Moment Methods in Electromagnetics*, John Wiley & Sons, Inc., New York, 1991.
13. R. F. Schwartz, "Input Impedance of a Dipole or Monopole," *The Microwave Journal*, Vol. 15, No. 12, p. 22, December 1972.
14. K. Fujimoto and J. R. James, *Mobile Antenna Systems Handbook*, Artech House, Norwood, MA, 1994.
15. M. A. Jensen and Y. Rahmat-Samii, "Performance Analysis of Antennas for Hand-Held Transceivers Using FDTD," *IEEE Trans. Antennas Propagat.*, Vol. 42, No. 8, pp. 1106–1113, August 1994.
16. M. A. Jensen and Y. Rahmat-Samii, "EM Interaction of Handset Antennas and a Human in Personal Communications," *Proc. IEEE*, Vol. 83, No. 1, pp. 7–17, January 1995.
17. C. A. Balanis, K. D. Katsibas and P. A. Tirkas, "Antenna Considerations for Wireless Communication Systems and Networks," 5th International Conference on Advances in Communication and Control (ComCon 5), June 26–30, 1995, Rethymnon, Crete, Greece.
18. R. E. Collin and F. J. Zucker (eds.), *Antenna Theory Part 2*, Chapters 23 and 24 (by J. R. Wait), McGraw-Hill, New York, 1969.
19. P. R. Bannister, "Image Theory Results for the Mutual Impedance of Crossing Earth Return Circuits," *IEEE Trans. Electromagn. Compat.*, Vol. 15, No. 4, 1973, pp. 158–160.
20. D. E. Kerr, *Propagation of Short Radio Waves*, MIT Radiation Laboratory Series, McGraw-Hill, New York, 1951, Vol. 13, pp. 98–109, 112–122, 396–444.
21. L. E. Vogler and J. L. Noble, "Curves of Input Impedance Change due to Ground for Dipole Antennas," U.S. National Bureau of Standards, Monograph 72, January 31, 1964.
22. H. R. Reed and C. M. Russell, *Ultra High Frequency Propagation*, Boston Technical Publishers, Inc., Lexington, Mass., 1964, Chapter 4, pp. 102–116.
23. C. A. Balanis, R. Hartenstein, and D. DeCarlo, "Multipath Interference for In-Flight Antenna Measurements," *IEEE Trans. Antennas Propagat.*, Vol. AP-32, No. 1, pp. 100–104, January 1984.
24. J. R. Wait and A. M. Conda, "Pattern of an Antenna on a Curved Lossy Surface," *IRE Trans. Antennas Propagat.*, Vol. AP-6, No. 4, October 1958, pp. 348–359.
25. P. Bechmann and A. Spizzichino, *The Scattering of Electromagnetic Waves from Rough Surfaces*, MacMillan, New York, 1963.
26. G. May, "Determining the Point of Reflection on MW Radio Links," *Microwave Journal*, Vol. 20, No. 9, September 1977, pp. 74, 76.
27. D. T. Paris and F. K. Hurd, *Basic Electromagnetic Theory*, McGraw-Hill Book Co., pp. 385–386, 1969.
28. C. A. Balanis, "Multipath Interference in Airborne Antenna Measurements," Final Report, prepared for Naval Air Station, Patuxent River, Maryland, May 28, 1982.
29. D. DeCarlo, "Automation of In-Flight Antenna Measurements," MSEE Problem Report, Dept. of Electrical Engineering, West Virginia University, July 1980.

PROBLEMS

4.1. A horizontal infinitesimal electric dipole of constant current I_0 is placed symmetrically about the origin and directed along the x-axis. Derive the
(a) far-zone fields radiated by the dipole
(b) directivity of the antenna

4.2. Repeat Problem 4.1 for a horizontal infinitesimal electric dipole directed along the y-axis.

4.3. For Problem 4.1 determine the polarization of the radiated far-zone electric fields (E_θ, E_ϕ) and normalized amplitude pattern in the following planes:
(a) $\phi = 0°$
(b) $\phi = 90°$
(c) $\theta = 90°$

4.4. Repeat Problem 4.3 for the horizontal infinitesimal electric dipole of Problem 4.2, which is directed along the y-axis.

4.5. An infinitesimal magnetic dipole of constant current I_m and length l is symmetrically placed about the origin along the z-axis. Find the
(a) spherical **E**- and **H**-field components radiated by the dipole in all space
(b) directivity of the antenna

4.6. For the infinitesimal magnetic dipole of Problem 4.5, find the far-zone fields when the element is placed along the
(a) x-axis
(b) y-axis

4.7. An infinitesimal electric dipole is centered at the origin and lies on the x-y plane along a line which is at an angle of 45° with respect to the x-axis. Find the far-zone electric and magnetic fields radiated. The answer should be a function of spherical coordinates.

4.8. Repeat Problem 4.7 for an infinitesimal magnetic dipole.

4.9. Derive (4-10a)–(4-10c) using (4-8a)–(4-9).

4.10. Derive the radiated power of (4-16) by forming the average power density, using (4-26a)–(4-26c), and integrating it over a sphere of radius r.

4.11. Derive the far-zone fields of an infinitesimal electric dipole, of length l and constant current I_0, using (4-4) and the procedure outlined in Section 3.6. Compare the results with (4-26a)–(4-26c).

4.12. Derive the fifth term of (4-41).

4.13. For an antenna with a maximum linear dimension of D, find the inner and outer boundaries of the Fresnel region so that the maximum phase error does not exceed
(a) $\pi/16$ rad
(b) $\pi/4$ rad
(c) 18°
(d) 15°

4.14. The boundaries of the far-field (Fraunhofer) and Fresnel regions were selected based on a maximum phase error of 22.5°, which occur, respectively, at directions of 90° and 54.74° from the axis along the largest dimension of the antenna. For an antenna of maximum length of 5λ, what do these maximum phase errors reduce to at an angle of 30° from the axis along the length of the antenna? Assume that the phase error in each case is totally contributed by the respective first higher order term that is being neglected in the infinite series expansion of the distance from the source to the observation point.

4.15. The current distribution on a terminated and matched long linear (traveling wave) antenna of length l, positioned along the z-axis and fed at its one end, is given by

$$\mathbf{I} = \hat{\mathbf{a}}_z I_0 e^{-jkz'}, \quad 0 \le z' \le l$$

where I_0 is a constant. Derive expressions for the
(a) far-zone spherical electric and magnetic field components
(b) radiation power density

4.16. A line source of infinite length and constant current I_0 is positioned along the z-axis. Find the
(a) vector potential **A**
(b) cylindrical **E**- and **H**-field components radiated

$$\text{Hint: } \int_{-\infty}^{+\infty} \frac{e^{-j\beta\sqrt{b^2+t^2}}}{\sqrt{b^2+t^2}}\,dt = -j\pi H_0^{(2)}(\beta b)$$

where $H_0^{(2)}(\alpha x)$ is the Hankel function of the second kind of order zero.

4.17. Show that (4-67) reduces to (4-68) and (4-88) to (4-89).

4.18. A thin linear dipole of length l is placed symmetrically about the z-axis. Find the far-zone spherical electric and magnetic components radiated by the dipole whose current distribution can be approximated by

$$\text{(a) } I_z(z') = \begin{cases} I_0\left(1 + \dfrac{2}{l}z'\right), & -l/2 \le z' \le 0 \\ I_0\left(1 - \dfrac{2}{l}z'\right), & 0 \le z' \le l/2 \end{cases}$$

$$\text{(b) } I_z(z') = I_0 \cos\left(\frac{\pi}{l}z'\right), \quad -l/2 \le z' \le l/2$$

$$\text{(c) } I_z(z') = I_0 \cos^2\left(\frac{\pi}{l}z'\right), \quad -l/2 \le z' \le l/2$$

4.19. A center-fed electric dipole of length l is attached to a balanced lossless transmission line whose characteristic impedance is 50 ohms. Assuming the dipole is resonant at the given length, find the input VSWR when
(a) $l = \lambda/4$ (b) $l = \lambda/2$
(c) $l = 3\lambda/4$ (d) $l = \lambda$

4.20. Use the equations in the book or the computer program at the end of the chapter. Find the radiation efficiency of resonant linear electric dipoles of length
(a) $l = \lambda/50$ (b) $l = \lambda/4$
(c) $l = \lambda/2$ (d) $l = \lambda$
Assume that each dipole is made out of copper [$\sigma = 5.7 \times 10^7$ S/m], has a radius of $10^{-4}\lambda$, and is operating at $f = 10$ MHz. Use the computer program at the end of the chapter to find the radiation resistances.

4.21. Write the far-zone electric and magnetic fields radiated by a magnetic dipole of $l = \lambda/2$ aligned with the z-axis. Assume a sinusoidal magnetic current with maximum value I_{mo}.

4.22. A resonant center-fed dipole is connected to a 50-ohm line. It is desired to maintain the input VSWR = 2.
(a) What should the largest input resistance of the dipole be to maintain the VSWR = 2?
(b) What should the length (in wavelengths) of the dipole be to meet the specification?
(c) What is the radiation resistance of the dipole?

4.23. The radiation field of a particular antenna is given by:

$$\mathbf{E} = \hat{\mathbf{a}}_\theta j\omega\mu k \sin\theta \frac{I_0 A_1 e^{-jkr}}{4\pi r} + \hat{\mathbf{a}}_\phi \omega\mu \sin\theta \frac{I_0 A_2 e^{-jkr}}{2\pi r}$$

The values A_1 and A_2 depend on the antenna geometry. Obtain an expression for the radiation resistance. What is the polarization of the antenna?

4.24. For a $\lambda/2$ dipole placed symmetrical along the z-axis, determine the
(a) vector effective height
(b) maximum value (magnitude) of the vector effective height
(c) ratio (in percent) of the maximum value (magnitude) of the vector effective height to its total length
(d) maximum open-circuit output voltage when a uniform plane wave with an electric field of

$$\mathbf{E}^i|_{\theta=90^\circ} = -\hat{\mathbf{a}}_\theta 10^{-3} \text{ volts/wavelength}$$

impinges at broadside incidence on the dipole

4.25. A $\lambda/2$ dipole situated with its center at the origin radiates a time-averaged power of 600 W at a frequency of 300 MHz. A second $\lambda/2$ dipole is placed with its center at a point $P(r, \theta, \phi)$, where $r = 200$ m, $\theta = 90^\circ$, $\phi = 40^\circ$. It is oriented so that its axis is parallel to that of the transmitting antenna. What is the available power at the terminals of the second (receiving) dipole?

4.26. A half-wave dipole is radiating into free space. The coordinate system is defined so that the origin is at the center of the dipole and the z-axis is aligned with the dipole. Input power to the dipole is 100 W. Assuming an overall efficiency of 50%, find the power density (in W/m^2) at $r = 500$ m, $\theta = 60^\circ$, $\phi = 0^\circ$.

4.27. The input impedance of a $\lambda/2$ dipole, assuming the input (feed) terminals are at the center of the dipole, is equal to $73 + j42.5$. Assuming the dipole is lossless, find the
(a) input impedance (real and imaginary parts) assuming the input (feed) terminals have been shifted to a point on the dipole which is $\lambda/8$ from either end point of the dipole length
(b) capacitive or inductive reactance that must be placed across the new input terminals of part (a) so that the dipole is self-resonant
(c) VSWR at the new input terminals when the self-resonant dipole of part (b) is connected to a "twin-lead" 300-ohm line

4.28. A linear half-wavelength dipole is operating at a frequency of 1 GHz, determine the capacitance *or* inductance that must be placed *across* the input terminals of the dipole so that the antenna becomes resonant (make the total input impedance real). What is then the VSWR of the resonant half-wavelength dipole when it is connected to a 50-ohm line?

4.29. The field radiated by an infinitesimal electric dipole, placed along the z-axis a distance s along the x-axis, is incident upon a waveguide aperture antenna of dimensions a and b, mounted on an infinite ground plane, as shown in the figure. The normalized electric field radiated by the aperture in the E-plane (x-z plane; $\phi = 0^\circ$) is given by

$$\mathbf{E} = -\hat{\mathbf{a}}_\theta j \frac{\omega\mu b I_0 e^{-jkr}}{4\pi r} \frac{\sin\left(\frac{kb}{2}\cos\theta\right)}{\frac{kb}{2}\cos\theta}$$

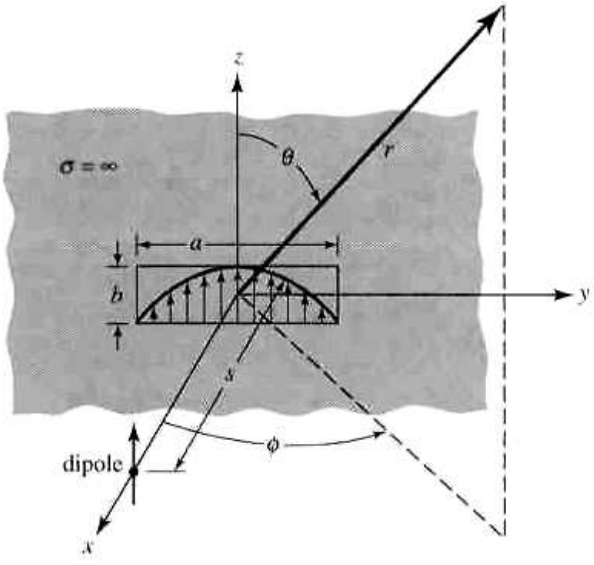

Assuming the dipole and aperture antennas are in the far field of each other, determine the polarization loss (in dB) between the two antennas.

4.30. We are given the following information about antenna A:

(a) When A is transmitting, its radiated far-field expression for the E field is given by:

$$\mathbf{E}_a(z) = E_0 \frac{e^{-jkz}}{4\pi z}\left(\frac{\hat{\mathbf{a}}_x + j\hat{\mathbf{a}}_y}{\sqrt{2}}\right) \qquad V/m$$

(b) When A is receiving an incident plane wave given by:

$$\mathbf{E}_1(z) = \hat{\mathbf{a}}_y e^{jkz} \qquad V/m$$

its open-circuit voltage is $V_1 = 4e^{j20^\circ}$ V.

If we use the same antenna to receive a second incident plane given by:

$$\mathbf{E}_2(z) = 10(2\hat{\mathbf{a}}_x + \hat{\mathbf{a}}_y E^{j30^\circ})e^{jkz} \qquad V/m$$

find its received open-circuit voltage V_2.

4.31. A 3-cm long dipole carries a phasor current $I_0 = 10e^{j60}$ A. Assuming that $\lambda = 5$ cm, determine the E- and H-fields at 10 cm away from the dipole and at $\theta = 45^\circ$.

4.32. The radiation resistance of a thin, lossless linear electric dipole of length $l = 0.6\lambda$ is 120 ohms. What is the input resistance?

4.33. A lossless, resonant, center-fed $3\lambda/4$ linear dipole, radiating in free space is attached to a balanced, lossless transmission line whose characteristic impedence is 300 ohms. *Calculate* the

(a) radiation resistance (referred to the current maximum)

(b) input impedance (referred to the input terminals)

(c) VSWR on the transmission line

For parts (a) and (b) use the computer program at the end of the chapter.

4.34. Repeat Problem 4.33 for a center-fed $5\lambda/8$ dipole.

4.35. A dipole antenna, with a triangular current distribution, is used for communication with submarines at a frequency of 150 kHz. The overall length of the dipole is 200 m, and its radius is 1 m. Assume a loss resistance of 2 ohms in series with the radiation resistance of the antenna.

(a) Evaluate the input impedance of the antenna including the loss resistance. The input reactance can be approximated by

$$X_{in} \simeq -j120\,\frac{[\ln(l/2a) - 1]}{\tan(\pi l/\lambda)}$$

(b) Evaluate the radiation efficiency of the antenna.

(c) Evaluate the radiation power factor of the antenna.

(d) Design a conjugate-matching network to provide a perfect match between the antenna and a 50 ohms transmission line. Give the value of the series reactance X and the turns ratio n of the ideal transformer.

(e) Assuming a conjugate match, evaluate the instantaneous 2 : 1 VSWR bandwidth of the antenna.

4.36. Derive (4-102) using (4-99).

4.37. Determine the smallest height that an infinitesimal vertical electric dipole of $l = \lambda/50$ must be placed above an electric ground plane so that its pattern has only one null (aside from the null toward the vertical), and it occurs at 30° from the vertical. For that height, find the directivity and radiation resistance.

4.38. A $\lambda/50$ linear dipole is placed vertically at a height $h = 2\lambda$ above an infinite electric ground plane. Determine the angles (in degrees) where all the nulls of its pattern occur.

4.39. A linear infinitesimal dipole of length l and constant current is placed vertically a distance h above an infinite electric ground plane. Find the first five smallest heights

(in ascending order) so that a null is formed (for each height) in the far-field pattern at an angle of 60° from the vertical.

4.40. A vertical infinitesimal linear dipole is placed a distance $h = 3\lambda/2$ above an infinite perfectly conducting flat ground plane. Determine the
(a) angles (*in degrees* from the vertical) where the *array factor* of the system will achieve its *maximum* value
(b) angle (*in degrees* from the vertical) where the maximum of the *total field* will occur
(c) relative (compared to its maximum) field strength (*in dB*) of the total field at the angles where the array factor of the system achieves its maximum value (as obtained in part a)

4.41. A half-wavelength dipole is placed vertically on an infinite electric ground plane. Assuming that the dipole is fed at its base, find the
(a) radiation impedance (referred to the current maximum)
(b) input impedance (referred to the input terminals)
(c) VSWR when the antenna is connected to a lossless 50-ohm transmission line

4.42. An infinitesimal dipole of length ℓ is placed a distance s from an air-conductor interface and at an angle of $\theta = 60°$ from the vertical axis, as shown in the figure. Determine the location and direction of the image source which can be used to account for reflections. Be very clear in indicating the location and direction of the image. Your answer can be in the form of a very clear sketch.

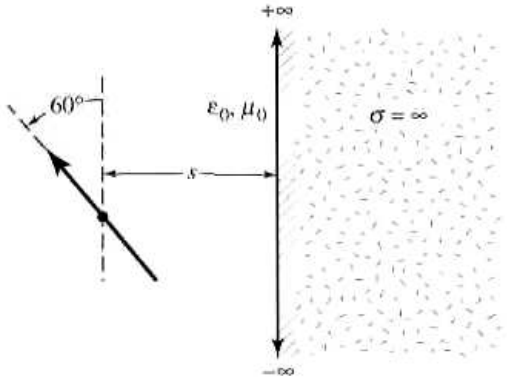

4.43. It is desired to design an antenna system, which utilizes a vertical infinitesimal dipole of length ℓ placed a height h above a flat, perfect electric conductor of infinite extent. The design specifications require that the pattern of the array factor of the source and its image has only one maximum, and that maximum is pointed at an angle of 60° from the vertical. Determine (in wavelengths) the height of the source to achieve this desired design specification.

4.44. A very short ($l \leq \lambda/50$) vertical electric dipole is mounted on a pole a height h above the ground, which is assumed to be flat, perfectly conducting, and of infinite extent. The dipole is used as a transmitting antenna in a VHF ($f = 50$ MHz) ground-to-air communication system. In order for the communication system transmitting antenna signal not to interfere with a nearby radio station, it is necessary to place a null in the vertical dipole system pattern at an angle of 80° from the vertical. What should the shortest height (in meters) of the dipole be to achieve the desired specifications?

4.45. Derive (4-118) using (4-116).

4.46. An infinitesimal horizontal electric dipole of length $l = \lambda/50$ is placed parallel to the y-axis a height h above an infinite electric ground plane.
(a) Find the smallest height h (excluding $h = 0$) that the antenna must be elevated so that a null in the $\phi = 90°$ plane will be formed at an angle of $\theta = 45°$ from the vertical axis.
(b) For the height of part (a), determine the (1) radiation resistance and (2) directivity (for $\theta = 0°$) of the antenna system.

4.47. A horizontal $\lambda/50$ infinitesimal dipole of constant current and length l is placed parallel to the y-axis a distance $h = 0.707\lambda$ above an infinite electric ground plane. Find *all* the nulls formed by the antenna system in the $\phi = 90°$ plane.

4.48. An infinitesimal magnetic dipole is placed vertically a distance h above an infinite, perfectly conducting electric ground plane. Derive the far-zone fields radiated by the element above the ground plane.

4.49. Repeat Problem 4.48 for an electric dipole above an infinite, perfectly conducting magnetic ground plane.

4.50. Repeat Problem 4.48 for a magnetic dipole above an infinite, perfectly conducting magnetic ground plane.

4.51. An infinitesimal vertical electric dipole is placed at height h above an infinite PMC (perfect magnetic conductor) ground plane.

(a) Find the smallest height h (excluding $h = 0$) to which the antenna must be elevated so that a null is formed at an angle $\theta = 60°$ from the vertical axis

(b) For the value of h found in part (a), determine

1. the directive gain of the antenna in the $\theta = 45°$ direction
2. the radiation resistance of the antenna normalizd to the intrinsic impedance of the medium above the ground plane

Assume that the length of the antenna is $l = \frac{\lambda}{100}$.

4.52. A vertical $\lambda/2$ dipole, operating at 1 GHz, is placed a distance of 5 m (with respect to the tangent at the point of reflections) above the earth. Find the total field at a point 20 km from the source ($d = 20 \times 10^3$ m), at a height of 1,000 m (with respect to the tangent) above the ground. Use a $\frac{4}{3}$ radius earth and assume that the electrical parameters of the earth are $\epsilon_r = 5$, $\sigma = 10^{-2}$ S/m.

4.53. Two astronauts equipped with handheld radios land on different parts of a large asteroid. The radios are identical and transmit 5 W average power at 300 MHz. Assume the asteroid is a smooth sphere with physical radius of 1,000 km, has no atmosphere, and *consists of a lossless dielectric material with relative permittivity* $\epsilon_r = 9$. *Assume that* the radios' antennas can be modeled as vertical infinitesimal electric dipoles. Determine the signal power (in microwatts) received by each radio from the other, if the astronauts are separated by a range (distance along the asteroid's surface) of 2 km, and hold their radios vertically at heights of 1.5 m above the asteroid's surface.

Additional Information Required to Answer this Question: Prior to landing on the asteroid the astronauts calibrated their radios. Separating themselves in outer space by 10 km, the astronauts found the received signal power at each radio from the other was 10 microwatts, when both antennas were oriented in the same direction.

4.54. A satellite S transmitts an electromagnetic wave, at 10 GHz, via its transmitting antenna. The characteristics of the satellite-based transmitter are:

(a) The power radiated from the satellite antenna is 10 W.

(b) The distance between the satellite antenna and a point A on the earth's surface is 3.7×10^7 m, and

(c) The satellite transmitting antenna directivity in the direction SA is 50 dB

Ignoring ground effects,

1. Determine the magnitude of the E-field at A.
2. If the receiver at point A is a $\lambda/2$ dipole, what would be the voltage reading at the terminals of the antenna?

4.55. Derive (4-134) based on geometrical optics as presented in section 13.2 of [7].

COMPUTER PROGRAM - LINEAR DIPOLE

```
C**********************************************************************
C
C THIS IS A FORTRAN PROGRAM THAT COMPUTES THE:
C
C     I.  MAXIMUM DIRECTIVITY (DIMENSIONLESS AND IN dB)
C     II.  RADIATION RESISTANCE
C     III.  INPUT  RESISTANCE
C
C FOR A SYMMETRICAL DIPOLE OF FINITE LENGTH.  THE DIPOLE IS
C RADIATING IN  FREE SPACE.
C
C THE DIRECTIVITY, RADIATION RESISTANCE AND INPUT
C RESISTANCE ARE CALCULATED USING THE TRAILING EDGE
C METHOD IN INCREMENTS OF 1° IN THETA.
C
C
C          **INPUT  PARAMETERS
C          1.  L:  DIPOLE LENGTH (in wavelengths)
C
C          **NOTE
C          THE FAR-ZONE ELECTRIC FIELD COMPONENT  E_θ
C          EXISTS FOR 0°≤ Θ ≤180° AND 0°≤ Φ ≤360°.
C
C
C**********************************************************************
```